HafenCity University Hamburg

Technical Infrastructure Management Insights Vol. II

Ingo Weidlich (Editor)
HafenCity University

Legal Notice

Publisher
First published 2026
HafenCity Universität Hamburg
Henning-Voscherau-Platz 1, 20457 Hamburg

Professorship
Technisches Infrastrukturmanagement

Print
oeding print GmbH

Editor
Univ.-Prof. Dr.-Ing. Ingo Weidlich

Contact
E-mail: ingo.weidlich@hcu-hamburg.de
Tel. : +49(0)40 300 880 5700

ISBN: 978-3-947972-92-0
DOI: 10.34712/142.81

Technical Infrastructure Management
Insights Vol. II

Ingo Weidlich (Editor)
HafenCity University

Hamburg - 2026

Authors:

M.Sc. Stefan Dollhopf
M.Sc. Moritz Laack
M.Sc. Pakdad Langroudi
Dipl.-Ing. Dennis Lottis
M.Sc. Violeta Madan
M.Eng. Marcel Ramler
M.Sc. Samira Shokouhi
Prof. Dr.-Ing. Ingo Weidlich
M.Sc. Aaron Wieland

Peer Review Committee:

Dipl.-Ing. Stefan Hay
Dr.-Ing. Dinah E. Hollermann
Dipl.-Ing. (FH) Marcus Illguth M.Eng.
Dr.-Ing. Andrej Jentsch
Dr. Irina Lokteva
Prof. Dr. Jürgen Quarg-Vonscheidt
Dipl.-Ing. Gerd Schaldach
M.Eng. Florian Spirkl
Dr.-Ing. Bernd Wagner

Composition and layout:

Maryam Hosseinzadeh
Samira Shokouhi

Content

Introduction

Having successfully introduced the work in the field of Technical Infrastructure Management in 2022 with our first issue, “Insights - Einblicke”, we now aim, four years later with “Insights Vol. II”, to once again offer interested readers the opportunity to learn more about our activities. This document therefore also serves to communicate current research efforts transparently and to facilitate the transfer of knowledge. All research staff members in the team have contributed an article, and external PhD students have also supported the publication with a contribution. The academic quality has been reviewed, monitored and enhanced by our peer review committee. Thank you very much for your support. As this collection presents only the latest scientific findings, this work also contributes to expanding our current understanding.

I therefore hope I have sparked your interest and that you enjoy reading it.

Third-party-funded research

A lot has happened in the four years since the last edition, and it is certainly not possible to cover every detail, so we will focus primarily on the key highlights. Firstly, three major nationally funded collaborative projects were successfully completed during this period, for which the final reports are freely available. The project “Instandhaltung-FW -Entwicklung von neuen und verbesserten Instandhaltungsstrategien für kleine und große Wärmeverteilnetze durch Kombination statistischer Alterungsmodelle mit materialbasierten Nutzungsdauermodellen” (BMWi project code: 03ET1625B) was carried out and completed by M.Sc. Pakdad Pourbozorgi Langroudi. This has led to the development of innovative computer models that have laid the foundations for a new approach to asset management.

In the project “Zustandsbewertung von erdverlegter systemrelevanter Infrastruktur zur proaktiven Charakterisierung von Schäden und Gewinnung von technisch realen Entscheidungshilfen”, led and completed by Dr. Gersena Banushi (BMBF FKZ: 03G0886C), earthquake loads were investigated in a full-scale test facility unique in Germany and numerically modelled at the HCU. Footage of the experiments can be found on the project website (https://edac.biz/projekte/zuversicht). Due to a lack of follow-up funding, Dr. Banushi left HafenCity University when the project came to an end. We wish her all the best for the future.

In addition, the project led by Dipl.-Ing. Sven Büschken, entitled “Fernwärmeleitungsbau 4.0 mit zeitweise fließfähigen selbstverdichtenden Verfüllbaustoffen für niedrige und hohe Betriebstemperaturen” (BMWi FKZ: 03EN3022D), has been completed. Besides a wide range of findings from the research activities, the project established a scientific discourse on the use of temporarily flowable self-compacting backfill materials (TFSB) at HafenCity University. This took the form of various knowledge-transfer events with industry partners, such as “Tech Talk I, Hamburg” (2023) and “Tech Talk II, Göttingen” (2024), as well as the seminar “Innovativer und nachhaltiger Leitungsbau mit ZFSV / Flüssigboden” (2025) at HCU, focusing on TFSB technology in infrastructure construction. Since this research project at HCU, the knowledge transfer events have achieved a certain degree of continuity. Within the Working Group 13 “Preinsulated district heating pipe systems - Design and installation” of CEN TC 107 “Pre-fabricated district heating pipe systems”, we are currently working within the “Bedding Materials” ad hoc group to motivate that TFSB is also incorporated into European standardisation. The topic of TFSB was new to Sven, but he threw himself into learning about it with great dedication. Nevertheless, after the project, he has returned to the wind energy sector. We wish him every success in his future endeavours!

The “Urban Turn” project (FKZ 03EN3029F), led by M.Sc. Stefan Dollhopf, is at the end of its funding period. An impressive research infrastructure has been established in Kassel, enabling the thermal and mechanical interaction behaviour of district heating pipes in the ground to be investigated in the field on a 1:1 scale. Stefan Dollhopf was responsible for the conceptual design of the measurement technology used for this project and closely accompanied and oversaw its installation in Kassel. We believe that this has laid the foundations for further research projects in this field. The final report is currently being prepared, which we await with curiosity.

The growing focus on sustainability within the district heating sector and the promising results from the “FW-Instandhaltung” project formed the basis for a further research proposal addressing these

issues. With the approval of the "SAM-FW" project (FKZ 03EN3078B) – where SAM stands for Sustainable Asset Management – the proposal was converted into a project, thereby securing continued employment for Pakdad Langroudi for the next years.

As employment periods are strictly tied to the duration of the projects, it is difficult to retain research staff. Depending on when next funding is approved, gaps in employment may arise, which can rarely be filled without difficulty. For excellent researchers this is a pretty inconvenient working condition, which has to be bridged sometimes. Stefan Dollhopf is also contributing his expertise in life-cycle assessment to the project through his work. The "SAM-FW" project is in full swing and has already produced a number of important publications.

A casual meeting with Dr. Bernd Rüger from Munich's municipal utility in 2018, during which we agreed to work together on addressing grid ageing issues in Munich, was followed by efforts to submit a research proposal on this topic. In conjunction with the aim of enabling the automated control of district heating and cooling networks, the "EnEff:Netzregelung" project (FKZ 03EN3076B) was launched in 2023. The project aims to achieve greater sustainability and more efficient use by extending the service life of the pipelines and reducing energy losses, with a particular focus on geothermal energy. The project is being led by M.Sc. Aaron Wieland, who has joined the team for this project and has brought fresh perspectives, particularly in terms of the economic aspects of network ageing. Welcome to the team Aaron!

One notable particularity was the "Facets of REAP" project, funded by the Claussen-Simon Foundation, which was largely due to the initiative and commitment of the student representatives for the "Resource Efficiency in Architecture and Planning" degree programme. One day, the students came into my office wanting to submit this application, which we did together and were successful. This led to the creation of an engaging podcast about the REAP programme.

Most recently, the "ABM4Energy" project (FKZ 03EN3125A) was launched in November 2025. Following several years of preparation, a compelling proposal was drawn up, which was approved in light of the new requirements of the Substitute Building Materials Ordinance (EBV). For the first time, the project is being chaired by the Technical Infrastructure Management. Another distinctive feature is the direct collaboration within HCU with our colleague Joche Schiewe, Professor of Geoinformatics and Geovisualisation. Together with the other project partners, the aim is to establish a digital material flow platform that takes environmental considerations into account. We expect the position for the project to be filled shortly.

Self-financed research at the HafenCity University

Some research activities are self-financed. These include financing and conducting preliminary research, enabling purchases and activities for internal doctorates at HafenCity, as well as the expenses of supervising external doctorates.

Once the importance of research questions relating to material cycles in the field of supply networks had become apparent, the work of Lucia Doyle in particular laid the foundations for gaining new insights in this area. Her PhD thesis, entitled "A Circular Economy Approach to Multifunctional Sandwich Structures: Polymeric Foams for District Heating Pre-Insulated Pipes", completed at HCU in 2022, brought the findings in this field to the public's attention. After successfully completing her PhD, Lucia soon returned to Madrid, where she has continued her work in materials research. We hope to continue joint research activities in the future, even though securing funding for cross-border research is always very difficult. There is often a lack of targeted funding schemes whose grants can be obtained with a reasonable amount of effort and a reasonable chance of success. Lucia also stays in touch with HCU through some teaching, so I very much hope that our joint research ideas can be put into practice one day.

We are delighted that Violeta Madan has returned to HCU following a year's parental leave, bringing with her her professional expertise and cheerful disposition. Whilst Pia Peters handled the stand-in role with great professionalism and provided us with valuable support, particularly in the field of "urban water management", Violeta's return was by no means certain. Balancing family life and research is a constant challenge for all researchers with children, and could benefit from significantly more support. Violeta is now back, and her input is extremely valuable when it comes to energy infrastructure. I would have loved for Pia to stay with us too, but she has chosen a different path.

In order to strengthen research at HCU, the HCU Präsidium succeeded in standardising the teaching load for professorships from 12 LVS to 9 LVS. At the same time, the support provided to professorships by research assistants was increased from a half-

time to a full-time position, so that the shortfall in LVS could be somehow equilibrated. I would like to express my sincere thanks to the Präsidium for these strategically astute measures, as they do indeed leave us with more time to produce publications and research proposals. The expansion of our research staff has enabled us to strengthen our team with the addition of M.Sc. Samira Shokouhi, as Violeta wished to remain on a 50% contract. Samira is an architect. Together with her, we are exploring a new approach: 'Form Follows Exergy'. On closer inspection, it becomes clear that exergy-driven design in architecture makes it possible to numerically demonstrate the ecological benefits of a design. We very much hope that this concept will gain acceptance within the architectural sector, so that the building industry can become more environmentally friendly. In any case, the concept provides the ground for many interdisciplinary research collaborations and has the potential to bring about significant change. Welcome to the team, Samira!

External doctoral collaborations were maintained through regular coordination meetings. As a result, the doctoral research of Marcel Ramler and Dennis Lottis progressed steadily, even though various obstacles had to be overcome. Provided the necessary perseverance is maintained throughout these procedures, I believe we can expect these doctoral examinations to be successfully completed in the near future. Another successfully accepted external research proposal was "Investigation into the ageing of gas pipelines and development of a predictive maintenance concept for a natural gas distribution network" by Moritz Laack in 2024. Thanks to his expertise in the field of gas supply to urban areas, Moritz Laack enriches the "collective intelligence" within the field of technical infrastructure management. By taking on the 'Leitungsbau' course in the summer semester of 2024, Moritz Laack also demonstrated his teaching skills and his willingness to share his knowledge. I would like to take this opportunity to thank him once again for his support.

Speaking of teaching support. For more than two years now, Dr.-Ing. Mark Klameth has been enriching the Master's course "Bauverfahren Technischer Infrastruktur" with his expertise in Liner-statics. This subject is very rare in the academic world and highlights the unique expertise that students acquire at HCU. I am delighted that we have been able to bring Mark on board here.

In parallel with the activities mentioned above, preliminary investigations are also carried out on an ongoing basis to prepare research proposals. One example is bending tests on district heating twin pipes, carried out to optimise the permissible free-lengths for the exposure of twin pipes under operation. A full scientific analysis of the experiments and the determination of the resulting free-lengths are still pending. This is representative of various efforts to lay the groundwork for new research and is intended to serve as an incentive for you to continue following our research activities.

Aknowlegement

We would like to extend our special thanks to Mr. Marcus Illguth, Dipl.-Ing., and his laboratory team. It has become clear that our research questions cannot be answered without experimental research, and that we continue to rely on the HCU's civil engineering laboratory. Bringing together the many tasks involved in experimental work to produce high-quality scientific results is a particular challenge. We greatly appreciate the patience shown towards us, as well as the valuable advice and ideas regarding the conduct of the research in the lab.

We would also like to thank all our internal and external funding bodies.

Thank you.

Prof. Dr.-Ing. Ingo Weidlich, April 2026

Publications 2025-2026

2026

- Weidlich I., Dollhopf S., (2026) "Alternative Bettungsmaterialien im Leitungsbau", Kanal- und Rohleitungsbau - Bau und Sanierung, Ernst u. Sohn Verlag, Mrz. 2026, pp. 26-30, ISSN: 2750-5030
- Dollhopf, Stefan; Weidlich, Ingo, (2026) "Experimental Investigation on the Thermal Conductivity of Alternative Backfill Materials for District Heating Networks". In: Dirk Vanhoudt (Hg.): Proceedings of the 19th International Symposium on District Heating and Cooling), S. 109–118., 2026, link.springer.com/chapter/10.1007/978-3-032-09844-3_11
- Langroudi, P., Weidlich, I. (2026). "Foam Density Distribution Analysis in Pre-insulated Pipes Using Non-destructive X-Ray Microscopy." In: Vanhoudt, D. (eds) Proceedings of the 19th International Symposium on District Heating and Cooling. DHC 2025. Lecture Notes in Networks and Systems, vol 1700. Springer, Cham. doi.org/10.1007/978-3-032-09844-3_16
- Wagner, B., Hay, S., Neidhart, T., Spirkl, F., Ried, M., Zrenner, L., Weidlich, I., Gabriel, E. & Banning, T., (2026) "TFSB as Bedding Material in District Heating Pipe Construction–Scientifically Proven Long-Term Experience", Proceedings of the 19th International Symposium on District Heating and Cooling - The International Research Conference on Heating and Cooling Networks - Under the Supervision of IEA DHC. Vanhoudt, D. (Hrsg.). Springer Science and Business Media Deutschland GmbH, S. 99-108 10 S. (Lecture Notes in Networks and Systems; Band 1700 LNNS).

2025

- Langroudi P., Weidlich I. (2025) Developing an Algorithmic Framework for Sustainable Asset Management of District Heating Networks: A Scenario-Based Approach, Environmental and Climate Technologies, 2025, vol. 29, no. 1, pp. 840–850, doi.org/10.2478/rtuect-2025-0056
- Dollhopf, Stefan; Weidlich, Ingo (2025): Potenzialanalyse für den Einsatz von Recyclingbaustoffen als nachhaltige Lösung im Fernwärmeleitungsbau. In: Ingo Weidlich, Petrit Vuthi und Lange Constantin (Hg.): Tagungsband (2. Version) - 2. Konferenz der Norddeutschen Wärmeforschung. HafenCity University Hamburg, S. 16–23.
- Cadenbach, Anna; Lottis, Dennis; Wecker, Mathias; Thalemann, Fabian; Hay, Stefan; Heiler, Daniel et al. (2025): Technologien zur experimentellen Untersuchung der Wandlung der urbanen leitungsgebundenen Wärmeversorgung. In: Ingo Weidlich, Petrit Vuthi und Lange Constantin (Hg.): Tagungsband (2. Version) - 2. Konferenz der Norddeutschen Wärmeforschung. HafenCity University Hamburg, S. 9–15.
- EnEff:Wärme - FW-ZFSV_4-0 - Fernwärmeleitungsbau 4.0 mit zeitweise fließfähigen selbstverdichtenden Verfüllbaustoffen ür niedrige und hohe Betriebstemperaturen : Abschlussbericht zum Verbundforschungsvorhaben / Herausgeber: AGFW, Der Energieeffizienzverband für Wärme, Kälte und KWK e. V. ; Autoren: Timo Che Banning, Sven Büschken, Eugen Gabriel, Stefan Hay, Thomas Neidhart, Michael Ried, Florian Spirkl, Bernd Wagner, Ingo Weidlich, Louis Zrenner, (2025), DOI: 10.2314/KXP:1926093372, edocs.tib.eu/files/e01fb25/1926093372.pdf
- Dollhopf, S., Wieland, A. & Weidlich, I. (2025). Thermal Behaviour of Piggyback-Laid District Heating and District Cooling Pipes. Environmental and Climate Technologies, 29(1), 2025. 500-511. doi.org/10.2478/rtuect-2025-0034
- Weidlich I., (2025), Essay Technischer Infrastruktur - Kontaktmechanik im Leitungsbau, link: doi.org/10.34712/142.69, Verlag: HafenCity Universität Hamburg
- Weidlich I., Vuthi P., Lange C., (2025) Tagungsband - 2. Konferenz der Norddeutschen Wärmeforschung: Gemeinsam die Wärmewende voranbringen. link: doi.org/10.34712/142.68, HafenCity Universität Hamburg

- Shokouhi, S. & Weidlich, I. (2025). An LCA Study of Various Office Building Shapes Focusing on Operational Energy—A Case of Hamburg. Sustainability, 17(4), 1659. doi.org/10.3390/su17041659

Of course, publications were also released in 2023 and 2024, but listing them all would go beyond the aim of this document. If you are interested, you can find the older publications online.

Master and Bachelor Theses 2022-2026

Master Theses

2026

- Benchmarking LCA Transparency in District Heating Pipelines: A Comparative Analysis of EPDs and Scientific Studies

2025

- Towards a Framework for Exergy-Based Life Cycle Assessment of Residential Buildings
- Risikoabschätzung und Phasenplanung für die Maßnahmen zum Aufbau der Wasserstoffinfrastruktur in Hamburg
- Untersuchung der Materialeigenschaften von ZFSV bei Temperaturen unter 5° Celsius
- Bewertung des komplementären hybriden Redispatch im Kontext kommunaler Wärmeplanung: Groß Molzahn als Modellregion
- Life Cycle Assessment of Onshore Wind Turbine: Exploring Circular Economy Strategies for Repowering in Germany
- Implementation of Construction Demolition Waste for Slope Stabilization
- Analysis of the critical buckling force of district heating pipes
- Impact of different development scenarios of a real estate portfolio on a remaining Co2 budget, considering embodied emissions as a strategic indicator. - A Case Study

2024

- Entwicklung eines KI-basierten Bildverarbeitungstools zur automatisierten Erkennung und Vermessung von Zellen in PUR-Hartschaumproben für die Qualitätsprüfung von Fernwärmeisoliermaterialien
- Untersuchung der thermischen Effizienz von Fernwärmerohrsystemen
- Transition to Smart Micromobility Synergising Micromobility Infrastructures and Intelligent Technologies for sustainable mobility scenario in Barmbek Nord, Hamburg
- Vergleich des Regelwerks ATV-DVWK-A 127 (2000) mit den Arbeitsblättern DWA-A 127-1 und -2 (2022 ff.)
- Exploring Bioleaching in Sustainable Construction Practices
- Democratic Energy Transition in Tunisia
- Untersuchung von Solaranlagen als Verschattungselement für Haltestellen
- Implementing a regional circular economy approach in the district of Altona Hamburg

2023

- Energy Management of Mines in Ghana: Optimising Sustainability and Efficiency
- Unlocking the Potential of Smart Contact Application in Renewable Energy Industry
- Investigation of the strategic challenges for the transition of the DH and GAS infrastructure in Hamburg and its mutual dependencies
- Monitoring the heat transition of Germany
- Standard key performance indicator framework for the maintenance management of wind turbines
- Green hydrogen production and export through sector coupling in Namibia - A case study for HyPAT project using open-source technologies.
- An analysis of maintenance cost in District Heating. A study of pre-insulated district heating distribution lines in Northern Europe
- Heat Gain Analysis of Distribution Pipes to Optimize District Cooling Systems in Hot Countries
- Betrachtung von Fernwärme-Subnetzstrukturen in Gebieten mit geringer Wärmebedarfsdichte
- Laserbasierte Erfassung der wassergehaltsabhängigen Volumenänderung kohäsiver Böden zur Ableitung empirischer Prognoseverfahren schrumpfungsbedingter Setzungen

2022

- Application of LCA for material selection and energy requirements for new office buildungs: A case study in Oberndorf
- A Suitable District Cooling System for A New Development Area in Thailand
- Wärmeverluste von Fernwärmeleitungen in zeitweise fließfähigen selbstverdichtenden Verfüllbaustoffen
- ZFSV im Statikprogramm "Rohr 2" für Fernwärmesysteme
- Investigation of the viability of using BIM to reduce CO2 emissions when intervening in an existing building
- Investigating the effects of adding a new skin to the facade as a energy efficient refurbishment scenario in residential building.

Bachelor Theses

2026

- Ökobilanzierung der Glasfaserverlegung - Analyse eines Streckenabschnitts in offener Bauweise

2025

- Optimierung der solaren Energiegewinne eines Gebäudeentwurfs durch Lage- und Ausrichtungsfestlegung im vorgegebenen Gelände
- Untersuchung von Großrohreffekten im Fernwärmeleitungsbau
- Setzungsberechnung von Fernwärmeleitungen - Ein Vergleich verschiedener Berechnungsansätze
- Korrekturfaktor für Volllastzyklen in der Ermüdungsanalyse von Kunstoffmantelrohren
- Untersuchung der Scherfestigkeit der Dämmung von Fernwärmerohren bei definierter Dehnung
- Bemessungswerte und -Methode für Abwasseranlagen, Erfordernisse für die Behandlung von Mikroplastik
- Untersuchung der Auswirkung des anstehenden Bodens auf die lateralen Verschiebungen von Fernwärmeleitungen
- Wärmeableitung in ZFSV beim Betrieb von Starkstromleitungen
- Resilienz der Siedlungswasserwirtschaft in Singapore
- Untersuchung der Grenzen und Möglichkeiten für die Reduzierung von Grabenbreiten beim Einsatz von Flüssigboden
- Internationaler Vergleich normativer Vorgaben im Fernwärmeleitungsbau
- Bodenähnlichkeit von zeitweise fließfähigen, selbsverdichtenden Verfüllbaustoffen
- Gegenüberstellung von konventionellen und recycelbaren Dehnpolstern im Fernwärmeleitungsbau
- Untersuchung der Verbundscherfestigkeit von Kunststoffmantelrohren nach erfolgter Knickbelastung

2024

- Potentialanalyse von Floating Photovoltaik im Kontext der Energiewende
- Energetische Nachhaltigkeit von Wärmepumpen im Vergleich zu traditionellen Heizsystemen
- Entwässerungsmethoden in der Antike und heute
- Analyse der Auswirkungen des Gebäudeenergiegesetzes (GEG) auf die Planung und Umsetzung von Wärmeschutzmaßnahmen im Vergleich zur Energieeinsparverordnung (EnEV)
- Eine vergleichende Analyse von Standard – und modernen Entwässerungsmethoden auf einer Konzept-Tankstelle
- Potenziale recycelbarer Verfüllbaustoffe im Leitungsbau für Abwasserleitungen
- Statistische Analyse der Ausfalldaten von Fernwärmenetzen
- Legionellenentwicklung in wasserführenden Bauteilen von Bestandsgebäuden - Beobachtung der Kaltwassertemperaturen in einem 4. -geschossigen Mehrfamilienhaus aus dem Jahre 1905
- Erddruck auf Abwasserrohre unter Verwendung recycelter Bettungsmaterialien
- Vergleich von LAGA und Ersatzbaustoffverordnung beim Erdaushub im urbanen Raum

- Auswirkungen der Geothermie als Energiequelle auf den Betrieb von Fernwärmenetzen
- Europas Klimaziele und die Bedeutung der Fernkälte für Deutschland
- Untersuchung der lateralen Bettungswiderstände im Fernwärmeleitungsbau in Abhängigkeit der Dämmserie
- Optimierung von baubetrieblichen Prozessen im Fernwärmeleitungsbau unter Betrachtung verschiedener Rohrleitungssysteme
- Anforderungen an Leitungsgräben hinsichtlich Geometrie und Korngröße vor dem Hintergrund der Ersatzbaustoffverordnung

2023

- Wärmedämmung von Außenwänden in Europa
- Untersuchung zu Eigenbauoptionen von Solarkollektoren mit Blick auf die Energieeffizienz und die Wirtschaftlichkeit
- Automatisierung von Nachweisen im Fernwärmeleitungsbau am Beispiel eines 90°-Bogens
- Grabenlose Sanierung von Trinkwasserleitungen – Eine Untersuchung des Press-/ Ziehverfahrens hinsichtlich Umsetzbarkeit, Ökologie und Wirtschaftlichkeit
- Untersuchung der Energieeffizienz elektrischer Baumaschinen im Rohrleitungsbau
- Potenziale der Abwärmenutzung von Leistungstransformatoren
- Energetische Optimierungspotentiale bei Einfamilienhäusern Fallstudie
- Energetische Modernisierung von Wohngebäuden, trotz Einschränkungen durch den Denkmalschutz, am Beispiel des Warmwasserblocks auf der Veddel
- Potentialanalyse für Windenergie unter aktuellen Randbedingungen
- Der Beitrag der Kaltetechnik zur Steigerung der Energieeffizienz von Gebauden
- Skalierungseffekte bei der Bemessung von Pflanzenkläranlagen in Abhängigkeit der Anzahl und Typologie von Gebäuden in einer kleinen Gemeinde
- Vergleich von Energieeffizienz, Wirtschaftlichkeit und Umweltauswirkungen bei konventionellen und ökologischen Dämmstoffen

2022

- Erddruck auf flexible Rohre eingebettet in zeitweise fließfähiges selbstverdichtendes Verfüllmaterial
- Untersuchung der Einwirkungen von Nutzlasten auf Kunststoffmantelrohrleitungen im Erdreich für unterschiedliche Dimensionen
- Wurzelschutz von Rohrleitungen Eine Analyse von Ursachen, möglichen Schäden und Reparatur- sowie Schutzmaßnahmen
- Untersuchung von Potentialen der Gebäudeautomation für energieeffiziente Gebäude
- Neuartige Sanitärsysteme und Sanitärkonzepte für autarke Ein- und Zweifamilienhäuser
- Energeieverbrauch von Reihenhäusern - Wie unterscheidet sich der Energieverbrauch eines Reihenhauses von dem eines freistehenden Hauses

Due to data protection, the authors of these papers are not listed. However, students generally have the option of publishing their theses via the HCU publication server. A few of these theses can be found there.

From Concept to Implementation: Hands on the pipe test bench at District Lab in Kassel

Stefan Dollhopf
stefan.dollhopf@hcu-hamburg.de HafenCity University, Hamburg

Abstract

The transformation of district heating networks (DHN) towards lower operating temperatures and more dynamic operating conditions provides an occasion to examine the mechanical and thermal behaviour of buried pre-insulated bonded pipes under these new conditions in detail. This paper presents the development and implementation of a full-scale pipe test bench (PTB) at the District Lab research facility in Kassel, Germany, established within the UrbanTurn research project. The PTB consists of a buried pipe loop with high- and low-temperature circuits and two test fields with different bedding materials, enabling an experimental investigation of pipe–soil interaction. A comprehensive measurement concept was implemented, comprising 54 local sensors and a distributed fibre-optic temperature monitoring system along the test section. The paper documents the iterative design process, the alignment of investigation objectives with the technical infrastructure, and the practical implementation under real construction conditions. The results highlight key challenges in integrating measurement technology into civil engineering works and underline the importance of detailed as-built documentation for experimental infrastructure.

Introduction

The transformation of German district heating (DH) networks in the course of decarbonisation is a challenging project, on the one hand, a major expansion of the networks (DHN) is forecasted (Agora Think Tanks, 2024), and on the other hand, these networks must be adapted to new, mostly decentralised heat generation and new operating parameters (Hay et al., 2022). To address this situation, it is essential accompany the transformation by broad-based research. The network-transformation often is being planned using digital simulations (Schmidt et al., 2023) and calculations. However, to improve simulations they should be validated, at least in part, by experimental investigations to ensure their transferability to reality. In Germany, there are a few DH test sections, e.g. the Chemnitz test-section (Villalobos et al., 2019 & Hay et al., 2022) the AGFW test-section in Frankfurt (Grimm et al., 2017) and other measuring points (e.g. in Dollhopf et al., 2025) in DHN to monitor the infrastructure and provide opportunities for scientific investigation.

To meet the need, a laboratory for experimental investigation of DH infrastructure, was set up at the Fraunhofer Institute for Energy Economics and Energy System Technology (IEE) in Kassel (see Figure 1). The so-called District Lab (Kallert et al., 2021) consists of the main building with heat generation, a consumer structure and a flexible-test-network. In addition, a pipe test bench (PTB) was also set up for the detailed investigation of buried pipes. Test-tracks are often connected to DH grids and are therefore limited in their performance. In implementing the District Lab, the capacity, was tailored to the research objectives to ensure the widest possible application for DH networks with operational temperatures ranging from second generation DH (2GDH) to fourth generation DH (4GDH) according to (Lund et al., 2014). This is necessary to account existing framework conditions, in Germany where these DH generations are represented (AGFW, 2024).

However, the broad spectrum of investigation-opportunities required a targeted, scientific development for the detailed design. Within the framework of the UrbanTurn joint research project, this was ensured by a broad-based project consortium, where the IEE took the lead, coordinating the overall project, while GEF Ingenieur AG developed the technical design. HafenCity University Hamburg (HCU) was responsible for planning and implementing the investigations on the pipe test bench (PTB) while the DH association AGFW

DOI: 10.34712/142.81-1

supported the implementation of the PTB with their expertise. BRUGG Pipes provided the pre-insulated bonded pipes and was responsible for the pipeline construction works and DANFOSS provided equipment, such as heat exchangers and further technical facilities. The overall aim was to develop specific investigation objectives and align them to a corresponding infrastructure and measurement equipment.

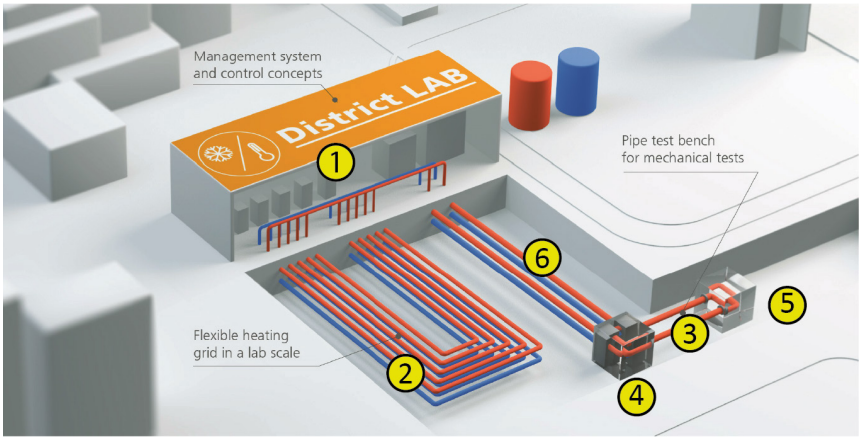

Figure 1: Concept-Drawing of District Lab (Fraunhofer IEE) with own edit (numbers)

In the end of 2025, the pipeline construction work and the installation of the measurement technology on the pipe test track were successfully completed. Four years passed from the start of the UrbanTurn project to the implementation of the PTB. This provides an opportunity to reflect in detail on the process. The focus thereby is set on the consistent further development of the investigation-objectives and the test infrastructure within the detailed planning and the implementation at the District Lab construction site. Since the construction of a research test track is neither a trivial process nor a frequent occurrence, this work shares experience and should serve as a reference for future projects.

Methodology

This paper provides comprehensive documentation of the implementation of the PTB and analyses the process from the basic concept until the completion of construction work on the building site.

The implementation will be analysed using a three-phase approach based on the chronological sequence. This begins with the conceptual-design of the pipe test section at the start of the UrbanTurn research project in 2021, with a broad spectrum of investigation possibilities at the concept planning stage. The detailed-design of the pipe test track, which includes the specification of the investigation objectives, is then discussed. The designation of detailed investigation objective based on the current challenges of DHN expansion and approaches also innovative construction methods for DHN design. The detailed planning also included the development of the accompanying measurement-concept, the development of a test schedule and the technical final design for the test infrastructure (working drawings for structures etc.). The third phase represents the implementation of the buried pipe test track in the end of 2025, during which the structures and pipelines were constructed, and the measurement equipment was installed.

In the concluding discussion, a qualitative review will be drawn, optimisation possibilities will be identified, and correlations and critical points in the implementation will be presented. Furthermore, deviations from the planning will be presented and important inter-dependencies highlighted.

Conceptual-Design

The Distric Lab test centre (see Figure 1). consists of the District Lab main-building (1) where the central

technical and control facilities are located, the flexible-test-network (FTN) (2) on a neighbourhood scale and the pipe test track (PTB) (3) for pipe-specific tests. For information regarding the FTN find the article “Fibre optic and embedded sensing concept for long term monitoring of district heating pipes at the District-LAB Kassel“ by Dennis Lottis within the “Insights Vol. II” publication. The PTB is generally used to carry out mechanical tests on buried pipes for district heating networks. Within the conceptual-design the investigation opportunities at the PTB included testing extreme operational modes, component tests, installation techniques, the investigation of bedding materials and quality assurance on the construction site (Kallert et al., 2021). The test infrastructure of the PTB consists of two structures (4 and 5) and the test section between them (3), into which the pipes are fed for testing purposes. The heating and cooling water from the central generation units is fed to the control structure via pipes (6) coming from the main building. The PTB is operated via the technical facilities in the structure. The supply line from the main-building and PTB are separated water circuits. From the control structure (4), the pipes of the PTB are routed towards an additional shaft (5). There, they are deflected in a U-bend and returned towards the control structure. The length of the pipe test section has been defined as 42 m, which corresponds the production length of pre-insulated bonded pipes (usually lengths of 3/6/12 m). Due to the route layout and the deflection of the pipes in the shaft, it is initially only possible to carry out tests on a straight section of pipe.

During the conceptional-design, various options of pipe-types and -systems for the PTB were considered but no further details such as pipe dimensions or pipe types were specified. The focus on the pipe-soil interaction was outlined in the UrbanTurn investigation-objective and the further development was done within the detailed-design to align the infrastructure to the specified research objectives. The control building was planned with a basement from which the pipes would branch off towards the test section. These results in an overburden height of the PTB of approximately 80 cm. The capacity of the main building defined the upper limits for the pipe test section. Accordingly, temperatures of up to 140 °C and pressures of up to 12 bar can be applied to the PTB. The supply line from the District Lab main building to the control structure is defined as a pre-insulated bonded pipe of diameter DN 125.

Detailed-Design

Based on theoretical investigations at the start of the UrbanTurn project, the experimental investigations on the pipe test section were elaborated. A key element of the DHN transformation is the reduction of flow temperatures in the heating networks. Also, an increase of thermohydraulic dynamics is expected. The design criteria for static calculations must therefore be reviewed and aligned and these requirements are to be investigated on the PTB. The framework is set within three technology-sets, the commissioning of the PTB, investigation of mechanical stresses and thermal behaviour, both with focus on the pipe-soil interaction.

Various pipe systems were discussed as subjects for investigation. To best represent the transformation of existing networks, achieve the broadest possible application of the investigation results and to validate investigation results of other test-tracks, pre-insulated bonded pipes with steel medium pipes were selected as the subject of investigation. These are the most commonly used pipe systems in Germany (Weidlich, 2015) and will also be the major construction technology used in the upcoming network expansion. This also allows to test extreme operating modes and the performance limits of the laboratory. Other pipe systems, such as pipes with polymer medium pipes, wouldn’t be suitable for this purpose.

The pipes are arranged as a single pipe system with two pipes per trench and are operated at different temperature levels as low-temperature (LT) and high-temperature (HT) lines (see Figure 2). In terms of dimensions, bonded pipes with DN 100 and an outer diameter of 200 mm were specified. By laying the pipes in a loop, two test fields with otherwise identical boundary conditions are created. Different installation conditions and bedding materials are used in the test fields. In test field 1, a conventional construction method is implemented, which represents the usual installation of district heating pipes in an urban environment. The pipe trench is filled with natural sand for pipe bedding and a sand-gravel-mix for backfilling. Due to the transformation of DHN, the use of alternative bedding materials represents a promising approach (Dollhopf & Weidlich, 2025; Weidlich & Grajcar, 2017) but further research into their application is needed. Therefore in the second test field, crushed concrete is used as bedding material (0/10) and

backfill-material (0/32) to promote research into circular economy-compliant construction methods for the upcoming network expansion.

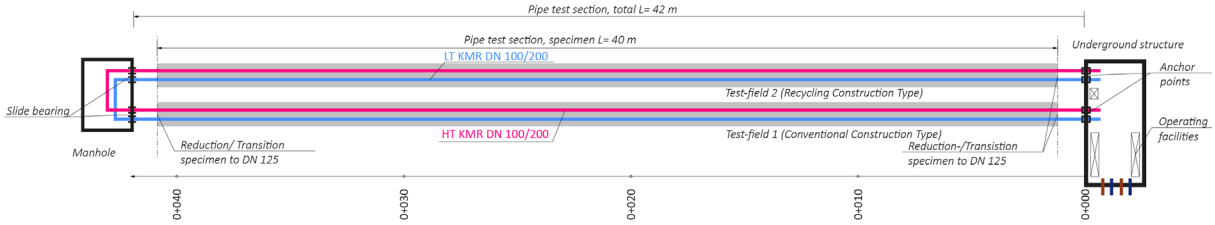

Figure 2: Overview of PTB (Detailed-Design)

Furthermore, due to advantages in execution and other planning requirements, it was decided that the control structure should be constructed as an underground shaft structure. Due to the change in construction details of the shafts, the elevation of the PTB also was adjusted. This results in an overburden-height of 1,05 m. Due to the trench depths, the ground conditions and the short distance between the test fields (see Figure 3), the pipe trenches were planned with an excavation pit shoring.

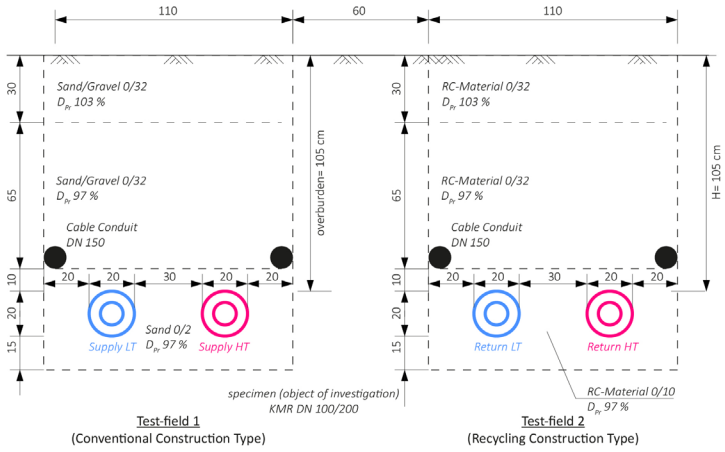

Figure 3: Cross-section of PTB with DN 100 bonded pipes(Detailed-Design)

In addition to working out the structural details, the requirements for the operating parameters were also further specified and refined to design load cases. The facilities in the main building of the DistrictLab and in the control building are designed so that operating temperatures of 20 to 130°C and temperature gradient (TG) of up to 100 K/h can be achieved in the HT pipe loop, and operating temperatures of 10 to 80°C and TG of up to 10 K/h can be achieved in the LT pipe loop. A test schedule was also developed during this. The plan is to initially carry out the commissioning in two scenarios. The target temperature is a flow temperature of 60°C in the HT pipe loop. During the first heating, this is carried out at a TG of 10 K/h in accordance with the DIN EN 13941 standard. After cooling down, a second process with a TG of 60 K/h will be carried out. Subsequently, the temperatures at the pipe test section will be gradually increased in various test scenarios. This phase is designated as “transformed operating modes I”. Temperatures of 75/85/90/110/130°C will be approached for the first time. High pipe friction is expected when the temperatures are first reached. The aim is to generate findings for district heating networks with lower design temperatures (< 130°C). After 130°C has been reached cyclically over a longer period of time and at different rates of change, the “transformed operating modes II” phase follows. Here, the temperatures are gradually reduced again. The aim is to simulate the effects of reducing the flow temperature in existing networks.

A comprehensive detailed measurement concept was further developed within the detailed design. In particular, the measurement resolution within the pipe trench area was increased. In order to measure mechanical and thermal behaviour, approximately 50 sensors are installed in the pipe test section. These

are located in measurement fields (see Figure 4 and Figure 5) in areas relevant to the investigation, e.g. strain measurement points at the point furthest away from the slide bearing. Rod extensometers, and earth pressure sensors are installed to record the mechanical behaviour. Resistance thermometers, soil moisture sensors, heat flux sensors and a fibre-optic linear temperature measuring device are installed to investigate the thermal interactions. The sensor cables are routed to the nearest shaft via cable conduits where the sensor signals are recorded.

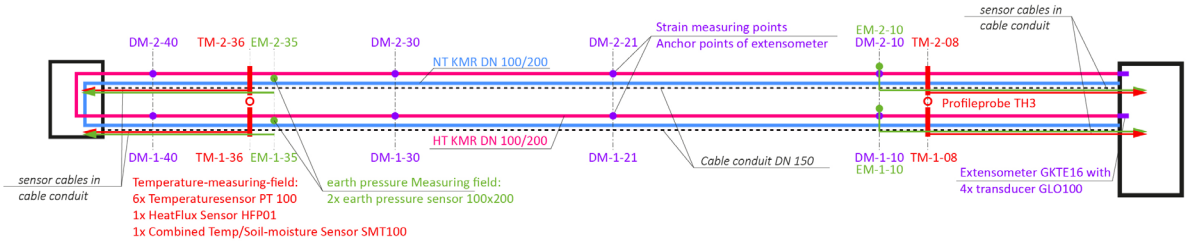

Figure 4: Measurement Concept - Sensor Locations

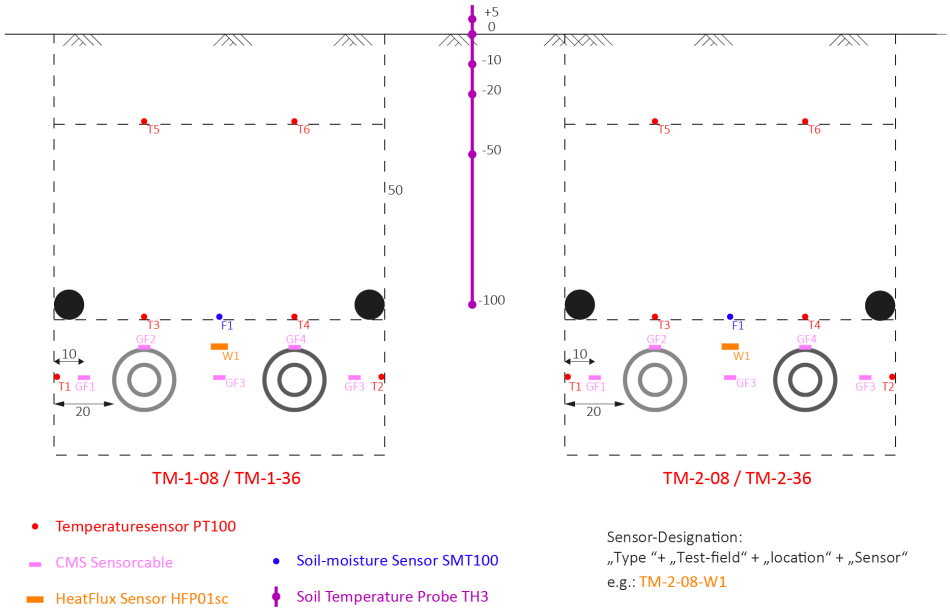

Figure 5: Measurement Concept - Cross section Temperature-measuring-field

As the measurement equipment contents various sensors with different measurement signals, external conversion of the measurement signals is often necessary to simplify connection to the programmable logic controller. A concept for signal conversion for data acquisition was therefore also developed.

Implementation of the PTB

Due to the complexity of the entire laboratory, it was initially not possible to find a general contractor for the implementation. Only after the construction work had been divided among several building-trades, construction companies could be found. This resulted in a delay in the start of construction work and a significantly shorter time span for execution. The excavation of the pipe trenches and thus the start of construction on the pipe test section began on September and the work was completed on December with the final backfilling of the trenches.

The construction with the use of continuous trench shoring proved to be impractical. Due to the obstacles created by the shoring, such as the cross struts between the shoring panels and a reduced working space, it would not have been possible to install the sensors and their cabling in the time available. Pulling the shoring boxes within the backfilling process would also have posed a major risk to the position and

integrity of the sensor technology. Therefore, an open construction method with a sloped pipe trench was chosen (see Figure 6). As a result, the existing soil between the test fields was not interlocked with natural soil as originally planned. Nevertheless, the excavated soil was reinstalled during the pipe trench backfilling between the test fields, creating a clear separation between the test fields (see Figure 7). The modified design is not expected to have any relevant impact on the research results. During the construction work, soil samples were taken from the existing soil and the delivered building materials, which are to be examined at the HCU laboratory as part of the project.

The distance between the shaft structures is 41,85 m, which represents the length of the pipe test section. The pipe test section was constructed as a loop with two single pipes, each with a diameter of DN 100/200 with three joint connections within the DN 100 route and two joint connections at the reduction from DN 125 to DN 100. Before being inserted into the shafts, the diameter was adjusted to DN 125, as all pipes within the shafts are DN 125 pipes. This ensures a simplified change of testing objects within the PTB for future investigations. At the control shaft the pipes are fixated within the shafts wall, at the additional shaft, slide bearings ensure the axial elongation of the pipes into the shaft.

Figure 6: Trenching with sloped Walls

Figure 7: Backfill with different Materials for test-fields

The pipe bedding and backfilling were carried out as planned with different materials for the test fields. Within Test-field 1 a natural Sand with grain-size 0/2 was used. In Test-field 2 recycled material of Class RC-1 according to the Substitute Building Materials Ordinance with a 40 % content of crushed concrete, 35 % crushed rock and 25 % crushed asphalt material was used. Because of changes within the implementation of the shafts also the overburden height had to be aligned to the situation. The overburden height of the route corresponds to 95 cm, with the height adjusted to 1,5 m close to the control shaft and approx. 85 cm above the additional shaft. As deviations occurred within the implementation subsequently the terrain heights were measured.

The tight schedule for the construction work meant that the installation of the measurement technology had to take place partly in parallel with the civil engineering work. Due to the flexible construction process, the implementation had to be planned and adapted during construction, which required close cooperation between the project participants. The installation of the measurement technology was successfully implemented with only minor deviations from the original plan, and the measurement concept for the pipe test section was thus fully realised by the project partners Fh IEE and HCU, as well as external support. To investigate the mechanical stress, extensometer (see Figure 8 and 10) anchors and earth pressure sensors (Figure 9) were applied to the pipeline at the designated locations. This was done using plastic-saddles, which were first positioned, then calibrated and finally attached to the pipe jacket using a plastic welding process. The implementation proved to be very practical as the position of the sensors is well secured.

Figure 8: Rod-Extensometer applied to Shaft-Wall

Figure 9: Earth-pressure sensor on plastic saddle

To investigate the thermal interaction between the pipeline and the surrounding bedding material, fibre optic measuring equipment from OSSCAD was laid along loops within the pipeline trench. In addition, temperature sensors (see Figure 11), humidity sensors and heat flow plates were installed at various measuring points. The sensors were laid layer by layer after the pipe zone had been constructed. To do this, the positions of the sensors were subsequently exposed by hand and, after securing the sensor layers and pulling the sensor cables into empty conduits, backfilled by hand. This procedure was developed during the execution phase.

Figure 10: Extensometer - Anchor and fibre-optic cable(blue)

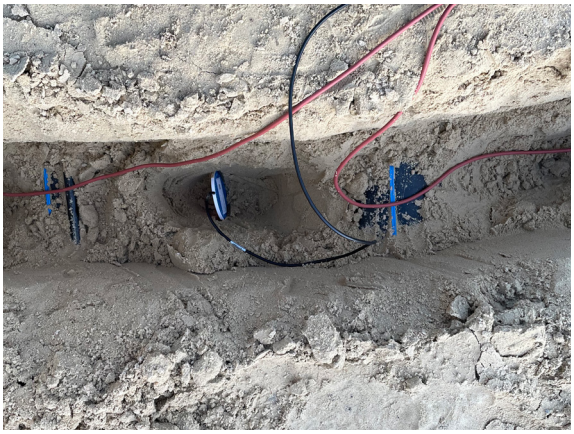

Figure 11: Temperature and HeatFlux sensors (Dennis Lottis, IEE)

A total of 54 measuring points were implemented and the linear measuring device from OSSCAD, which was laid in a total of 10 loops, additionally provides the temperature at approx. 400 positions within the pipe test section. This corresponds to a very high density of measuring points. Due to the above-mentioned adjustments in the design of the pipe test section and the adjustment of the sensor positions, etc., it is necessary to digitally process the documentation in a high level of detail (see Figure 12). This is mandatory to enable scientific evaluation of the measurement data.

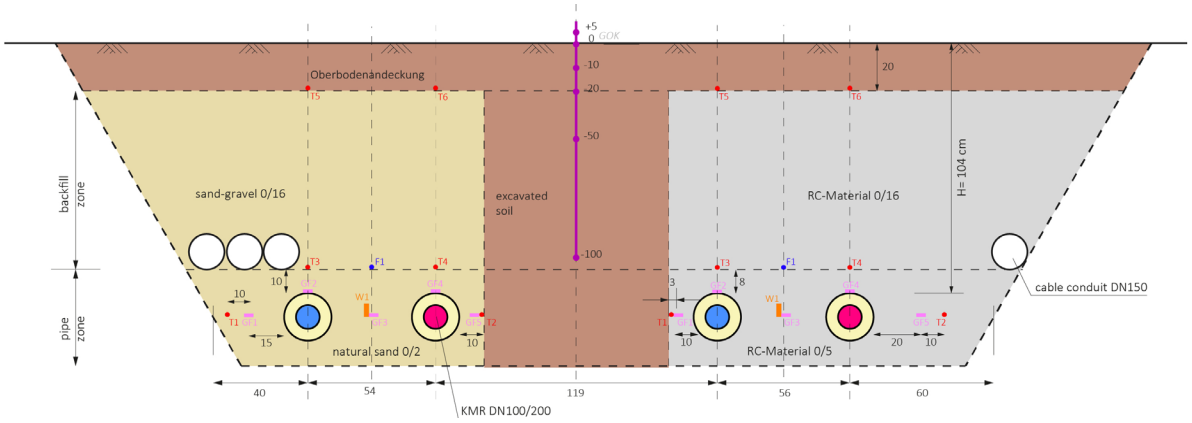

Figure 12: As-Built Documentation of Temperature measuring field 0+008

Discussion and conclusion

In the course of the project, the infrastructure was subsequently adapted to the further developed project goals. This proved to be necessary in light of the dynamic transformation of heating networks and elaborated construction technologies in DHN constructions. Specific investigation scenarios (technology sets) and installation conditions for both network expansion and the transformation of existing networks were created. The implementation of the PTB served as a reality check for the full-scale laboratory. The limited construction time required a particularly flexible approach. As is common on real construction sites, manufacturing-related deviations occurred and improved the transferability of scientific findings into practice.

At the PTB, the construction works involves earthworks which, despite GPS-supported surveying and controlled construction equipment, lead to deviations from the planning due to the construction equipment used and the heterogeneity of soils. Higher requirements regarding the precision must be explicitly specified in the items of the service specifications. In road construction, for example, usually tolerances of between -10% and 20% are permissible for the thickness of unbound layers. The excavation of the pipe trench as a continuous trench across both test fields with sloped trench walls deviates significantly from the planned route cross-section with built-in vertical trench shoring. Also, the overburden height also deviates from the plan. However, as explained above, these changes were discussed during the implementation and jointly decided upon in consideration of the static design and the scientific research approach.

In addition to deviations in civil engineering during the excavation and backfilling of trenches, deviations also occur in pipeline construction. This is due to numerous factors, such as surveying tolerances, but also production-specific deviations such as pipe connections or the introduction into shaft structures. Furthermore, the reduction in diameter from DN 125 to DN 100 had to be planned and implemented in situ. The measured length of the pipe test section shows a deviation of approx. -15 cm, which corresponds to a relative deviation of 0,03 %. Deviations here are due to inaccuracies in the surveying of the shaft structures and their construction. Due to an on-site adjustment of the shaft height, the elevation of the pipeline was also changed. The adjustments have no negative impact on the function or investigation possibilities at the PTB. While minor inaccuracies in actual construction work are generally accounted within the static calculation, for a Research-Facility it is important to document the exact “As-Built” inventory to provide a basis for scientific investigations. Therefore, manual measurements of the structural implementation were carried out, particularly at the measurement cross-sections.

Adjustments were also necessary on site regarding the measurement technology. The position of the extensometer anchors had to be adjusted to the lengths of the extensometer rods. Shortening the rods on site would have caused further delays to the work. As a result, the measuring points were moved slightly. The position of the plastic saddles was subsequently measured and documented. Sensors also had to be adjusted to the position of the pipes in the cross-section, but the measuring points were fixed in position in the bedding material and calibrated. Here, too, however, deviations from the plan occurred. In general, installing sensors in the bedding material during the accompanying civil engineering work is a challenging

task and required a flexible and coordinated approach. For example, the empty conduits for cable routing had to be constantly adjusted to the height of the backfill, and the sensors could only be installed retrospectively by digging them in manually after the layers had been backfilled. This also led to minor changes in the sensor position.

For future tenders, it is recommended that installation breaks for measurement technology be explicitly and specifically provided for this task. The high number of sensors used leads to a considerable amount of coordination effort for sensor cabling and data acquisition. These aspects should be considered when selecting the sensor technology and, if necessary, optimised in an iterative process. Under certain circumstances, it may be advisable to engage external services to ensure combability. The routing of empty conduits must also be consistently adapted to the construction process. Radio-based sensor technology may be an alternative in the future, provided that its suitability for installation in the ground is guaranteed.

The position of the sensor technology in the bedding material should be secured manually after backfilling, as compaction work and construction activities otherwise pose an increased risk. Overall, the application of sensor technology directly on the pipeline (e.g. fibre optic measuring cables, earth pressure sensors and extensometers) has proven to be practicable. After calibration, the measuring points can be assumed to be stable. Also, for the implementation of the measurement equipment a high-resolution inventory is required to compare simulation results with measurement data.

In principle, deviations between planning and execution are always to be expected in construction projects, which is why precise documentation of the existing situation, close construction supervision and clear communication on site are particularly important. Overall, the implementation of the pipe test section represents a significant milestone for the realisation of the DistrictLab. It creates a comprehensive and, in this form, unique test infrastructure for in-depth scientific investigations and practical insights into the transformation of heating networks.

Acknowledgement

This work is a result of the research project UrbanTurn (03EN3029F) which is nationally funded under the EnEff: Program by the Federal Ministry for Economic Affairs and Energy of Germany.

References

AGFW (2024). AGFW-Hauptbericht 2024: eng. Main-Report 2024.

Agora Think Tanks (2024). Climate-neutral Germany. From target-setting to implementation.

Dollhopf, S., & Weidlich, I. (2025). Potenzialanalyse für den Einsatz von Recyclingbaustoffen als nachhaltige Lösung im Fernwärmeleitungsbau. In I. Weidlich, P. Vuthi, & L. Constantin (Chairs), Tagungsband (2. Version) - 2. Konferenz der Norddeutschen Wärmeforschung. HafenCity University Hamburg.

Dollhopf, S., Wieland, A., & Weidlich, I. (2025). Thermal Behaviour of Piggyback-Laid District Heating and District Cooling Pipes. Environmental and Climate Technologies, 29(1), 500–511. https://doi.org/10.2478/rtuect-2025-0034

Hay, S., Kallert, A. M., Lottis, D [Dennis], Ziegler, R., Weidlich, I., & Dollhopf, S. (2022). Existing District Heating Networks in Context of German Climate Goals: Potentials for „UrbanTurn", 196–203.

Hay, S., Weidlich, I., Wolf, I., & Villalobos, F. A. (2022). Pipe axial displacements from a monitored pipeline connected to a district heating network. Proceedings of the Institution of Civil Engineers - Energy, 175(3), 150–161. https://doi.org/10.1680/jener.21.00100

Kallert, A., Lottis, D [D.], Shan, M., & Schmidt, D. (2021). New experimental facility for innovative district heating systems—District LAB. Energy Reports, 7, 62–69. https://doi.org/10.1016/j.egyr.2021.09.039

Lund, H., Werner, S., Wiltshire, R., Svendsen, S., Thorsen, J. E., Hvelplund, F., & Mathiesen, B. V. (2014). 4th Generation District Heating (4GDH). Energy, 68, 1–11. https://doi.org/10.1016/j.energy.2014.02.089

Schmidt, D.(ed.) et al. (2023). Guidebook for the Digitalisation of District Heating: Transforming Heat Networks for a Sustainable Future, Final Report of DHC Annex TS4.

Grimm, S, Huther,H., Neidhart, T., & Weidlich, I. (2017). Einsatz fließfähiger Verfüllstoffe zur KMR-Verlegung in Gräben und Haubenkanälen. Bbr : Leitungsbau, Brunnenbau, Geothermie, 68(5), 18–25.

Villalobos, F., Hay, S., & Weidlich, I. (2019). Monitoring in a District Heating Pipeline System. In A. Ferrari & L. Laloui (Eds.), Springer Series in Geomechanics and Geoengineering. Energy Geotechnics (pp. 132–139). Springer International Publishing. https://doi.org/10.1007/978-3-319-99670-7_17

Weidlich, I. (2015). Mantelrohrsysteme in der Wärmeverteilung. In H.-B. Horlacher & U. Helbig (Eds.), Rohrleitungen (pp. 1–16). Springer Berlin Heidelberg. https://doi.org/10.1007/978-3-642-45027-3_13-1

Weidlich, I., & Grajcar, M. (2017). Expected potential of bound and recycled backfill material in low temperature district heating networks. Energy Procedia, 128, 150–156. https://doi.org/10.1016/j.egypro.2017.09.035

Stationäre Methan- und Ethanmessungen in urbanen Gasverteilnetzen: Messkonzept, Standortwahl und Anforderungen an die Sensorik zur Kopplung mit Zustands- und Emissionsmodellen

Moritz Laack
moritz.laack@hcu-hamburg.de HafenCity University, Hamburg

Kurzfassung

Regulatorische Initiativen wie die EU-Methanverordnung und die DVGW-Merkblätter G 404, G 424 und G 425 fordern von Gasnetzbetreibern eine systematische Erfassung und Reduktion von Methanemissionen. Gleichzeitig besteht weiterhin eine Forschungslücke bei der Verknüpfung diffuser Methanemissionen aus erdverlegten Verteilnetzen mit dem Netzzustand und prädiktiven Instandhaltungsstrategien. Der Beitrag stellt ein Messkonzept für stationäre Methan- und Ethanmessungen in urbanen Gasverteilnetzen vor. Es umfasst (i) die Bewertung verschiedener Standortvarianten – eigenständige Stationen, Nutzung von Gasdruckregelanlagen (GDRA) sowie Integration in bestehende Luftqualitätsmessstationen – und identifiziert die Integration in Luftqualitätsmessstationen als pragmatische Vorzugsvariante. (ii) Darauf aufbauend werden zwingende und optionale Anforderungen an die Sensorik abgeleitet, einschließlich Messbereichen für Methan und Ethan, notwendiger Nachweisgrenzen, Einsatzbedingungen, Schnittstellen sowie Restriktionen durch vorhandene Luftschadstoffmessgeräte. (iii) Abschließend wird skizziert, wie die kontinuierlich erfassten Konzentrationsdaten unter Nutzung vorberechneter Windfelder und atmosphärischer Ausbreitungsmodelle als Eingang für ein Modul zur Methanrückverfolgung und Emissionshochrechnung dienen können. Das Konzept schafft damit eine praxisnahe Grundlage für eine kontinuierliche Überwachung des Rohrleitungsnetzes und eine netzzustandsbasierte Emissionsquantifizierung. Die vorgestellte Methode ergänzt einerseits die klassischen Methoden zur messtechnischen Quantifizierung von Methanemissionen nach DVGW G 425-1 Tabelle 1 und andererseits auch die Methoden zur sicherheitstechnischen Überwachung des Leitungsnetzes nach DVGW G\,465-1-4. Der Einsatz der vorgestellten Vorgehensweise ermöglicht perspektivisch eine effizientere Instandhaltungsplanung in urbanen Gasverteilnetzen.

Einleitung

Die regulatorischen Anforderungen an Gasnetzbetreiber zur systematischen Erfassung und Reduktion von Methanemissionen haben sich in den vergangenen Jahren deutlich verschärft. Neben der EU-Methanverordnung (EU-Verordnung 2024/1787) (Europäisches Parlament & Rat der Europäischen Union, 2024) gewinnen insbesondere die DVGW-Merkblätter G 404 „Maßnahmen zur technischen Reduzierung von Methan- und Wasserstoffemissionen in der Gasinfrastruktur“, G 424 „Leitfaden zur Verringerung der Methanemissionen durch den Gastransport- und Gasverteilnetzbetrieb in Anlehnung an die Verordnung (EU) 2024/1787“ (DVGW e. V., 2024a) und G 425 „Methoden zur messtechnischen Quantifizierung von Methanemissionen“ (DVGW e. V., 2024b, 2024c) Teile 1 bis 5 an Bedeutung. Diese Regelungen konkretisieren den Rahmen für die Emissionsquantifizierung und -minderung im Gasbereich und werden im Folgenden zusammenfassend als „regulatorischer Rahmen“ bezeichnet. Die sicherheitstechnische Überwachung des Gasleitungsnetzes erfolgt zusätzlich nach den Regelungen G 465-1-4. Gleichzeitig besteht weiterhin eine Forschungslücke bei der Verknüpfung diffuser Methanemissionen aus erdverlegten Verteilnetzen mit dem Netzzustand und prädiktiven Instandhaltungsstrategien.

Während konventionelle Quellmessverfahren nach DVGW G 425-1 auf die Identifikation und Quantifizierung einzelner Leckagen fokussieren, adressieren sie die kontinuierliche übergeordnete Überwachung eines urbanen Gasverteilnetzes nur eingeschränkt (über Standort-Messungen). Hier setzen stationäre

DOI: 10.34712/142.81-2

Konzentrationsmessungen von Methan – ergänzt um Ethan als Tracer für fossiles Erdgas – in der Umgebungsluft an: Sie ermöglichen eine dauerhafte Beobachtung des städtischen Hintergrunds sowie die Detektion wiederkehrender Konzentrationserhöhungen, die mit Emissionsereignissen im Gasnetz in Verbindung stehen können.

Der vorliegende Beitrag stellt (i) ein Standortkonzept für stationäre Messstationen in urbanen Gasverteilnetzen vor, (ii) definiert zwingende und optionale Anforderungen an die eingesetzte Messtechnik und (iii) skizziert die Kopplung der kontinuierlichen Konzentrationsmessungen mit Ausbreitungs- und Emissionsmodellen. Ziel ist es, die Grundlage für eine netzzustandsbasierte Instandhaltungsplanung zu schaffen, die bestehende Quellmessverfahren ergänzt und für urbane Gasverteilnetze operationalisiert.

Methodik

Zentrale Bestandteile für die Festlegung des Messkonzepts sind die Standortwahl für stationäre Erdgaskonzentrationsmessungen, Anforderungen an die Sensorik und die Integration in Luftqualitätsmessstationen.

Standortwahl für stationäre Erdgaskonzentrationsmessungen

Für die stationäre Messung von Erdgaskonzentrationen in der Umgebungsluft werden drei grundsätzliche Standortvarianten untersucht: eigenständige Messstationen im öffentlichen Raum, Nutzung vorhandener Gasdruckregelanlagen (GDRA) und Integration der Messtechnik in bestehende Luftqualitätsmessstationen. Diese Varianten unterscheiden sich hinsichtlich baulicher Randbedingungen, betrieblicher Einbindung, messtechnischer Eignung sowie Wirtschaftlichkeit.

Zur systematischen Bewertung werden Kriterien wie Standortflexibilität, Nähe zu potenziellen Emissionsquellen, Repräsentativität für die Hintergrundbelastung, Nutzung bestehender Infrastruktur, Ex-Schutz-Anforderungen, Betriebsbedingungen, Vandalismusrisiko, organisatorische Komplexität, Wartungszugänglichkeit und Wirtschaftlichkeit herangezogen. In der Tabelle 1 sind die drei Standortvarianten anhand ausgewählter Kriterien zusammenfassend gegenübergestellt.

Der Vergleich zeigt, dass eigenständige Messstationen zwar eine hohe Standortflexibilität und eine gezielte Nähe zu vermuteten Emissionsquellen erlauben, dafür jedoch mit einem hohen Infrastruktur- und Betriebsaufwand einhergehen. GDRA-Standorte bieten eine unmittelbare Nähe zu kritischen Netzkomponenten, sind aber durch Ex-Schutz-Anforderungen, eingeschränkte Repräsentativität für die städtische Hintergrundbelastung und den stark anlagengebundenen Standort limitiert.

Luftqualitätsmessstationen weisen demgegenüber eine weitgehend vorhandene Mess- und Übertragungsinfrastruktur, klimatisierte Messcontainer, eine etablierte Qualitätssicherung sowie eine in der Regel gute Repräsentativität für die urbane Hintergrundbelastung auf. Einschränkungen resultieren daraus, dass deren Standorte primär nach luftqualitätsrelevanten Kriterien ausgewählt werden. Zudem erfordert die Integration zusätzliche organisatorische Abstimmungen mit den Betreibern des Luftmessnetzes.

Neben den hier betrachteten Hauptvarianten existieren weitere potenzielle Aufstellorte, etwa Transformatorengebäude, Wetterstationen der Stadtreinigung für den Winterdienst oder mobile Infrastruktureinheiten. Diese weisen in Bezug auf bauliche, betriebliche und messtechnische Randbedingungen überwiegend Zwischenpositionen zu den drei analysierten Standortkategorien auf und werden daher in diesem Beitrag nicht vertieft betrachtet.

Tabelle 1: Vergleich der Standortvarianten zur Messung von Erdgaskonzentrationen in der Umgebungsluft

Kriterium	Eigene Messstationen	GDRA	Luftqualitätsmessstationen
Standortflexibilität	hoch; freie Wahl gemäß Messkonzept	gering; an Anlagenstandort gebunden	sehr gering; bestehende, fest definierte Standorte
Nähe zu potenziellen Emissionsquellen	je nach Standortwahl gezielt herstellbar	hoch; unmittelbare Nähe zu Netzkomponenten	meist gering; auf luftqualitätsrelevante Lagen optimiert
Repräsentativität für Hintergrundbelastung	gut möglich bei entsprechender Standortwahl	eingeschränkt; stark an Anlagenumgebung gebunden	in der Regel gut; standortabhängig durch Messnetzkonzept
Nutzung bestehender Infrastruktur	gering; eigenständiger Aufbau erforderlich	mittel bis hoch; Nutzung von Flächen und ggf. Übertragungstechnik	hoch; bestehende Mess- und Übertragungsinfrastruktur
Ex-Schutz-Anforderungen	abhängig vom Standort; oft gering im öffentlichen Raum	hoch; Ex-Zonen und ex-geschützte Messtechnik erforderlich	in der Regel gering; keine Ex-Zonen
Betriebsbedingungen (Wärme, Witterung)	vollständig selbst bereitzustellen (z. B. Heizungen, Gehäuse)	teilweise vorhanden; abhängig von Anlagengebäude und Ausstattung	weitgehend erfüllt; klimatisierte Messcontainer
Vandalismus- und Diebstahlrisiko	je nach Lage; ggf. erhöht im öffentlichen Raum	gering; gesicherte Betriebsanlagen	mittel; meist umzäunte, aber sichtbare Infrastruktur
Organisatorische Komplexität	hoch; Flächenakquise, Aufbau, eigener Betrieb	mittel; Integration in Anlagenbetrieb und IT-Strukturen	mittel bis hoch; Abstimmung mit externem Betreiber
Wartungszugänglichkeit	flexibel gestaltbar; abhängig von Standort	gut im Rahmen von Anlagenbegehungen	eingeschränkt durch Zugangsregelungen der Station
Wirtschaftlichkeit (Invest und Betrieb)	höherer Aufwand durch eigenständige Infrastruktur	potenziell günstiger durch Mitnutzung bestehender Infrastruktur	abhängig von Vereinbarungen; Invest in Zusatztechnik, aber geringe Zusatzinfrastruktur

Anforderungen an die Sensorik

Zentrale Zielgrößen der Messstationen sind Methan (CH4) und Ethan (C2H6). Methan ist die Hauptkomponente von Erdgas (Cerbe & Lendt, 2017) und aufgrund des hohen globalen Erwärmungspotenzials (Intergovernmental Panel On Climate Change (IPCC), 2023) die klimarelevante Leitkomponente der Emissionen aus der Gasinfrastruktur. Die EU-Methanverordnung definiert Methan zudem als regulatorisch relevante Messgröße (Europäisches Parlament & Rat der Europäischen Union, 2024). Ethan hingegen wird als Marker zur Abgrenzung fossiler Erdgasquellen von anderen anthropogenen oder natürlichen Methanquellen benötigt (McKain et al., 2015). Die Messung des Ethan-Anteils dient damit zur eindeutigen Zuordnung der Emissionsereignisse zum Erdgasnetz. Dies erfolgt über das Methan–Ethan-Verhältnis, das charakteristisch für die jeweilige Erdgaszusammensetzung ist (McKain et al., 2015).

Für Methan wird ein Messbereich von etwa 1.800 ppb – entsprechend der atmosphärischen Hintergrundkonzentration (Intergovernmental Panel On Climate Change (IPCC), 2023) – bis mindestens 50.000 ppb (50 ppm) spezifiziert. Damit werden sowohl Hintergrundbedingungen als auch lokale Konzentrationserhöhungen infolge von Leckagen abgedeckt (McKain et al., 2015).

Für Ethan ist ein möglichst niedriges Detektionslimit erforderlich, um auch kleine Emissionsereignisse sicher der Erdgasquelle zuordnen zu können. Um die notwendige Größenordnung des Ethan-Detektionslimits zu verdeutlichen, wird nachfolgend die zugehörige c_C2H6 für die untere Messgrenze von Methan mit 1.800 ppb hergeleitet. Hierzu wird eine konstante Erdgaszusammensetzung angenommen mit $x_{CH_4} = 93\,\%$ und $x_{C_2H_6} = 4{,}3\,\%$ ($x_{Rest} = 93\,\%$). Damit ergibt sich für die Ethan-Konzentration bei gegebener Methankonzentration c_{CH_4} :

$$c_{C_2H_6} = c_{CH_4} \cdot \frac{x_{C_2H_6}}{x_{CH_4}} = c_{CH_4} \cdot \frac{4{,}3}{93}$$

Setzt man für c_CH4 die untere Messgrenze von 1.800 ppb an, so ergibt sich für Ethan:

$$c_{C_2H_6,min} = 1.800\,ppb \cdot \frac{4{,}3}{93} \approx 83\,ppb$$

Damit wird deutlich, dass das Detektionslimit für Ethan deutlich unterhalb von 100 ppb liegen muss, damit das Methan–Ethan-Verhältnis bereits ab der unteren Messgrenze von Methan zuverlässig nutzbar ist. Ein Ethan-LOD im Bereich einiger 10 ppb ist daher anzustreben.

Aus den Anforderungen an die Messaufgabe leiten sich folgende Mindestanforderungen an die Messtechnik ab: Als Messgrößen werden Methan und Ethan kontinuierlich erfasst. Bei Bedarf werden zusätzlich Temperatur und relative Luftfeuchte zur Messwertkorrektur herangezogen. Hinsichtlich der Messbereiche ist Methan ab etwa 1.800 ppb bis mindestens 50 ppm (50.000 ppb) zu messen, während Ethan ab 0 ppb mit einem möglichst niedrigen Detektionslimit erfasst werden soll. Die Messqualität muss so ausgelegt sein, dass Konzentrationserhöhungen von wenigen 100 ppb bis in den unteren ppm-Bereich sicher detektiert werden können. Zugleich ist ein geringes Signalrauschen anzustreben, das bei Bedarf durch geeignete Filterverfahren weiter geglättet wird. Für die Auslegung des Messsystems wird eine interne Messfrequenz von 1 s bis 5 s angestrebt, während die weiterverarbeitete Datenbasis aus 1minMittelwerten besteht, die bei Bedarf durch zusätzliche Kurzzeitmaxima zur Peakerkennung ergänzt werden.

In Bezug auf die Langzeitstabilität wird ein maximaler Drift von 2 % pro Jahr gefordert (vgl. Fulcrum Point Sustainability Consulting Co., Ltd., 2025), vorzugsweise in Kombination mit einer Selbstkalibrierung oder einer Kalibrierung im Rahmen einer jährlichen Wartung. Die Einsatzbedingungen umfassen eine Probentemperatur von −20 °C bis +50 °C sowie eine Betriebstemperatur des Geräts von 10 °C bis 35 °C im klimatisierten Messcontainer. Die Schnittstellen müssen die Übertragung der Messdaten an vorhandene Daten-

logger der Luftqualitätsstationen über einen Netzwerkanschluss und/oder RS232 ermöglichen. Darüber hinaus darf das Messsystem keine relevanten Querempfindlichkeiten gegenüber den in den Luftqualitätsstationen bereits eingesetzten Geräten zur Messung von SO_2, NO, NO_2, NO_X, Ozon und Feinstaub aufweisen, um eine Beeinflussung der laufenden Luftschadstoffmessungen zu vermeiden.

Aus Sicherheitsgründen werden Messprinzipien, die Brenngas benötigen, ausgeschlossen, da sie mit erhöhten Explosions- und Brandgefahren, zusätzlichen Genehmigungsanforderungen (z. B. Gaswarnsysteme) sowie einem erhöhten betrieblichen Aufwand verbunden wären. Anwendbare Messprinzipien für die geplante Messtechnik sind beispielsweise OF-CEAS (*engl. Optical Feedback Cavity Enhanced Absorption Spectroscopy)* oder OAICOS (*engl. OffAxis Integrated Cavity Output Spectroscopy*).

Als optionale Kriterien sind Anforderungen an die Energieversorgung und Wartungsfreundlichkeit zu nennen. Bevorzugt wird eine Stromversorgung über eine Batterie mit maximal einem Batteriewechsel pro Jahr, um zusätzliche Anfahrten außerhalb der regulären Wartungszyklen zu vermeiden. Alternativ ist ein fester Stromanschluss möglich. Weiterhin wird eine Selbstdiagnose und -kalibrierung der Messtechnik als vorteilhaft bewertet, um den personellen Aufwand im Routinebetrieb zu reduzieren und die Datenqualität langfristig sicherzustellen.

Integration in Luftqualitätsmessstationen

Die Integration der Erdgaskonzentrationsmessung in bestehende Luftqualitätsmessstationen erfordert die Beachtung baulicher, technischer und messtechnischer Randbedingungen. Die Messcontainer der Luftqualitätsstationen bieten in der Regel einen standardisierten 19ZollEinbauraum. Für das Methan/Ethan-Analysegerät steht eine Einbaubreite von 19 Zoll mit einer Höheneinheit nach DIN EN 602973100 zur Verfügung (DIN EN 602973100, 2009). Die klimatisierte Umgebung ermöglicht einen Betrieb der Geräte im Temperaturbereich von 10 °C bis 35 °C, während die Probenluft im Bereich von −20 °C bis +50 °C auftreten kann.

Die Probenentnahme erfolgt über die bestehende Probenluftverteilung der Station. Dabei wird die Außenluft über einen Ansaugkopf eingezogen und über einen Glasverteiler („Glasharfe“) mit Laboranschlüssen (GL 14 auf 6 mm PFA-Schlauch) auf die verschiedenen Analysegeräte verteilt. Das Erdgasanalysegerät wird als zusätzlicher Abzweig in diese Verteilung integriert. Die Abluft wird über einen 6 mm PFA-Schlauch durch den Containerboden ins Freie geleitet.

Zur Anbindung an das vorhandene Daten- und Übertragungssystem werden die Messdaten des CH4/C2H6-Analysegeräts an einen Datenlogger mit Fernübertragung übergeben. Hierzu stehen Netzwerk- und RS232Schnittstellen zur Verfügung. Die Messwerte werden über geeignete Filterverfahren von Rauschen bereinigt, um eine konsistente Weiterverarbeitung zu ermöglichen.

Ein wesentliches Integrationskriterium besteht darin, die laufenden Messungen in der Luftqualitätsstation nicht zu beeinträchtigen. Das zusätzliche Analysegerät darf daher weder den Probenstrom so verändern, dass die anderen Geräte beeinflusst werden, noch störende elektromagnetische, thermische oder chemische Effekte verursachen. Insbesondere sind Querempfindlichkeiten zu den bereits installierten Analysatoren für SO2, NO, NO2, NOX, Ozon und Feinstaub zu vermeiden.

Ergebnisse

Auswahl der Vorzugsvariante für den Standort

Aus dem Vergleich der Standortvarianten in Tabelle 1 stellt sich die Variante zur Installation der Erdgasmesstechnik in vorhandenen Luftqualitätsmessstationen als Vorzugsvariante dar. Entscheidend sind die Verfügbarkeit klimatisierter Messcontainer, die die Anforderungen an Temperaturstabilität und Witterungsschutz der Messtechnik weitgehend erfüllen, die vorhandene Mess- und Übertragungsinfrastruktur inklusive Datenloggern und Netzwerkanschlüssen und die in der Regel gute Repräsentativität für die stadtweite Hintergrundbelastung, die für die Detektion von Konzentrationserhöhungen auf dem atmosphäri-

schen Methanhintergrund entscheidend ist.

Die Nachteile – insbesondere die begrenzte Standortflexibilität in Bezug auf das Gasnetz und die organisatorische Komplexität der Kooperation mit den Messnetzbetrieben – werden als akzeptabler Kompromiss bewertet. Die Vorzugsvariante fokussiert damit nicht auf die unmittelbare punktgenaue Lokalisierung einzelner Leckagen, sondern auf die Identifikation von Netzbereichen mit erhöhter Emissionswahrscheinlichkeit in einem Testgebiet um die Messstandorte. Im Hinblick auf die spätere geplante Nutzung als Absicherung für Netzbereiche mit einem hohen Anteil älterer und damit potenziell leckageanfälliger Leitungen ist das akzeptabel.

Zusammenfassung der spezifizierten Sensoranforderungen

Die in Abschnitt 2 hergeleiteten Anforderungen an die Sensorik lassen sich in drei Gruppen zusammenfassen: (i) funktionale Messanforderungen, (ii) integrative Anforderungen für den Einsatz in Luftqualitätsmessstationen und (iii) Anforderungen an Langzeitstabilität und Betrieb.

Zentrale Messgrößen sind Methan (CH4) und Ethan (C2H6). Für Methan wird ein Messbereich von etwa 1.800 ppb bis mindestens 50 ppm gefordert; Ethan ist ab einem möglichst niedrigen Detektionslimit zu erfassen. Aus der dargestellten Herleitung in Kapitel 2 ergibt sich, dass bei einer Methankonzentration von 1.800 ppb eine zugehörige Ethankonzentration von nur rund 83 ppb zu erwarten ist. Zielgröße ist daher ein Ethan-LOD im Bereich weniger 10 ppb, damit das Methan–Ethan-Verhältnis bereits ab der unteren Messgrenze von Methan zuverlässig nutzbar ist.

Hinsichtlich der Messqualität werden eine sichere Detektion von Konzentrationserhöhungen im Bereich weniger 100 ppb bis in den unteren ppm-Bereich sowie ein geringes Signalrauschen gefordert. Für die zeitliche Auflösung ist eine interne Messfrequenz von 1–5 s vorgesehen; die weitere Verarbeitung erfolgt auf Basis von 1minMittelwerten, bei Bedarf ergänzt um Kurzzeitmaxima zur Peakerkennung. Die Langzeitstabilität der Sensorik soll einen maximalen Drift von 2 % pro Jahr nicht überschreiten.

Für die Integration in Luftqualitätsmessstationen sind Einsatzbedingungen von −20 °C bis +50 °C Probentemperatur und 10–35 °C Gerätetemperatur im Messcontainer maßgeblich. Erforderlich sind zudem standardisierte Schnittstellen (Netzwerk, RS232) zur Anbindung an vorhandene Datenlogger sowie eine Probenanbindung an die bestehende Glasharfe. Querempfindlichkeiten gegenüber den in den Stationen betriebenen Luftschadstoffmessgeräten sind zu vermeiden; Messprinzipien mit Brenngaseinsatz werden aus Sicherheits- und Betriebsgründen ausgeschlossen.

Diskussion

Der vorliegende Beitrag stellt ein Messkonzept für stationäre Methan- und Ethanmessungen in urbanen Gasverteilnetzen vor. Im Mittelpunkt stehen die Standortwahl für Messstationen, die Ableitung von Sensoranforderungen sowie die Integration in bestehende Luftqualitätsmessstationen als Grundlage für eine spätere Kopplung mit Ausbreitungs- und Emissionsmodellen. Das vorgestellte Messkonzept ist vor dem Hintergrund des verschärften regulatorischen Rahmens zu sehen. Die EU-Methanverordnung sowie die DVGW-Regelwerke G 404, G 424 und G 425 definieren Anforderungen an die Erfassung und Reduktion von Methanemissionen, während G 4651 bis -4 die sicherheitstechnische Überwachung des Leitungsnetzes adressieren.

Die Analyse der drei Standortvarianten zeigt, dass eigenständige Messstationen zwar eine hohe Standortflexibilität und eine gezielte Nähe zu vermuteten Emissionsquellen erlauben, jedoch mit erheblichem Investitions- und Betriebsaufwand verbunden sind. GDRA bieten eine unmittelbare Nähe zu kritischen Netzkomponenten, sind aber durch Ex-Schutz-Anforderungen und eine eingeschränkte Repräsentativität für die urbane Hintergrundbelastung limitiert. Die Integration in Luftqualitätsmessstationen stellt sich als pragmatischer Kompromiss dar: Sie ermöglicht die Nutzung bestehender Infrastruktur, etablierter Qualitätssicherungsprozesse und repräsentativer Hintergrundmessungen, erfordert jedoch eine enge Abstim-

mung mit den Messnetzbetrieben und akzeptiert eine geringere Standortflexibilität im Hinblick auf das Gasnetz.

Aus den Anforderungen an die Messaufgabe werden die Mindestanforderungen an die Sensorik abgeleitet. Besonders hervorzuheben sind der geforderte Messbereich für Methan ab etwa 1.800 ppb bis mindestens 50 ppm und die Notwendigkeit eines sehr niedrigen Detektionslimits für Ethan, da bereits bei der unteren Methangrenze von 1.800 ppb nur rund 83 ppb Ethan zu erwarten sind und das Detektionslimit daher im Bereich weniger 10 ppb liegen muss. Ergänzend werden Anforderungen an Drift, Einsatzbedingungen, Schnittstellen und Probenführung formuliert, die eine robuste Integration in bestehende Messcontainer und Dateninfrastrukturen ermöglichen sollen.

Gleichzeitig sind Grenzen und Unsicherheiten des Ansatzes zu berücksichtigen. Die stationären Messungen liefern keine direkte, punktgenaue Lecklokalisierung, sondern Konzentrationszeitreihen, die erst im Zusammenspiel mit Windfeldern und Ausbreitungsmodellen interpretiert werden können. Die Qualität der Emissionsrückrechnung hängt daher wesentlich von der Güte der meteorologischen Eingangsdaten und der verwendeten Ausbreitungs- und Inversionsmodelle ab. Hinzu kommt die begrenzte räumliche Auflösung, die durch die Anzahl und Lage der Luftqualitätsmessstationen vorgegeben ist. Diese Einschränkungen begründen die Notwendigkeit einer sorgfältigen Modellierung, Validierung und Kombination mit klassischen Leitungsprüf- und Quellmessverfahren.

Fazit und Ausblick

Die in Luftqualitätsmessstationen kontinuierlich erfassten Methan- und Ethankonzentrationen bilden eine zentrale Eingangsdatenbasis für modellgestützte Verfahren zur Rückverfolgung von Emissionsquellen und zur Emissionshochrechnung im urbanen Gasverteilnetz. Anhand vorberechneter Windfelder und atmosphärischer Ausbreitungsmodelle sind mögliche Leckageorte zu identifizieren.

Konzeptionell lässt sich der Ansatz wie folgt beschreiben: Zunächst werden die stationären Konzentrationszeitreihen einer Qualitätssicherung unterzogen und zeitlich mit meteorologischen Daten (insbesondere Windrichtung und -geschwindigkeit) synchronisiert. Auf Basis vorberechneter Windfelder aus einem mesoskaligen Modell für das urbane Gebiet, z. B. METRASPCL, berechnet ein Ausbreitungsmodell die zu erwartenden Konzentrationen an den Messstationen für gegebene Emissionsszenarien.

Durch den Vergleich der modellierten Konzentrationen mit den tatsächlich gemessenen Werten kann in einem inversen Verfahren iterativ auf die räumliche Verteilung und Stärke der Emissionsquellen geschlossen werden. Nachfolgend werden einerseits die möglichen Leckageorte mit den vorhandenen Leitungen aus dem grafischen Informationssystem verschnitten, um den Überprüfungsumfang in der Nähe befindlicher Leitungen einzugrenzen. Durch gezielte Auswertung der Netz- und Anlagendaten (z. B. Leitungsmaterial, Alter, Druckstufe, Störungs- und Schadenshistorie) für den Zielbereich werden die Leitungsteile mit der größten „Leckagewahrscheinlichkeit“ identifiziert. Nach Überprüfung der Leckageorte durch Befahrung oder Begehung werden die Ergebnisse der Überprüfung ins Modell rückgespeist zur Modellverbesserung. Übergeordnet werden alle Überprüfungsergebnisse zusammen mit den Netzdaten kontinuierlich ausgewertet, um Muster zu identifizieren und Anhaltspunkte für eine netzzustandsbasierte Instandhaltungsplanung abzuleiten.

Die detaillierte Ausgestaltung der Ausbreitungs- und Inversionsmodelle, die Quantifizierung von Unsicherheiten sowie die Modellierung des Bewertungstools zur netzzustandsbasierten Instandhaltungsplanung sind Gegenstand weiterer Forschungen im Zuge der Dissertation. Der im vorliegenden Beitrag vorgestellte Fokus auf Standortwahl und Sensoranforderungen bildet jedoch die notwendige Grundlage, um stationäre Methan- und Ethanmessungen verlässlich in ein solches modellbasiertes Emissionsquantifizierungssystem einzubinden.

Insgesamt schafft der Beitrag eine fachlich und regulatorisch eingebettete Grundlage für das Konzept stationärer Methan- und Ethanmessungen in urbanen Gasverteilnetzen, die Standortwahl, Sensoranforderungen und Integrationsaspekte zusammenführt und in die Perspektive einer modellgestützten Emissionsbewertung stellt. Aus Sicht der Emissionsüberwachung und Netzsicherheit liegt der zentrale Mehrwert in der Kombination aus kontinuierlicher, netzweiter Beobachtung und der Kopplung an Zustands- und Emissionsmodelle, die klassische Quellmess- und Leitungsprüfverfahren nicht ersetzt, aber gezielt ergänzt und fokussiert.

Literatur

Cerbe, G., & Lendt, B. (Hrsg.). (2017). Grundlagen der Gastechnik: Gasbeschaffung – Gasverteilung – Gasverwendung (8., vollständig überarbeitete Auflage). Hanser.

DIN EN 60297-3-100:2009-09, Bauweisen für elektronische Einrichtungen – Maße der 482,6mm (19Zoll) Bauweise – Teil 3100: Hauptmaße von Frontplatten, Baugruppenträgern, Einschüben, Gestellen und Schränken (IEC 602973100:2008); Deutsche Fassung EN 602973100:2009. (2009). https://doi.org/10.31030/1530142

DVGW e. V. (2024a). DVGW-Merkblatt G 424 2024-10: Leitfaden zur Verringerung der Methanemissionen durch den Gastransport- und Gasverteilnetzbetrieb in Anlehnung an die Verordnung (EU) 2024/1787.

DVGW e. V. (2024b). DVGW-Merkblatt G 425-1 2024-10: Methoden zur messtechnischen Quantifizierung von Methanemissionen Teil 1 Allgemeine Grundlagen.

DVGW e. V. (2024c). DVGW-Merkblatt G 425-2 2024-10: Methoden zur messtechnischen Quantifizierung von Methanemissionen Teil 2 Absaugmethode an erdverlegten Installationen.

Europäisches Parlament & Rat der Europäischen Union. (2024). Verordnung (EU) 2024/1787 des Europäischen Parlaments und des Rates über die Verringerung der Methanemissionen im Energiesektor und zur Änderung der Verordnung (EU) 2019/942. https://eur-lex.europa.eu/legal-content/DE/TXT/HTML/?uri=OJ:L_202401787

Fulcrum Point Sustainability Consulting Co., Ltd. (2025, Dezember). What Is Acceptable Sensor Drift? Question. Verfügbar 11. März 2026 unter https://pollution.sustainability-directory.com/question/what-is-acceptable-sensor-drift/

Intergovernmental Panel On Climate Change (IPCC). (2023, Juli). Climate Change 2021 – The Physical Science Basis: Working Group I Contribution to the Sixth Assessment Report of the Intergovernmental Panel on Climate Change (1. Aufl.). Cambridge University Press. https://doi.org/10.1017/9781009157896

McKain, K., Down, A., Raciti, S. M., Budney, J., Hutyra, L. R., Floerchinger, C., Herndon, S. C., Nehrkorn, T., Zahniser, M. S., Jackson, R. B., Phillips, N., & Wofsy, S. C. (2015). Methane emissions from natural gas infrastructure and use in the urban region of Boston, Massachusetts. Proceedings of the National Academy of Sciences of the United States of America, 112(7), 1941–1946. https://doi.org/10.1073/pnas.1416261112

Assessment of Long-Term Aged Polyurethane Foam in District Heating Pipes and the Applicability of FTIR Spectroscopy

Pakdad Langroudi
pakdad.langroudi@hcu-hamburg.de HafenCity University, Hamburg

Abstract

Polyurethane (PUR) foam used in district heating pipe systems plays a critical role in the performance and service life of the pipe assembly. Besides providing thermal insulation, the foam contributes to the structural integrity of the system by supporting the steel service pipe, maintaining the cohesion between the steel pipe and the outer casing, and limiting pipe displacement caused by thermal expansion. Over time, however, PUR foam undergoes ageing and degradation, which lead to deterioration of its thermal and mechanical properties. Fourier Transform Infrared Spectroscopy (FTIR) is commonly used to evaluate the chemical degradation of PUR by monitoring changes in molecular bonds. In this study, PUR foam samples extracted from field-aged district heating pipes at the end of their service life were investigated using FTIR and complementary analytical techniques. The outer surface of the foam exhibited strong darkening and FTIR measurements performed directly on this layer showed a significant reduction or disappearance of characteristic absorption bands. After removing approximately 1 mm of the surface layer, the typical PUR spectral features became detectable again. Additional investigations using X-ray diffraction (XRD) and chemical analysis were carried out to determine whether iron oxides or metallic ions originating from the steel service pipe contributed to this phenomenon; however, no evidence of such contamination was detected. Furthermore, nuclear magnetic resonance (NMR) analysis was conducted to examine potential hydrogen redistribution across the foam from the steel pipe side toward the casing. The results indicate that surface alterations in severely aged PUR foam may influence FTIR measurements and should be considered when interpreting spectroscopic analyses of field-aged insulation materials.

Introduction

District heating (DH) systems play a central role in modern energy infrastructure by enabling efficient heat distribution from centralized sources to consumers. Pre-insulated district heating pipes typically consist of three main components: a steel service pipe, a rigid polyurethane (PUR) foam insulation layer, and an external high-density polyethylene (HDPE) casing. The PUR foam performs multiple functions within the pipe assembly. In addition to its primary role as thermal insulation, it provides mechanical support for the steel pipe, maintains the structural cohesion between the steel pipe and the casing, and restricts pipe displacement caused by thermal expansion during operation. The long-term performance and reliability of district heating networks therefore strongly depend on the durability of the PUR insulation material (Yarahmadi, Vega, und Jakubowicz 2017). During long-term service, PUR foam is exposed to elevated temperatures, mechanical stresses, and environmental influences that gradually lead to ageing and degradation of the polymer structure. Several degradation mechanisms have been reported for PUR insulation materials in district heating systems, including thermal ageing, oxidative degradation, and gas diffusion within the foam cells. These processes may cause structural changes in the polymer network, loss of mechanical strength, increased brittleness, and deterioration of thermal insulation properties (Yarahmadi und Sällström 2014). Previous studies have demonstrated that the chemical degradation of PUR foams is largely governed by thermo-oxidative processes, which lead to changes in the molecular structure of the polymer (Yarahmadi, Vega, und Jakubowicz 2017). Accelerated ageing experiments have shown the formation of additional carbonyl groups and the reduction of methylene (CH_2) groups in the polymer backbone when PUR foams are exposed to elevated temperatures in the presence of oxygen. These chemical modifications are directly associated with the progressive deterioration of the polymer structure (Yarahmadi, Vega, und Jakubowicz

DOI: 10.34712/142.81-3

2017).

Spectroscopic techniques, particularly Fourier Transform Infrared Spectroscopy (FTIR), are widely used to investigate the chemical degradation of polyurethane materials. FTIR enables the monitoring of characteristic absorption bands associated with urethane linkages, carbonyl groups, and other functional groups within the polymer chain, allowing researchers to track chemical changes during ageing. Several investigations of naturally and artificially aged PUR foams have demonstrated that degradation processes can be identified through systematic changes in FTIR spectra, particularly in the carbonyl and aromatic regions of the spectra (França De Sá u. a. 2017). In the context of district heating systems, FTIR has been frequently used to analyze the ageing behavior of PUR insulation materials and to correlate chemical changes with the mechanical and thermal performance of the pipes. However, the degradation process in PUR insulation is complex and may involve several phases, including early physical ageing followed by progressive chemical degradation. These processes may occur differently depending on the local thermal and mechanical conditions within the insulation layer (Alberto Vega 2018). Despite the extensive use of FTIR in polymer degradation studies, the interpretation of spectra from naturally aged materials recovered from long-term field operation remains challenging. Field-aged insulation materials may exhibit heterogeneous ageing patterns due to gradients in temperature, oxygen diffusion, and mechanical stress across the insulation layer. In district heating pipes, the most severe conditions often occur near the interface between the steel service pipe and the PUR foam, where thermal loads and mechanical stresses are highest (Weidlich u. a. 2020).

The present study investigates PUR foam insulation extracted from district heating pipes that have been in field operation for 27 years. Particular attention is given to the chemical characterization of the foam using ATR-FTIR spectroscopy and the evaluation of potential factors influencing the spectroscopic measurements. Complementary analytical techniques, including X-ray diffraction (XRD) and chemical detection methods for iron species, were employed to examine whether possible migration of corrosion products from the steel pipe could influence the spectroscopic response. In addition, nuclear magnetic resonance (NMR) analysis was conducted to explore potential changes in hydrogen distribution within the foam structure. By combining these analytical approaches, this work aims to improve the understanding of ageing phenomena in PUR insulation under real operating conditions and to evaluate potential limitations of FTIR analysis when applied to severely aged polyurethane materials from district heating systems.

Methodology

Sample Material

PUR foam samples were obtained from district heating pipe assemblies that had been in field operation for approximately 27 years. The investigated pipes had reached the end of their service life and were removed from operation. The PUR foam functions as the thermal insulation and structural support material between the steel service pipe and the outer casing of the district heating pipe system. Visual inspection of the recovered samples revealed a distinct color gradient within the foam structure (see Figure 1 Measurement locations on a PUR foam sample). The region of the foam directly adjacent to the steel service pipe exhibited strong darkening and appeared almost black in color. Moving away from the steel pipe toward the outer casing, the foam gradually became lighter, indicating a gradient in the degree of ageing or chemical modification across the insulation layer. Foam specimens were therefore collected from different positions within the insulation thickness in order to evaluate potential differences between the steel-side interface region and the foam regions closer to the casing.

FTIR Spectroscopy (ATR Mode)

FTIR measurements were performed using the Attenuated Total Reflection (ATR) technique in order to analyze chemical changes in the polyurethane structure caused by long-term ageing. Initial FTIR measurements were carried out directly on the darkened surface layer of the foam. Subsequently, approximately 1 mm of the surface layer was mechanically removed, and the measurement was repeated on the newly exposed material. This approach allowed the comparison between the surface layer and the underlying

bulk material. The spectra were analyzed with particular focus on characteristic polyurethane absorption bands, including those associated with urethane linkages, carbonyl groups, and C–H stretching vibrations. The measurements were used to evaluate the presence or absence of identifiable polymer bond structures in both the surface and subsurface layers of the foam.

X-Ray Diffraction (XRD)

XRD analysis was conducted to investigate whether crystalline inorganic phases were present within the darkened surface layer of the aged PUR foam. The objective of this analysis was to determine whether materials originating from the steel service pipe, such as iron oxides, had migrated into the foam and could potentially influence the FTIR measurements. Samples from the surface region of the foam were analyzed using XRD to identify any crystalline phases. The diffraction patterns were evaluated and compared with reference patterns for common iron oxide phases.

Chemical Detection of Iron Compounds

To further investigate the possible presence of iron species within the foam, qualitative chemical analysis was performed using an acid extraction followed by colorimetric detection. Polyurethane foam samples were treated with nitric acid (HNO_3) to extract potential metal ions from the material matrix. The resulting solution was subsequently reacted with potassium ferrocyanide ($K_4[Fe(CN)_6]$), which forms a characteristic blue complex (Prussian blue) in the presence of iron species.

This procedure was applied to assess whether iron-containing materials originating from the steel service pipe had migrated into the foam structure during long-term operation.

Results

FTIR spectroscopy using the ATR technique was performed on the PUR foam samples recovered from district heating pipes that had been in service for approximately 27 years. The spectra obtained were analyzed to identify the characteristic functional groups associated with the polyurethane structure. Assignment of the absorption bands was carried out according to previously reported studies on PUR foams and their degradation behavior (Doyle und Weidlich 2021; França De Sá u. a. 2017; Hatchett, Kinyanjui, und Sapochak 2007). To ensure the reliability of the measurements, repeatability tests were performed, and the resulting spectra showed a high degree of overlap when measured repeatedly at the same location, confirming the consistency of the FTIR measurements. The analysis was conducted at four different positions across the insulation thickness in order to investigate possible spatial variations in chemical structure associated with long-term ageing.

The investigated locations included:

1. The interface between the PUR foam and the steel service pipe
2. A depth of approximately 1 mm from the steel interface toward the casing
3. A depth of approximately 5 mm toward the casing
4. The interface between the PUR foam and the outer casing

The measurement locations are illustrated in Figure 1 Measurement locations on a PUR foam sample.

Figure 1 Measurement locations on a PUR foam sample

The FTIR spectra revealed a pronounced difference between the foam region directly adjacent to the steel service pipe and the regions located further inside the insulation layer. Figure 2 FT-IR spectrum of naturally aged polyurethane foam insulation from a district heating pipeline after 27 years of in-field operation. illustrates the spectrum measured at the immediate interface shows a substantial deviation from the spectra obtained in the interior regions of the foam. At the steel–foam interface, where the material visually exhibited strong darkening and appeared nearly black, most of the characteristic absorption bands associated with the polyurethane structure were significantly reduced or nearly absent. In particular, absorption bands related to key functional groups of PUR, including isocyanurate structures, urethane carbonyl groups (C=O), ether linkages (C–O–C), and N–H stretching vibrations, were either strongly diminished or completely lost in the spectrum. The mentioned functional groups have been used in multiple studies for identification and degradation purposes (França De Sá u. a. 2017; Hatchett, Kinyanjui, und Sapochak 2007; A. Vega, Yarahmadi, und Jakubowicz 2018). In contrast, the FTIR spectra obtained from the 1 mm and 5 mm depths toward the casing exhibited clear and well-defined absorption bands corresponding to these functional groups. The spectra recorded at these locations showed a high degree of overlap with each other, indicating that the underlying foam material retained a consistent molecular structure across these regions (Jakubowicz u. a. 2022). The reappearance of the characteristic PUR bands after removal of approximately 1 mm of the surface layer suggests that the spectroscopic signal disruption is confined primarily to the outermost region of the foam adjacent to the steel pipe. The spectrum obtained at the foam–casing interface also displayed identifiable polyurethane absorption bands, although slight variations in intensity were observed compared with the spectra obtained at intermediate depths. The observed disappearance of characteristic PUR absorption bands at the steel interface represents a significant challenge when using FTIR spectroscopy to assess the degradation state of long-term field-aged district heating insulation materials. In cases where the foam surface has undergone severe discoloration, resulting in a dark or nearly black appearance, the altered surface layer can interfere with infrared measurements and obscure the characteristic absorption features typically used to evaluate polymer degradation. This phenomenon complicates the establishment of reliable spectroscopic benchmarks for determining the end-of-service-life condition of PUR insulation in district heating pipes. When FTIR measurements are performed directly on such darkened surfaces, the absence of identifiable absorption bands could potentially lead to incorrect conclusions regarding the chemical state of the material.

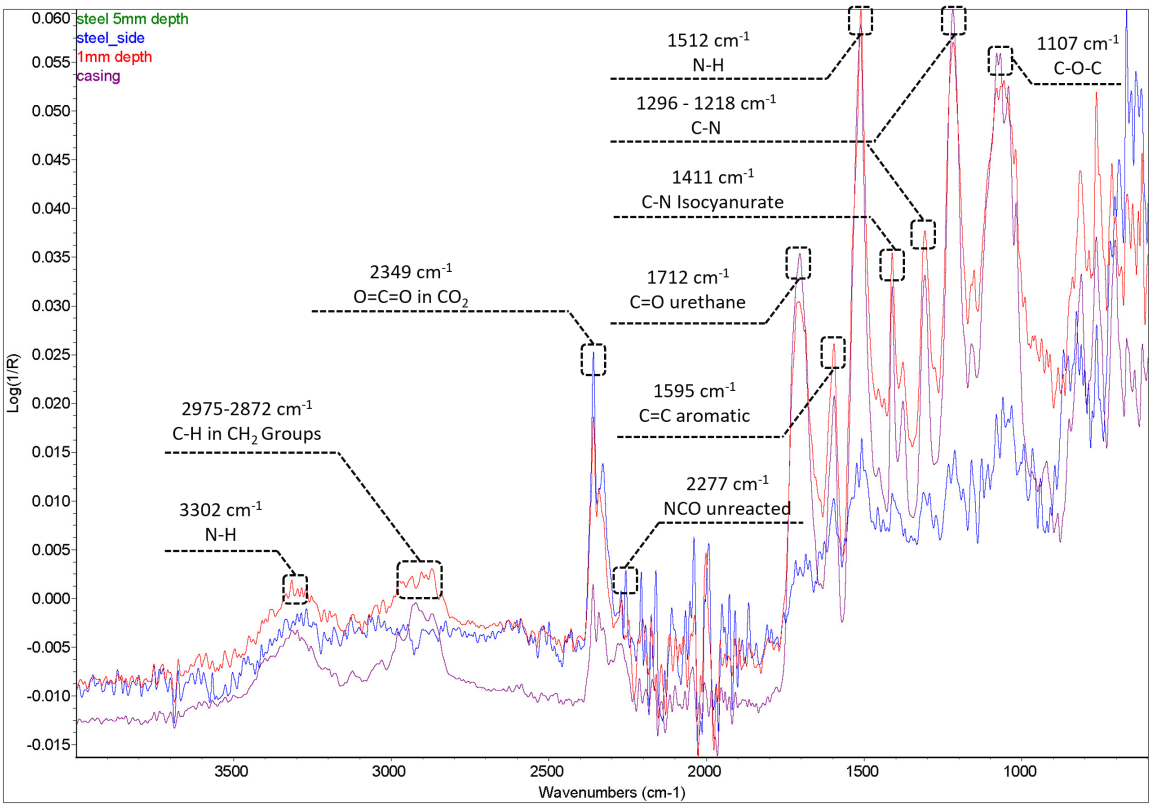

Figure 2 FT-IR spectrum of naturally aged polyurethane foam insulation from a district heating pipeline after 27 years of in-field operation.

The loss of spectral features, especially within the range of 2000 to 1000 cm^{-1} at the steel interface therefore raises an important question regarding the underlying cause of the signal disruption. One possible explanation could be the presence of inorganic contaminants, such as iron ions or iron oxide particles originating from corrosion processes in the steel service pipe. Such species could potentially interfere with infrared absorption or modify the surface characteristics of the foam.

To investigate whether inorganic phases were present in the darkened foam region located at the interface with the steel service pipe, XRD analysis was performed. The purpose of this analysis was to determine whether crystalline corrosion products, particularly iron oxides originating from the steel pipe, had migrated into the polyurethane foam during long-term operation and could potentially influence the FTIR measurements. XRD is commonly used for the identification of crystalline phases in materials and is widely applied in corrosion studies to detect iron oxide products formed during steel oxidation processes (Cornell und Schwertmann 2003; Cullity und Stock 2001). Samples taken from the darkened interface region of the foam were subjected to XRD analysis, and the obtained diffraction patterns were compared with reference patterns of common iron oxide phases, including hematite (Fe_2O_3), magnetite (Fe_3O_4), and goethite (FeOOH). These phases represent the most frequently observed corrosion products formed during the oxidation and environmental degradation of iron and steel (Cornell und Schwertmann 2003; Revie und Uhlig 2008). Under long-term service conditions, corrosion products from steel components may in some cases migrate into adjacent materials or accumulate at interfaces, potentially altering local chemical environments (Revie und Uhlig 2008). Figure 3 Diffractometer Analysis of Foam–Pipe Interface illustrates that the XRD patterns obtained from the investigated foam samples within the 10–80° (2θ) scan range do not show any detectable diffraction peaks corresponding to crystalline iron oxide phases. Instead, the diffraction pattern exhibits a broad amorphous halo, which is characteristic of polymeric materials such as polyurethane. The sharp diffraction peaks expected for common iron oxide phases are indicated in red in the figure; however, no such reflections are observed in the measured pattern. Polymers typically lack long-range crystalline order and therefore produce diffuse diffraction patterns rather than sharp Bragg peaks in XRD measurements (Alexander 1985; Sperling 2006). The absence of identifiable crystalline peaks suggests that

no significant amount of crystalline inorganic phases is present within the analyzed foam region.

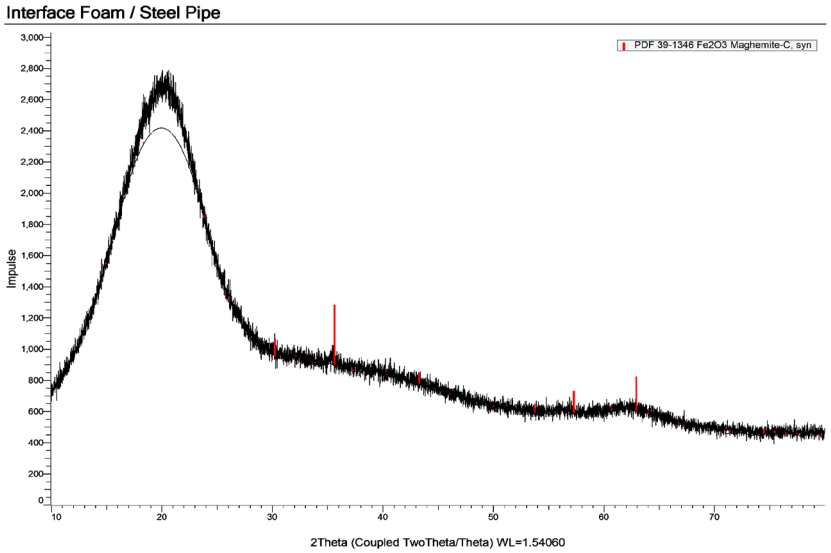

Figure 3 Diffractometer Analysis of Foam–Pipe Interface

These findings indicate that the darkened surface layer observed at the steel–foam interface is not associated with the presence of crystalline corrosion products from the steel service pipe. Consequently, the disappearance of FTIR absorption bands at this interface cannot be attributed to the presence of crystalline iron oxide phases within the foam structure.

In order to further evaluate the possibility of iron ion migration from the steel service pipe into the polyurethane foam, qualitative chemical analyses were performed to detect the presence of ferric ions (Fe^{3+}). The detection method was based on the well-known reaction between iron(III) ions and potassium ferrocyanide ($K_4[Fe(CN)_6]$), which results in the formation of a deep blue complex commonly referred to as Prussian blue. This reaction is highly sensitive and widely used for the qualitative identification of ferric ions (Harris 2007; Skoog u. a. 2022). The formation of Prussian blue results from the coordination reaction between ferric ions and hexacyanoferrate complexes, producing the characteristic intense blue precipitate that allows visual detection of Fe^{3+} ions even at relatively low concentrations (Inorganic Chemistry 2018). Two different approaches were applied during the chemical analysis. First, the darkened foam material taken from the interface region was directly exposed to a solution containing potassium ferrocyanide ($K_4[Fe(CN)_6]\cdot 3H_2O$) in order to observe whether a color reaction indicating the presence of Fe^{3+} ions would occur. Second, foam samples were subjected to acid digestion using nitric acid (HNO_3) to extract any potential metal ions embedded within the polymer matrix. Acid digestion is commonly used in analytical chemistry to dissolve solid samples and release metal ions into solution prior to qualitative or quantitative analysis (Harris 2007; Skoog u. a. 2022). The resulting solution was then reacted with potassium ferrocyanide to test for the presence of dissolved ferric ions.

In both cases, no characteristic blue coloration associated with Prussian blue formation was observed. This result indicates that detectable concentrations of ferric ions were not present in the analyzed foam samples (see Figure 4 Chemical Analysis for Detection of Iron Oxides at the Pipe–Foam Interface in PU Insulation). The chemical tests therefore support the XRD findings, suggesting that iron ions or corrosion products originating from the steel pipe have not significantly migrated into the polyurethane foam. The

absence of detectable iron species further suggests that the observed loss of FTIR absorption signals at the interface region cannot be attributed to interference caused by metallic contamination or corrosion products.

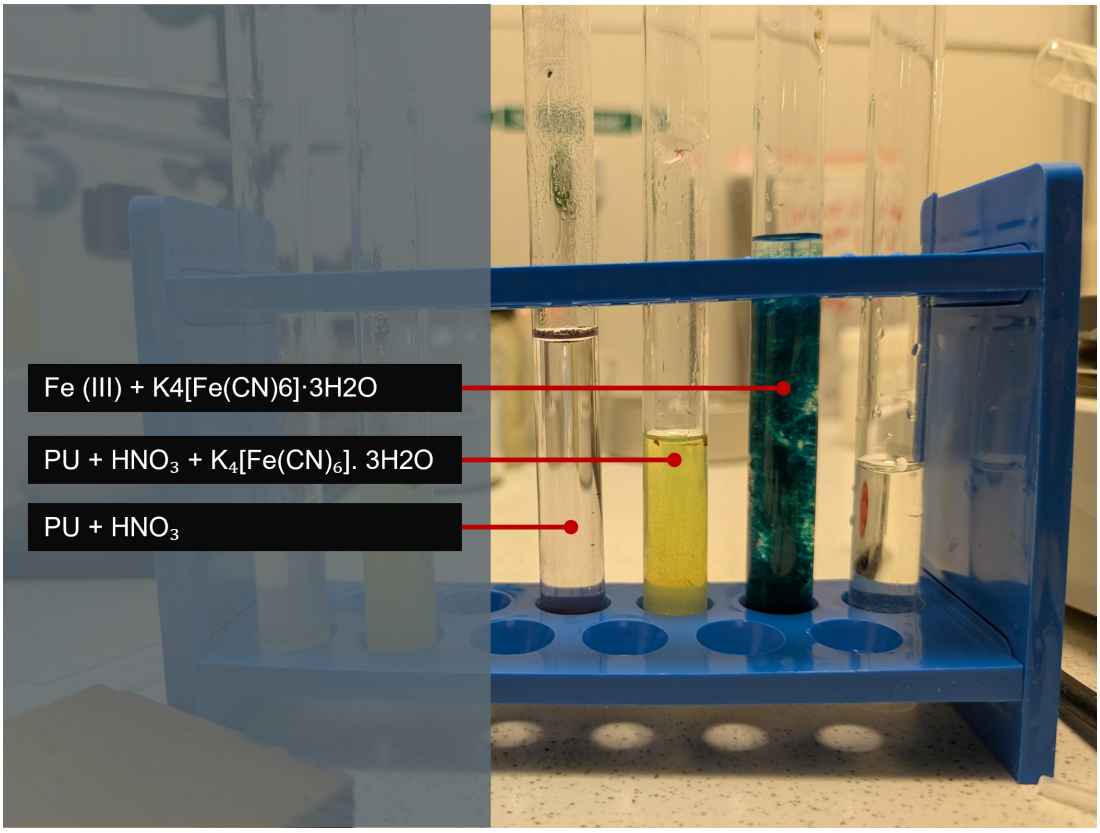

Figure 4 Chemical Analysis for Detection of Iron Oxides at the Pipe–Foam Interface in PU Insulation

To further investigate possible structural changes within the polyurethane foam resulting from long-term service conditions, nuclear magnetic resonance (NMR) analysis was performed with particular focus on hydrogen distribution within the material. NMR spectroscopy is widely used for the characterization of polymer structures because it provides detailed information about the local chemical environment and mobility of hydrogen atoms within polymer chains (Claridge 2016; Keeler 2011). In polymer systems, variations in NMR signals can reveal changes in molecular structure, cross-linking density, and degradation processes that occur during ageing (Mehring 1996; Schmidt-Rohr und Spiess 1994). The NMR measurements were conducted across the insulation thickness in order to examine potential variations in hydrogen-related signals between the steel pipe interface and the outer casing region. This approach allowed the evaluation of possible gradients in polymer structure that may have developed during the extended operational lifetime of the pipe. Spatial variations in NMR signals have previously been used to investigate structural heterogeneity and ageing gradients in polymeric materials exposed to long-term environmental or thermal stress (Schmidt-Rohr & Spiess, 1994; Claridge, 2016). The results indicated variations in the hydrogen-related signals across the insulation layer, suggesting changes in the molecular environment of hydrogen atoms within the polymer structure. These variations were more pronounced in the region adjacent to the steel service pipe, where the foam exhibited the strongest visual discoloration and where FTIR measurements showed the most significant loss of characteristic absorption bands (see Figure 5 . Change in hydrogen signal intensity as a function of depth, measured by NMR.). Changes in NMR signals in polymer systems are often associated with modifications in chain mobility, chemical bonding, or cross-linking within the polymer matrix (Keeler 2011; Schmidt-Rohr und Spiess 1994). The observed changes in the NMR signals therefore suggest that structural modifications within the polyurethane matrix may have occurred in the interfacial region during long-term operation, potentially associated with thermal exposure or other ageing processes. Thermo-oxidative degradation of polyurethane materials can lead to chain scission,

cross-linking reactions, and the formation of new chemical structures, which may alter the local hydrogen environments detectable by NMR spectroscopy (Doyle und Weidlich 2021; França De Sá u. a. 2017). Such changes may contribute to the formation of the darkened surface layer observed at the steel interface, where the ageing conditions are expected to be most severe.

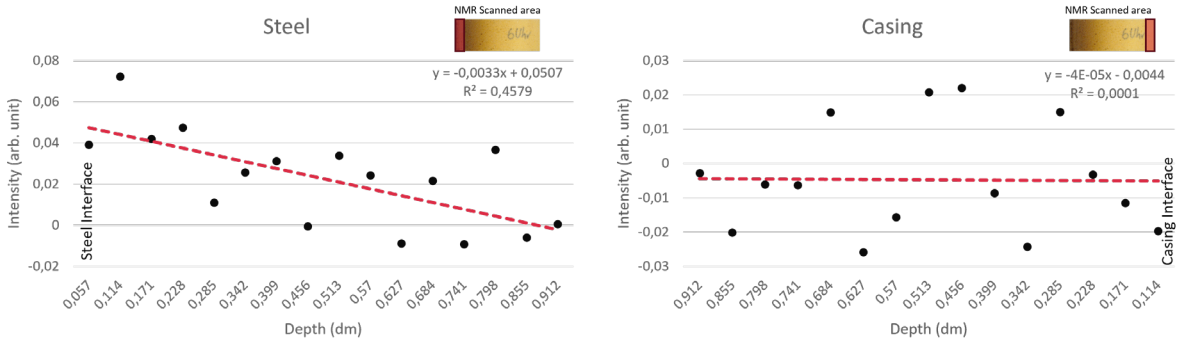

Figure 5 . Change in hydrogen signal intensity as a function of depth, measured by NMR.

Taken together, the results from FTIR, XRD, chemical analysis, and NMR indicate that the loss of FTIR absorption bands at the steel–foam interface is not related to the presence of iron ions or crystalline corrosion products. Instead, the findings suggest that the phenomenon is likely associated with ageing-related modifications of the polymer structure occurring in the interfacial region during long-term service.

Discussion

The FTIR analysis revealed that the PUR foam located directly at the interface with the steel service pipe exhibits a strong darkening, accompanied by the disappearance of most characteristic infrared absorption bands associated with polyurethane functional groups. In contrast, spectra obtained from locations only 1 mm beneath the interface display well-defined absorption bands corresponding to urethane carbonyl groups (C=O), ether linkages (C–O–C), N–H stretching vibrations, and isocyanurate structures. These functional groups are typically used as diagnostic absorption bands in FTIR analysis of polyurethane materials (França De Sá u. a. 2017; Hatchett, Kinyanjui, und Sapochak 2007). The observation therefore suggests that the loss of FTIR spectral features is limited to a very thin surface layer and is not representative of the bulk polymer structure. One plausible explanation for the disappearance of FTIR signals is the formation of a highly altered surface layer resulting from long-term thermo-oxidative degradation of the polyurethane matrix. Prolonged exposure to elevated temperatures and oxidative conditions can lead to extensive chemical transformations within the polymer network, including chain scission, cross-linking reactions, and the formation of new oxidation products (Doyle und Weidlich 2021; França De Sá u. a. 2017). During advanced degradation stages, these reactions may lead to the formation of conjugated carbon-rich structures within the polymer matrix, which are commonly associated with progressive discoloration and darkening of polymeric materials (Grassie und Scott 1988).

Such carbon-rich or highly conjugated materials typically exhibit broad and featureless infrared absorption behavior due to their disordered molecular structure and extensive electronic delocalization. In addition, darkened or partially carbonized surfaces tend to strongly absorb and scatter infrared radiation. As a result, the incident infrared beam used in ATR-FTIR measurements may be significantly attenuated before it can interact effectively with the underlying polymer bonds responsible for the characteristic absorption peaks. Consequently, the FTIR spectrum obtained from this altered surface layer may appear largely featureless or show a substantial reduction in the intensity of the expected polymer absorption bands (Stuart 2008). Another contributing factor may be the optical properties of the blackened surface layer. Dark materials generally exhibit high broadband absorbance across the infrared spectral range, which can reduce the penetration depth of the evanescent infrared wave generated during ATR measurements. Because ATR-FTIR typically probes only the upper few micrometers of a material surface, the presence of an optically dense or highly absorbing layer can effectively prevent the spectroscopic detection of the underlying polymer

structure (Griffiths und De Haseth 2007; Stuart 2008).

The results of the XRD and chemical analyses further support this interpretation. The absence of detectable iron oxide phases and the lack of ferric ion detection indicate that the signal suppression cannot be attributed to inorganic contamination originating from the steel service pipe. Instead, the phenomenon appears to be associated primarily with intrinsic chemical modifications of the polyurethane surface resulting from long-term ageing.

PUR foam in district heating pipe assemblies performs several essential functions that directly influence the service life of the system. In addition to acting as thermal insulation, the foam contributes to the structural integrity of the pipe assembly by supporting the steel service pipe, maintaining the bond between the steel pipe and the outer casing, and restricting pipe movement caused by thermal expansion (Alberto Vega, Yarahmadi, und Jakubowicz 2021). During long-term operation, however, PUR foam is exposed to thermal, chemical, and environmental stresses, which gradually lead to degradation of the polymer network and a loss of its initial mechanical and thermal performance (Doyle und Weidlich 2021; França De Sá u. a. 2017). Consequently, reliable analytical methods are required to evaluate the ageing state of the insulation material and to support lifetime assessment of district heating pipelines.

Conclusion

FTIR is widely used to study degradation mechanisms in polyurethane materials because it enables the identification of changes in molecular bonds within the polymer structure. In the present investigation, PUR foam samples taken from district heating pipes that had reached the end of their service life were analyzed using FTIR and complementary characterization techniques. The outer surfaces of the recovered foams were strongly darkened, and FTIR measurements performed directly on these surfaces showed a substantial reduction or complete loss of characteristic absorption bands associated with polyurethane structures. However, when approximately 1 mm of the surface layer was mechanically removed, the typical FTIR spectral features reappeared, indicating that the underlying material still retained detectable molecular characteristics. This observation suggests that the surface layer formed during long-term service interferes with infrared measurements and may mask the spectral information of the underlying polymer.

To determine whether this effect could be related to contamination from the steel service pipe, XRD and chemical analyses were performed to identify possible iron oxide phases or metallic ion migration into the foam. The results showed no detectable traces of iron oxides or other metallic compounds on the foam surface. In addition, NMR analysis was conducted to investigate potential changes in hydrogen distribution across the foam structure, particularly from the steel pipe interface toward the outer casing.

The combined results indicate that the loss of FTIR absorption bands at the foam surface is not associated with metallic contamination but rather with surface modifications that develop during long-term ageing in service. According to (França De Sá u. a. 2017; Grassie und Scott 1988; Stuart 2008), it is hypothesized that these modifications are associated with advanced thermo-oxidative degradation of the polyurethane, leading to the formation of carbon-rich structures, which are known to accompany discoloration in aged polymers. Given the surface sensitivity of ATR-FTIR measurements, such a highly absorbing surface layer may attenuate the infrared signal and obscure the characteristic absorption bands of the underlying materia (Stuart 2008). These findings highlight an important limitation of FTIR when applied directly to severely aged PUR insulation materials. Surface conditions can significantly influence spectroscopic measurements and may lead to misinterpretation of degradation levels if sample preparation is not carefully considered. Therefore, removing the altered surface layer and employing complementary analytical techniques are recommended when assessing the ageing state of PUR foam in district heating systems.

Acknowledgement

The author gratefully acknowledges the financial support of the Federal Ministry for Economic Affairs and Energy of Germany through the project SAM-FW (project number 03EN3078B).
The author also gratefully acknowledges the support and facilities provided by the Civil Engineering Department laboratory at HafenCity Universität Hamburg.

Literatur

Alexander, Leroy E. 1985. X-Ray Diffraction Methods in Polymer Science. Reprint ed. with corr., 3. print. Malabar, Flo: Krieger.

Claridge, Timothy D. W. 2016. High-Resolution NMR Techniques in Organic Chemistry. Third edition. Amsterdam London: Elsevier.

Cornell, Rochelle M., und Udo Schwertmann. 2003. The Iron Oxides: Structure, Properties, Reactions, Occurrences, and Uses. 2nd, completely rev. and extended ed Aufl. Weinheim: Wiley-VCH GmbH & Co. KGaA. doi:10.1002/3527602097.

Cullity, B. D., und Stuart R. Stock. 2001. Elements of X-Ray Diffraction. 3. ed. Upper Saddle River, NJ: Prentice Hall.

Doyle, Lucía, und Ingo Weidlich. 2021. „Effects of Thermal and Mechanical Cyclic Loads on Polyurethane Pre-insulated Pipes". Fatigue & Fracture of Engineering Materials & Structures 44(1): 156–68. doi:10.1111/ffe.13347.

França De Sá, Susana, Joana Lia Ferreira, Isabel Pombo Cardoso, Rita Macedo, und Ana Maria Ramos. 2017. „Shedding New Light on Polyurethane Degradation: Assessing Foams Condition in Design Objects". Polymer Degradation and Stability 144: 354–65. doi:10.1016/j.polymdegradstab.2017.08.028.

Grassie, Norman, und Gerald Scott. 1988. Polymer Degradation & [and] Stabilisation. 1st paperback ed. Cambridge: Cambridge Univ. Press.

Griffiths, Peter R., und James A. De Haseth. 2007. Fourier Transform Infrared Spectrometry. 2nd ed. Hoboken, N.J: Wiley-Interscience.

Harris, Daniel C. 2007. Quantitative Chemical Analysis. 7. ed., 2. print. New York: Freeman.

Hatchett, David W., John M. Kinyanjui, und Linda Sapochak. 2007. „FTIR Analysis of Chemical Gradients in Thermally Processed Molded Polyurethane Foam". Journal of Cellular Plastics 43(3): 183–96. doi:10.1177/0021955X07076665.

Inorganic Chemistry. 2018. 5. Auflage. Harlow: Pearson Education, Limited.

Jakubowicz, Ignacy, Jan Henrik Sällström, Alberto Vega, und Nazdaneh Yarahmadi. 2022. LIFETIME PREDICTIONS AND STATUS ASSESSMENTS OF DISTRICT HEATING PIPELINES. https://energiforsk.se/media/31455/liftetime-predictions-and-status-assessments-energiforskrapport-2022-872.pdf.

Keeler, James J. 2011. Understanding NMR Spectroscopy. Second edition. Chichester: Wiley.

Mehring, M. 1996. „K. Schmidt-Rohr and H. W. Spiess: "Multidimensional Solid-State NMR and Polymers" , Academic Press, London 1994, ISBN 0-12-626630-1, S. 478, Preis: 65 £". Berichte der Bunsengesellschaft für physikalische Chemie 100(6): 1091–1091. doi:10.1002/bbpc.19961000669.

Revie, R. Winston, und Herbert Henry Uhlig. 2008. Corrosion and Corrosion Control: An Introduction to Corrosion Science and Engineering. Fourth edition. Hoboken, NJ: Wiley-Interscience. doi:10.1002/9780470277270.

Schmidt-Rohr, Klaus, und Hans Wolfgang Spiess. 1994. Multidimensional Solid-State NMR and Polymers. London San Diego New York [etc.]: Academic Press.

Skoog, Douglas A., Donald Markham West, F. James Holler, und Stanley R. Crouch. 2022. Fundamentals of Analytical Chemistry. Tenth edition. Australia Brazil: Cengage.

Sperling, Leslie Howard. 2006. Introduction to Physical Polymer Science. 4th ed. New York: J. Wiley & sons.

Stuart, Barbara H. 2008. Infrared Spectroscopy: Fundamentals and Applications. Chichester: Wiley.

Vega, A., N. Yarahmadi, und I. Jakubowicz. 2018. „Optimal Conditions for Accelerated Thermal Ageing of District Heating Pipes". Energy Procedia 149: 79–83. doi:10.1016/j.egypro.2018.08.171.

Vega, Alberto. 2018. „Degradation mechanisms and long-term performance of PUR insulation in district heating pipes". Licentiate of Engineering. CHALMERS UNIVERSITY OF TECHNOLOGY. https://research.chalmers.se/publication/500596/file/500596_Fulltext.pdf.

Vega, Alberto, Nazdaneh Yarahmadi, und Ignacy Jakubowicz. 2021. „Cyclic Axial Loads and Thermal Ageing of District Heating Pipes". Energy Reports 7: 105–9. doi:10.1016/j.egyr.2021.09.033.

Weidlich, Ingo, Gersena Banushi, Nazdaneh Yarahmadi, Ignacy Jakubowicz, Jan Henrik Sällström, Alberto Vega, Jooyong Kim, u. a. 2020. Effects of Loads on Asset Management of the 4th Generation District Heating Networks. International Energy Agency Technology Collaboration Programme on District Heating and Cooling including Combined Heat and Power. https://www.iea-dhc.org/fileadmin/documents/Annex_XII/IEA_DHC_Final_summary_report_Asset_management.pdf?utm_source=chatgpt.com.

Yarahmadi, Nazdaneh, und Jan Henrik Sällström. 2014. Improved maintenance strategies for district heating pipe-lines. https://www.iea-dhc.org/fileadmin/documents/Annex_X/IEA_Annex_X_Final_Report_2014_-_Improved_Maintenance.pdf?utm_source=chatgpt.com.

Yarahmadi, Nazdaneh, Alberto Vega, und Ignacy Jakubowicz. 2017. „Accelerated Ageing and Degradation Characteristics of Rigid Polyurethane Foam". Polymer Degradation and Stability 138: 192–200. doi:10.1016/j.polymdegradstab.2017.03.012.

Fibre optic and embedded sensing concept for long term monitoring of district heating pipes at the District-LAB Kassel

Dennis Lottis
dennis.lottis@iee.fraunhofer.de Fraunhofer IEE, Kassel

Abstract

District heating systems are expected to operate with lower temperatures and a higher share of renewable and volatile heat sources, which increases the need for experimental data on pipe soil interaction and insulation behaviour. This paper presents the concept and realisation of a full-scale district heating test section within the flexible heating grid of the District-LAB at Fraunhofer IEE in Kassel. The measurement setup combines distributed fibre optic temperature sensing on the pipe surface, in the bedding and in the surrounding soil with embedded temperature and humidity sensors in the PUR foam and soil moisture sensors close to the pipes. The paper focuses on the design, installation and initial functional checks of this integrated measurement concept, which provides a platform for future investigations of heat losses, insulation ageing and moisture processes under realistic and dynamic operating conditions.

Introduction

District heating systems consist of heat generation units, distribution grids, and heat consumers. In particular, buried district heating pipe systems in densely populated areas are characterized by high investment costs (AGFW, 2021). This makes them a key leverage point for the politically intended expansion and transformation in the course of decarbonization in Germany and the EU in order to achieve the legally anchored climate protection targets (Deutschland. (2021); European Union. (2021)). Factory pre-insulated pipe systems are the most widely used pipe systems in Germany (AGFW, 2021). Their design and lifetime assessment require detailed knowledge of the thermo-mechanical properties of the pipe assemblies as well as the resulting heat losses. Improved condition monitoring enables an extension of service life and thus an increase in economic and resource efficiency.

In the course of the transformation, district heating systems are expected to be increasingly operated with renewable, often volatile heat sources in the future. It is anticipated that grid temperatures will be progressively reduced and the number of decentralized heat generation units will gradually increase (Lund et al., 2014). In parallel, the use of new pipe materials (e.g. plastics instead of steel), alternative bedding materials and innovative jointing technologies is foreseeable. These changes will have far-reaching impacts on district heating systems.

This work focuses on the thermal interaction between the pipe systems and the surrounding bedding material and their long-term behaviour. The resulting effects on heat losses, insulation ageing and structural integrity can only be predicted to a limited degree and with restricted reliability using conventional, predominantly steady-state models, particularly under dynamic operating conditions (Hay et al., 2025). Against this background, district heating systems are being investigated experimentally in the flexible heating grid of the “District-LAB” experimental facility at Fraunhofer IEE in Kassel (Kallert et al., 2021)but is also put in question. To face these challenges, research on innovative district heating concepts is required like the feed-in of decentralized renewable energy or the design of new modes of operation. Against this background, the new experimental facility District LAB is set up serving as a test and development platform for innovative district heating systems in close cooperation with collaborates from industry and research. By using the facility, it is targeted to investigate the system behaviour of flexible heating networks, to conduct component tests and to develop innovative control concepts for new management strategies. To

DOI: 10.34712/142.81-4

reach these goals the District LAB consists of a flexible heating grid, a pipe test bench for mechanical tests and management respectively control units. This way the possibilities of the already existing facilities are expanded. Compared to tests in real operating district heating grid (demonstration. One focus is on long-term monitoring in the bedding material as well as in the foam region of pipe and joint using fibre-optic distributed temperature sensing in combination with point-wise humidity and temperature sensors. The aim is to capture, by measurement, the influence of reduced operating temperatures and dynamic load profiles on heat losses, ageing processes and service life of the pipe systems, thereby improving the data basis for further investigations.

This paper describes the implemented measurement concept and its installation and presents the results of initial functional tests of the embedded sensors. In terms of its integrated design and density of fibre-optic instrumentation within a district heating test facility, the measurement concept is, to the best of current knowledge, novel. Against this background, the practical experience gained during installation of the measurement system is discussed.

Motivation

To begin with, the influence of ageing-dependent changes in the thermal conductivity of PUR foam on heat losses for an existing heating network with a total length of approx. 13.8 km and a known diameter-length distribution of the pipes is calculated in a motivating manner.

The thermal conductivity of PUR foam is determined by the proportions of solid material, radiation and cell gases, with the cell gases having a significant influence on the overall thermal conductivity. Due to permeation processes, the gases diffuse from the foam cells through the PE coating into the environment over the course of the product's service life. The cell gases originally contained in the foam, such as cyclopentane and carbon dioxide, which have low thermal conductivity, are replaced by ambient atmospheric gases such as oxygen and nitrogen, which have significantly higher thermal conductivity. This leads to a gradual increase in overall thermal conductivity and thus to higher heat losses.

In (Frederiksen & Werner, 2013), the change in thermal conductivity of PUR foam over 30 years is given for some nominal diameters (DN) of the insulation series one. To perform the calculation for the heating network, values for additional DNs are also required. These are determined using linear interpolation. The result is shown in Figure 1. Solid lines are values taken from (Frederiksen & Werner, 2013), while dotted lines are interpolated. It can be seen that the thermal conductivity is identical for all diameters immediately after manufacture and then increases over time. The magnitude of this increase depends on the diameter. A significantly greater increase can be seen for small diameters.

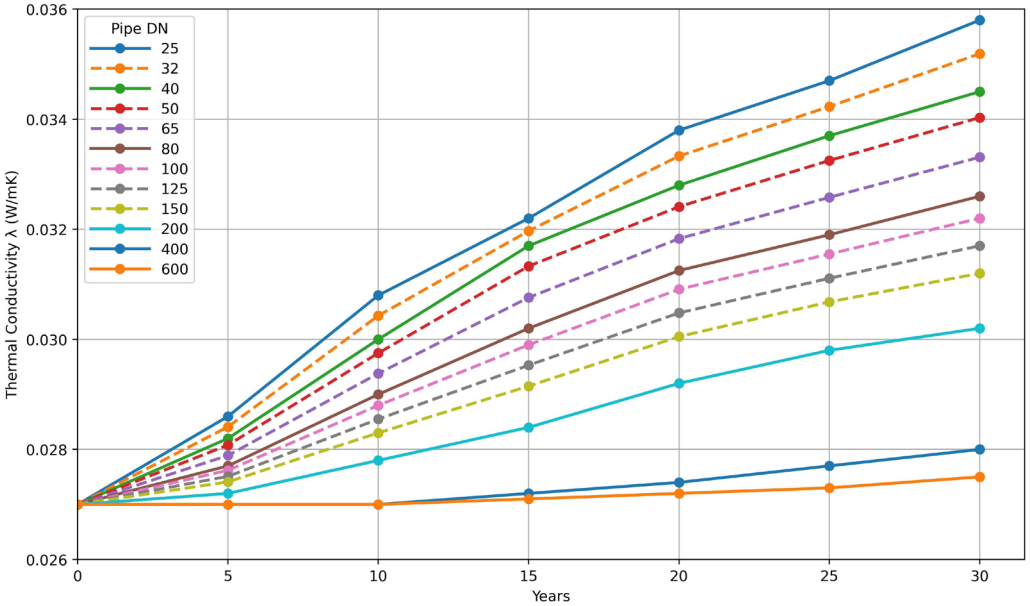

Figure 1: Change in the thermal conductivity of PUR foam over 30 years for insulation series one. Solid lines are taken from (Frederiksen & Werner, 2013); dotted lines are interpolated.

The heat losses $\dot{Q}_{loss}$ of pre-insulated pipe systems are calculated with Equations (1) and Equation (2) (Frederiksen & Werner, 2013, pp. 78–79). The definitions of the used geometric dimensions are shown in Figure 2. In order to perform the calculation, numerical values according to Table 1 are used in addition to the information on the length-diameter distribution in the heating network.

$$\dot{Q}_{loss} = L\pi d \frac{(T_{sup} - T_g) + (T_{ret} - T_g)}{R_i + R_g + R_c} \quad (1)$$

With the length of the pipe L, supply, return and ground temperature T_{sup}, T_{ret} and T_g and the thermal resistances R_i, R_g and R_c which are defined as:

$$R_i = \frac{d}{2\lambda} ln\left(\frac{D}{d}\right), \qquad R_g = \frac{d}{2\lambda_g} ln\left(\frac{4H}{D}\right), \qquad R_c = \frac{d}{2\lambda_g} ln\left(\sqrt{\left(\frac{2H}{s}\right)^2 + 1}\right) \quad (2)$$

with the cover height h, the pipe spacing a and the thermal conductivity of the soil λ_g (see Figure 2).

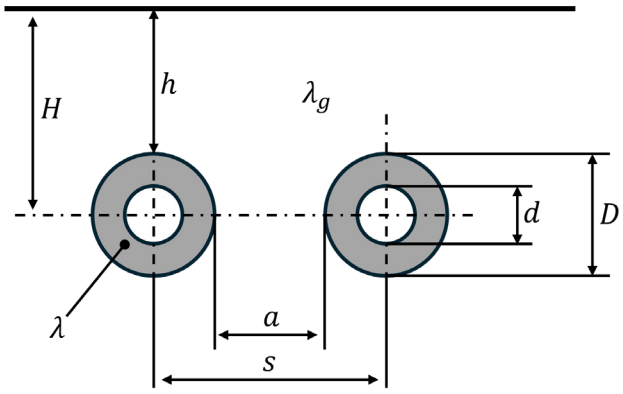

Figure 2: Definition of parameter names for geometry

Parameter	Value
T_{sup} [°C]	100
T_{ret} [°C]	60
T_g [°C]	10
h [m]	0.8
a [m]	0.2
λ_g [W/mK]	1.2

Table 1: Numerical values used for the calculation

Figure 3: Network-weighted relative heat loss Increase over time shows the calculated relative heat losses of the district heating system, along with the relative shares of pipe diameters used in the calculation. PUR ageing is represented solely by an increase of the thermal conductivity λ_{PUR} in and all other parameters are kept constant according to Table 1: Numerical values used for the calculation. Also, it is assumed that all pipes were manufactured at time $t = 0$. This point in time also serves as the reference for the percentage increase in the calculated relative heat losses. The black curve illustrates that, after 30 years, the heat losses increase by approximately 20 %. This increase is well approximated by a linear trend, represented by the red linear fit. The corresponding fit equation indicates that the relative heat losses rise by about 0.7 % per year.

These results suggest that ageing of the PUR insulation leads to a noticeable increase in distribution heat losses over the lifetime of a district heating system and should therefore be taken into account in long-term energetic, environmental, and economic assessments. However, the present calculation is based on a simplified steady-state approach with idealised, temporally constant operating temperatures. In real district heating systems, especially with the increasing integration of volatile renewable heat sources, frequent and sometimes rapid changes in operating conditions are to be expected. Such dynamic temperature variations may affect the ageing behaviour of the PUR foam and thus its effective thermal conductivity, potentially leading to deviations from the quasi-linear trend assumed here. Against this background, more detailed investigations under dynamic boundary conditions, for example using transient simulations or long-term field measurements, appear necessary in order to robustly quantify the impact of volatile operating strategies on the evolution of heat losses. In order to address these limitations and to better understand the coupled thermal and hygric behaviour of pre-insulated district heating pipes under realistic and

dynamic operating conditions, the following research questions are formulated, which guide the design of the implemented measurement concept in the District-LAB:

1. To what extent can distributed fibre optic temperature sensing capture asymmetric heat flows, thermal interaction between neighbouring pipes and locally altered heat transfer conditions, for example in expansion sections?
2. How do reduced operating temperatures and more volatile renewable heat inputs affect the ageing behaviour of PUR insulation and its effective thermal conductivity under realistic moisture conditions?
3. How do moisture dynamics in the PUR foam and in the sand bedding evolve over time, and how reliably can embedded humidity sensors and soil moisture sensors detect and quantify these processes?

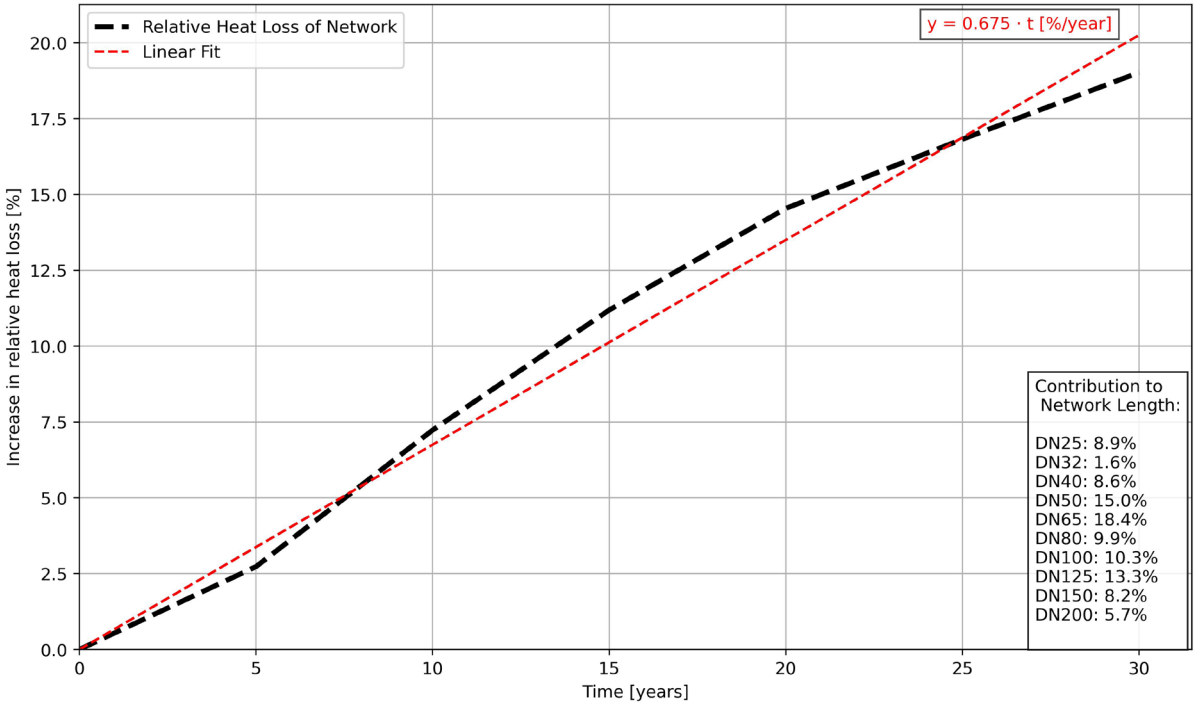

Figure 3: Network-weighted relative heat loss Increase over time

Methodology

Experimental setup/District-LAB

In Figure 4: Aerial view of the District LAB during construction work, with the experimental fields “pipe test bench” (blue) and “flexible heating grid” (green) marked., an aerial view of the District-LAB during the pipe construction work is shown. The test facility comprises two experimental areas: the area highlighted in blue shows the experimental field “pipe test bench”. Here, tests focusing on the interaction between pipelines and bedding material are carried out in close cooperation with the Technical Infrastructure Management group of Prof. Weidlich. Details on the setup and the measurement concept of the pipe test bench can be found in the contribution by Stefan Dollhopf within this “Insights”. The area highlighted in green contains the experimental field “flexible heating grid”, which also includes the long-term experiments discussed in this paper. This is necessary because only for these pipelines operating periods of several years are to be expected.

The flexible heating grid is approximately 35 m long and about 6 m wide and consists of two levels, each with five pipelines arranged in a U-shape. At the end, there is an expansion section with expansion pads. The gaps between the pipes as well as between the two pipe levels are backfilled with sand followed by

excavated material. The cover height above the upper pipelines is approximately 0.7 m to ensure the required mechanical and thermal properties. The cross-section of the flexible heating grid is shown in Figure 8: Cross-section of the flexible test grid and route of the fibre-optic measuring cable on the outer pipes. It illustrates further geometrical dimensions of the structure, including the spacing between individual pipes and the vertical distance between the levels. Further details and information can be found in (Kallert et al., 2021)but is also put in question. To face these challenges, research on innovative district heating concepts is required like the feed-in of decentralized renewable energy or the design of new modes of operation. Against this background, the new experimental facility District LAB is set up serving as a test and development platform for innovative district heating systems in close cooperation with collaborates from industry and research. By using the facility, it is targeted to investigate the system behaviour of flexible heating networks, to conduct component tests and to develop innovative control concepts for new management strategies. To reach these goals the District LAB consists of a flexible heating grid, a pipe test bench for mechanical tests and management respectively control units. This way the possibilities of the already existing facilities are expanded. Compared to tests in real operating district heating grid (demonstration.

Figure 4: Aerial view of the District LAB during construction work, with the experimental fields “pipe test bench” (blue) and “flexible heating grid” (green) marked.

Fibre optic measurement technology

Compared to conventional temperature measurement methods, in which temperatures are measured at specific points on the pipe or in the ground using individual sensors, fibre optic measurement technology enables continuous temperature measurement along the entire length of the laid fibre optic cable. This replaces a large number of individual sensors and allows temperature profiles to be recorded with high spatial resolution both on the outside of the pipes and in the surrounding bedding material. The District-LAB

uses the OSSCAD CMS-1022 system with a cable length of 2000 m.

The fibre optic measurement system essentially consists of a fibre optic cable that functions as a linear temperature sensor and an evaluation device equipped with a laser source and optoelectronic detectors. The measuring device injects short laser pulses into the fibre optic cable and detects the light scattered back along the fibre. The temperature as a function of position along the fibre can be determined from the time delay and spectral composition of this backscattered signal. In this way, a continuous temperature profile can be calculated over the entire length of the cable, allowing local temperature changes, leaks or anomalies in the network to be measured.

Figure 5: Course of the fibre optic measuring cable for longitudinal measurement

Figure 5: Course of the fibre optic measuring cable for longitudinal measurement shows the routing of the fibre-optic cable for the longitudinal measurement on the outer pipe in the lower level. The cables follow the U-shape and are installed once at the 12 o'clock position and once at the 6 o'clock position of the outer pipe. No longitudinal measurements are carried out on the four inner pipelines. The same configuration is used for the upper level.

The fibre-optic cable has continuous metre markings printed on it at regular intervals. These can also be seen in the yellow fields. During commissioning of the measurement system, they will be used to subdivide the individual measurement sections.

Figure 6: Installation of the fibre optic cable on the outer pipes

Figure 6: Installation of the fibre optic cable on the outer pipes shows details of the installation of the fibre-optic cable for the longitudinal measurement. The cable is taped to the upper side of the pipe (top left) as well as to the lower side of the pipe (top right). To keep the distance between cable and pipe as small as possible, the cable is also fixed firmly to the pipe at regular intervals using cable ties. This arrangement along the entire length enables continuous acquisition of the pipe surface temperature at the upper and lower edge of the pipe and thus possibly the detection of asymmetric temperature distributions.

Figure 6: Installation of the fibre optic cable on the outer pipes also shows the expansion pads and the routing of the fibre-optic cable in this area. Here, too, the fibre-optic measurement cables are fixed to the upper and lower sides of the pipe casing. Above the measurement cables, expansion pads and mats are installed. The primary function of the expansion pads is to accommodate thermal longitudinal expansion of the pipeline in a controlled manner and to dissipate mechanical stresses. This area is of scientific interest: in contrast to the rest of the pipeline section, the direct contact between the pipe wall and the surrounding sand is missing here, as the expansion pads act as a separating layer. This leads to locally altered heat transfer conditions and the associated temperature gradients along the pipe axis. The aim of using fibre optics in this area is to capture these temperature differences and to use them for a quantitative assessment of heat losses caused by heat accumulation in the expansion section.

In addition to the longitudinal measurements, transverse measurements were also implemented using fibre-optic sensing. The routing of the measurement cable for the transverse measurements is illustrated in Figure 7: Course of the fibre-optic measuring cable during transverse measurement. In the area of the crossings marked in blue, each pipeline is wrapped three times with the measurement cable. This is intended to enable the analysis of both local temperature gradients on the pipe surface and thermal interactions between adjacent pipes. In particular, the differences in temperature distribution between the sections facing neighbouring pipes and the outward-facing pipe sections are to be captured, allowing a more differentiated assessment of the thermal interaction within the pipe bundle.

The areas marked in orange indicate sections where the cable was placed directly on the slope at the interface between the natural soil and the sand bedding. The intention is to obtain comparative temperature measurements in practically unaffected ground. This configuration is identical on the upper and lower pipe levels.

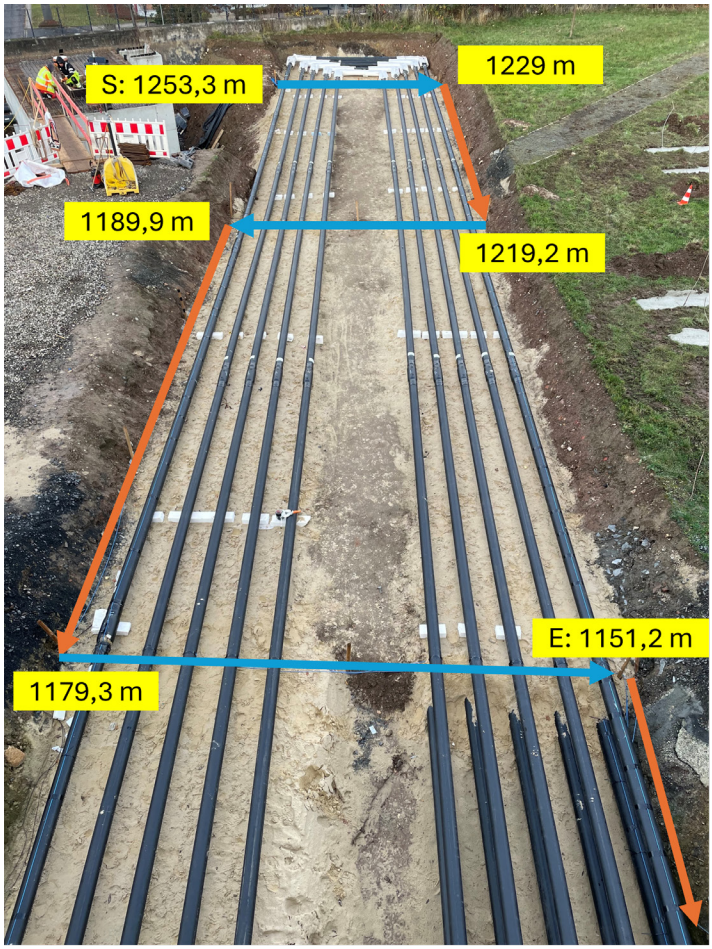

Figure 7: Course of the fibre-optic measuring cable during transverse measurement

The experimental implementation of the described measurement concept for the transverse measurements is shown in Figure 9: Installation of the fibre-optic measuring cable on the pipes by winding it around them and on the slope using wooden pegs.. The figure illustrates the actual routing of the measurement cable, the wrapping around the pipes, and the routing directly along the slope using wooden stakes, as well as its fixation to the pipe by means of adhesive tape and cable ties.

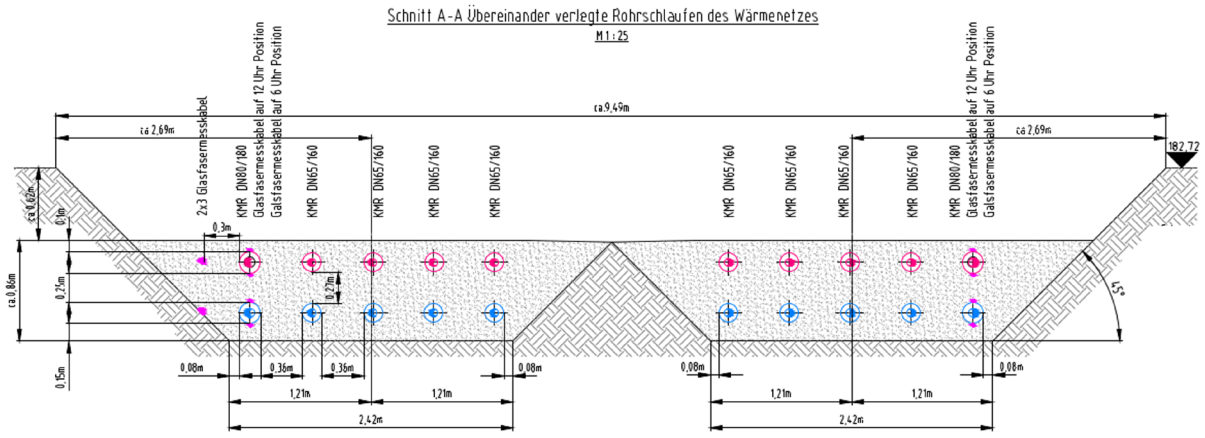

Figure 8: Cross-section of the flexible test grid and route of the fibre-optic measuring cable on the outer pipes

Figure 8: Cross-section of the flexible test grid and route of the fibre-optic measuring cable on the outer pipes shows the cross-section of the structure with the most important geometrical dimensions. The fibre-optic cable installation on the upper and lower sides of the outer pipes, as described above, as well as in the slope area is also illustrated.

Figure 9: Installation of the fibre-optic measuring cable on the pipes by winding it around them and on the slope using wooden pegs.

In addition to the longitudinal and transverse measurements directly on the pipelines, the fibre-optic cable was also installed in the sand bedding midway between the two levels and directly at the interface between sand and natural soil (see Figure 8: Cross-section of the flexible test grid and route of the fibre-optic measuring cable on the outer pipes). The aim of this installation is the continuous recording of thermal effects in the sand that arise as a result of the different temperature conditions in the pipelines. The cable routing geometries used for this purpose are shown in Figure 10 and Figure 11. Figure 10 illustrates the installation between the two pipe levels, and Figure 11 shows the installation at the interface between sand and natural soil.

Figure 10: Cable routing on the level between the pipes

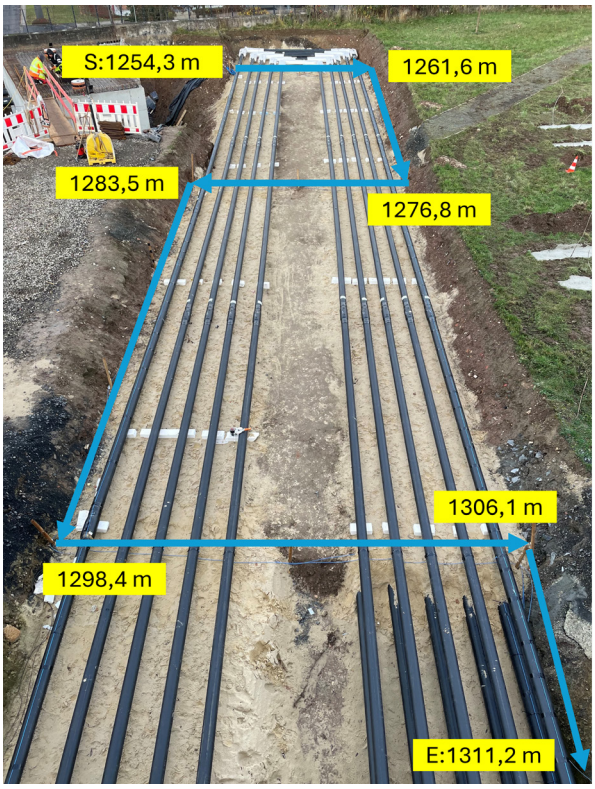

Figure 11: Cable routing at interface between sand and natural soil

Embedded sensors in PUR and joints

Even small amounts of water or moisture in the PUR foam can critically affect the material properties and, in extreme cases, lead to damage of the pipe. For this reason, leakage detection systems are used in district heating pipes in order to localize water ingress in the pipeline network at specific points and thus prevent more extensive damage. The most commonly used system consists of two wires that are foamed into the insulation. If water penetrates into the foam, for example due to a leak, damage to the outer casing, leakage at joints, or diffusion processes, the electrical resistance of the wires changes, enabling the fault to be detected and localized.

However, this system is not suitable for continuous monitoring of changes in the water content within the foam. To capture these changes under operating conditions, more advanced measurement technology is required. For this reason, the flexible test network was additionally equipped with embedded moisture sensors and temperature probes in the foam. In a pre-insulated pipe DN80/160, two sensors were installed before foaming: a PT1000 temperature sensor EU-325-G10000-0 from Driesen + Kern GmbH, positioned approximately 3 m from the pipe end directly on the outside of the carrier pipe, and a DKRF517 sensor from Driesen + Kern GmbH, which can measure both temperature and relative humidity and which was likewise placed at a distance of about 3 m from the pipe end, approximately midway between the outer surface of the steel pipe and the inner surface of the plastic jacket. The installation condition of the sensors is shown in Figure 12: Installation of the humidity and temperature sensor and the surface temperature sensor in the pipe. Figure 13: Sensors foamed into the pipe shows the sensors embedded in the pipe foam.

Figure 12: Installation of the humidity and temperature sensor and the surface temperature sensor in the pipe

Figure 13: Sensors foamed into the pipe

The embedded sensors were tested a few days later in order to verify their functionality. For this purpose, the fully foamed pre-insulated pipe was brought into a heated laboratory hall after spending a cool night outdoors. There, both sensors were connected to a control unit to display and record their output signals. First, a short-term recording was carried out, followed by a second short-term recording after a brief interval. Subsequently, a long-term recording was started. After the long-term recording had been running for some time, an additional sensor for measuring the room temperature was connected. The recorded temporal profiles of temperature and relative humidity are shown in Figure 15: Measurement results of the temperature sensors: PT1000 surface temperature sensor on the carrier pipe (blue), combined temperature and humidity sensor in the middle of the foam (red) and air temperature sensor in the laboratory

(yellow) and Figure 16: Measurement results of the relative humidity recorded by the sensor located in the middle of the foam..

An identical setup was implemented during the installation of the joint connection in the area of the first joint, i.e. after the first 6 m of the pipe section that had been prepared with sensors. For routing the sensor cables, a welded nozzle was used. Fibre-optic cable was subsequently also installed in this area. Finally, the nozzle was protected with expansion pads to prevent it from tearing off due to the temperature-induced expansion of the pipe. In the last step, SMT100-10-10000-0 soil moisture sensors from Driesen + Kern GmbH were placed in the sand bedding in the immediate vicinity of the measurements inside the pipe and the joint. This setup is shown in Figure 14: Joint with welded nozzle for routing the sensor cables.

Figure 14: Joint with welded nozzle for routing the sensor cables

Results

Testing of the embedded sensors

The following Figure 15: Measurement results of the temperature sensors: PT1000 surface temperature sensor on the carrier pipe (blue), combined temperature and humidity sensor in the middle of the foam (red) and air temperature sensor in the laboratory (yellow) shows the measured temperature profiles of the embedded sensors and of the test room over a period of approximately 23 hours. Here, blue indicates the PT1000 surface temperature sensor directly on the carrier pipe, red indicates the combined temperature and humidity sensor located in the middle of the foam, and yellow indicates a temperature sensor used to measure the air temperature in the laboratory hall.

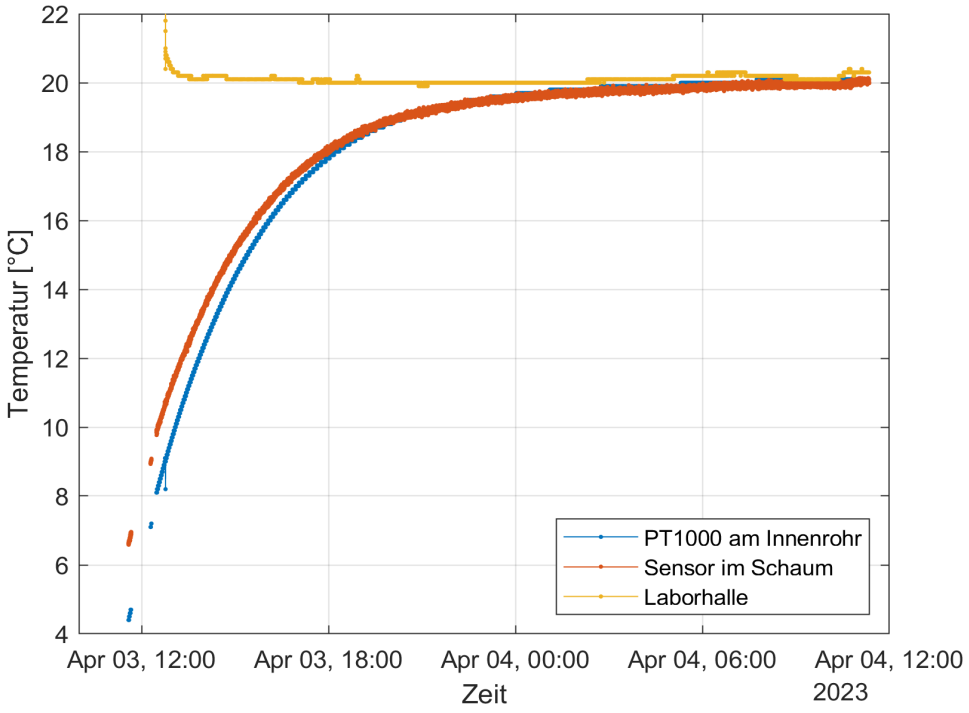

Figure 15: Measurement results of the temperature sensors: PT1000 surface temperature sensor on the carrier pipe (blue), combined temperature and humidity sensor in the middle of the foam (red) and air temperature sensor in the laboratory (yellow)

At the beginning of the measurements, the temperatures in the pipe were low due to outdoor storage combined with frost during the night. The differing initial temperature values can be explained by the morning sunlight to which the pipe was exposed outside. The sensor located in the middle of the foam was more strongly affected by this than the PT1000 sensor mounted on the inner pipe. Over the course of several hours, the temperatures inside the pipe adjusted to the room temperature. This demonstrated that both sensors are capable of capturing the heating process through the PUR foam and representing the thermal inertia of the pipe structure.

Figure 16: Measurement results of the relative humidity recorded by the sensor located in the middle of the foam. shows the development of the measured relative humidity. A slight decrease in relative humidity can be observed during the measurement period. This decrease can be attributed to the warming to room temperature: if the absolute moisture content in the foam remains constant, the relative humidity decreases as the temperature rises. Due to the installed position, it was not possible to deliberately expose the sensor to humid air during this test. Nevertheless, the measurement results confirm the fundamental functionality of the humidity sensor in the embedded condition.

From these results it can be concluded that the sensors withstood the foaming process well and remain fully functional.

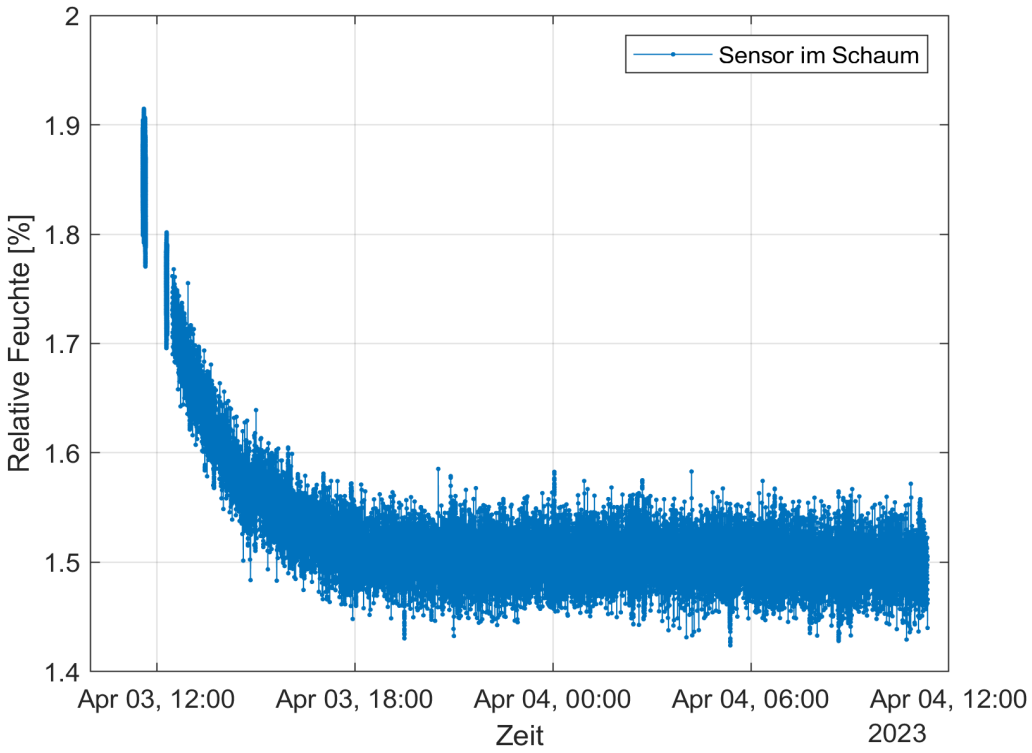

Figure 16: Measurement results of the relative humidity recorded by the sensor located in the middle of the foam.

Practical experience with fibre optic measurement technology

In practical use, the fibre optic measuring cable proved to be robust and durable overall. However, due to its stiffness, the cable tends to roll up on its own, so regular and sufficiently tight fastening is necessary to ensure accurate positioning. On the positive side, the cable can be cut if necessary and later reconnected by splicing. Fastening it to the pipes with adhesive tape and cable ties worked well as long as the pipes were completely accessible and dry. If the pipes were already partially filled or moist, mounting adhesive had to be used instead, which proved to be much more difficult and time-consuming. Overall, it became clear that careful planning of the cable routing is essential. In particular, accessible loops should be provided to enable subsequent sectioning, for example using cold spray. When laying the cable, it is very helpful to have several people working together to avoid tangling ('cable salad'). In addition, careful documentation of the laying process is necessary in order to be able to clearly assign the subsequent measurement data to specific locations. The measurement system has not yet been commissioned, so no results can be presented at this stage.

Discussion and Conclusion

The measurement concept implemented in the District-LAB combines fibre-optic measurement cables at the pipe surface and in the bedding with embedded temperature and humidity sensors in the PUR foam and soil moisture sensors in the surrounding sand. This provides a comprehensive basis for experimental investigation of district heating systems. Distributed fibre optic sensing enables spatially highly resolved and almost continuous temperature measurements along the pipe route, around the pipe circumference and in the bedding. This makes it possible to analyse stationary temperature fields and dynamic effects caused by volatile renewable heat inputs, reduced operating temperatures and innovative operating strategies. The transverse winding of the cable helps to detect asymmetric heat flows and thermal interaction

between neighbouring pipes, while the cable in the bedding captures the propagation of heat in the sand layers and the adjacent ground. The specific instrumentation in the expansion section allows a more detailed assessment of modified heat-transfer conditions and possible heat accumulation.

The embedded sensors in the PUR foam provide additional information on the condition of the insulation. The tests of the foamed in PT1000 sensor and the combined temperature and humidity sensor show that both the thermal inertia of the pipe structure and changes in relative humidity inside the foam can be captured. This enables more continuous and condition-based monitoring than with conventional leak detection alone. Together with the understanding of PUR ageing and the associated increase in thermal conductivity, the measurement setup offers the potential to estimate thermal conductivity, heat losses and service life of the pipe system more accurately under realistic operating conditions. In particular, the influence of lower operating temperatures and volatile renewable heat sources on PUR ageing and moisture ingress can be investigated, which is crucial for the long-term efficiency and stability of district heating systems.

In summary, the measurement concept realised in the District-LAB provides the basis for evaluating transformation strategies in the district heating sector in an experimentally supported way. These strategies include reduced temperature levels, the use of new pipe materials, alternative bedding materials and new operating concepts. The data obtained from the facility will make it possible to quantify more reliably how these measures affect heat losses, insulation condition and service life. This supports the targeted optimisation of future district heating networks with respect to efficiency, operational reliability and decarbonisation.

Declaration of Generative AI and AI-assisted technologies in the writing process

During the preparation of this work the author used FhGenie by Fraunhofer in order to improve the linguistic clarity and grammar. After using this tool/service, the author reviewed and edited the content as needed and takes full responsibility for the content of the publication.

Acknowledgments

This research was conducted as part of the Project EnEff:Wärme: UrbanTurn, which is funded by Federal Ministry for Economic Affairs and Energy (BMWE) under grant number 03EN3029A. The author gratefully acknowledges this support.

References

AGFW. (2021). Praxishilfe Fernwärmeleitungsbau – Verlegesysteme und Kosten.

Deutschland. (2021). Erstes Gesetz zur Änderung des Bundes-Klimaschutzgesetzes vom 18. August 2021. Bundesgesetzblatt I, 2021(54), 3905–3913. Abgerufen von https://www.bgbl.de/xaver/bgbl/start.xav?startbk=Bundesanzeiger_BGBl&jumpTo=bgbl121s3905.pdf

Frederiksen, S., & Werner, S. (2013). District heating and cooling. Studentliteratur.

Hay, S., Deselaers, T., Huther, H., Weidlich, I., Langgroudi, P., Dollhopf, S., Kropp, I., Schwarze, M., Cadenbach, A. M., Lottis, D., Dittmer, H., Urbaneck, T., & Zimmerling, N. (2025). Sustainable Asset Management Fernwärme: Wie vorausschauende Instandhaltungsstrategien und Nachhaltigkeitskriterien im Asset Management von Wärmenetzen genutzt werden können—Aktueller Stand und zukünftige Entwicklungen -. https://cloud.agfw.de/d/fe228d68960c4cd981e5/files/?p=/Praxisleitfaden%20Sustainable%20Asset%20Management.pdf

Kallert, A., Lottis, D., Shan, M., & Schmidt, D. (2021). New experimental facility for innovative district heating systems—District LAB. Energy Reports, The 17th International Symposium on District Heating and Cooling, 7, 62–69. https://doi.org/10.1016/j.egyr.2021.09.039

Lund, H., Werner, S., Wiltshire, R., Svendsen, S., Thorsen, J. E., Hvelplund, F., & Mathiesen, B. V. (2014). 4th Generation District Heating (4GDH). Energy, 68, 1–11. https://doi.org/10.1016/j.energy.2014.02.089

European Union. (2021). Regulation (EU) 2021/1119 of the European Parliament and of the Council of 30 June 2021 establishing the framework for achieving climate neutrality and amending Regulations (EC) No 401/2009 and (EU) 2018/1999 (European Climate Law). Official Journal of the European Union, L 243, 1–17.

The Role of Exergy and Emissions in Municipal Heat Planning: Insights from Hamburg

Violeta Madan
violeta.madan@hcu-hamburg.de HafenCity University, Hamburg

Abstract

As part of municipal heat planning, large cities such as Hamburg are required to develop a heat plan by the end of June 2026. A central challenge is the substitution of heat supply in urban areas currently connected to the gas network. For a sustainable heat supply, district heating networks mainly compete with decentralized heat supply using air-to-water heat pumps. The decision to implement a district heating network often relies on linear heat density as a key criterion. This study examines heat planning in three Hamburg districts, comparing current primary energy, greenhouse gas emission, and resource exergy factors for different heat supply options. The results suggest that the primary energy factor is influenced by political frameworks, while the greenhouse gas emission factor depends on the applied accounting methodology. The resource exergy factor provides a physically consistent evaluation metric for assessing the efficiency of local heat supply options and is the only factor investigated in this study that can distinguish among renewable energy sources. Considering the current electricity mix and the assumptions made, combined heat and power plants and waste heat utilization in district heating networks outperform air-to-water heat pumps. The study also reveals a prevailing tendency toward decentralized heat supply as a substitute for gas-connected districts, which poses significant lock-in risks. These risks stem primarily from the recent abolition of the so-called 65 % renewable energy obligation, which may prolong the use of fossil-fuel-based heating systems. At the same time, large-scale deployment of decentralized heat pumps may substantially increase electricity demand, so that both developments may adversely affect the energy transition. The findings suggest that linear heat density alone is insufficient and underscore the necessity of a holistic, locally differentiated assessment framework. Integrating exergy analysis and life cycle assessment into future municipal heat planning to assess efficiency and material consumption is proposed as a holistic approach to effectively achieve climate-neutral heat supply in Hamburg.

Introduction

Heating in buildings represents a crucial sector for meeting Hamburg's climate protection goals, as it accounts for around 30 % of both the city's final energy consumption and its greenhouse gas (GHG) emissions (FHH & BUKEA, 2024). The Heat Planning Act (WPG), embedded in the 2023 Climate Protection Plan, requires large cities and municipalities to prepare a heat plan by 2026 and 2028, respectively (WPG, 2023; FHH, 2023). Municipal heat planning is intended to provide a holistic framework for the systematic transformation of regional heat supply, involving relevant stakeholders in the planning process (BUKEA, 2025a).

According to the regional report of the German Association of Energy and Water Industries (BDEW), approximately 43 % of residential buildings in Germany were supplied by a central gas boiler in 2023. In Hamburg, around 53 % of residential buildings were connected to the gas network in the same year (BDEW, 2025). Hamburg's climate strategy envisages a gradual transition towards sustainable, low-carbon heat supply solutions. The phase-out of conventional natural gas supply is legally mandated by 2045; corresponding strategies foresee that parts of the existing gas network will be gradually decommissioned or repurposed for alternative energy carriers (Sandrock et al., 2025). According to the WPG, possible alternatives include repurposing gas networks by replacing natural gas with "green" gases, connecting buildings to district heating networks, or implementing decentralized heat supply systems. Until now, the Building Energy Act (GEG) has required a minimum share of renewable energy in new heating systems (WPG, 2023; GEG, 2020). However, a recent key issues paper by the German government proposes abolishing this requirement (the so-called 65 % rule), which would again allow the installation of fossil gas and oil heating

DOI: 10.34712/142.81-5

systems in the future (Bundesregierung, 2026).

This paper aims to analyse the evaluation criteria used in municipal heat planning in Hamburg. Heat supply alternatives are assessed from both GHG emission and resource exergy perspectives, with a particular focus on district heating systems and decentralised air-to-water heat pumps. The analysis is conducted for three case-study neighbourhoods with different local conditions. The alternatives are evaluated using primary energy, GHG emission, and resource exergy factors, and the gaps in the current evaluation framework are identified.

State of knowledge

Municipal heat planning in Hamburg

Municipal heat planning in the Free and Hanseatic City of Hamburg (FHH) aims to assess the suitability of climate-neutral options for supplying building and process heat. The planning process is defined in Section 13 of the Heat Planning Act (WPG) and comprises several steps, ranging from suitability testing to the development of an implementation strategy with concrete measures for achieving the target scenario.

Guidelines published by the Federal Ministry of Housing, Urban Development and Construction (BMWSB) require that the suitability of both district heating networks and hydrogen networks be assessed. Among other factors, the building structure of a neighbourhood can be used to evaluate the suitability of district heating. In areas with dense single-family housing, the economic operation of a heating network can only be ruled out if no existing heating network is present in the sub-area or its immediate vicinity and, at the same time, no favourable renewable energy source or unavoidable waste heat source can be utilised (BMWSB, 2024).

For the city of Hamburg, the Authority for the Environment, Climate, Energy and Agriculture (BUKEA) defines the following key assessment criteria for municipal heat planning:

- heat demand density
- surface characteristics of the installation area
- economic feasibility

According to the BUKEA guidelines, district heating networks and air-to-water heat pumps are considered the dominant future technologies for Hamburg's heat supply. District heating networks are prioritised in the guidelines because they enable the efficient and cost-effective distribution of renewable heat sources and unavoidable waste heat. Furthermore, the decision cascade proposed by BUKEA suggests that heat pumps are prioritised over other decentralised heat supply concepts (BUKEA, 2025a).

The resulting preliminary target scenario was published on 16 March 2026 in the Hamburg Heat Register, and the corresponding report was released by FHH & BUKEA (2026).

Linear heat density

The linear heat density of a district heating network is defined as the ratio of heat demand to the network route length (with supply and return pipes counted as a single route). In the Hamburg Heat Register, linear heat density is reported separately for renovated and unrenovated buildings in units of MWh/(m·a). In the context of municipal heat planning, Dochev et al. recommend using linear heat density as a key indicator, as it accounts for the network length and therefore requires hypothetical network modelling (Dochev et al., 2018).

The following table provides an overview of typical linear heat densities in various countries, as analysed in the International Energy Agency (IEA) status report on district heating systems.

Table1 : Typical linear heat densities for district heating systems in different countries

Country	Share of district heating in the final energy mix for heat supply* (Rambøll, 2020)	Typical linear heat densities (Nussbaumer & Thalmann, 2014)	Typical heat losses (Nussbaumer & Thalmann, 2014)
Germany	14 %	2.0 MWh/(ma)	17 %
Denmark	65 %	0.7 MWh/(ma)	25 %
Finland	38 %	1.9 MWh/(ma)	14 %
Switzerland	4 %	1.9 MWh/(ma)	12 %
Austria	14 %	1.1 MWh/(ma)	19 %

*The figures from (Rambøll, 2020) have been rounded to whole numbers

In general, the higher the linear heat density of an area, the more likely it is considered as a district heating area. Various reference values are used for evaluation. The guidelines published by BMWSB classify areas with a linear heat density of 0.7 MWh/(m·a) or higher as having “medium suitability” for district heating (BMWSB, 2024). In practice, a value of 1.5 MWh/(m·a) is often applied as the threshold for the economically viable operation of a heating network. This value serves primarily as an economic benchmark for network operators in Germany to ensure that investment costs and network losses remain proportionate to the amount of heat delivered (Pfnür et al., 2016). For municipal heat planning in Hamburg, the Heat Register specifies threshold values of 1.5 MWh/(m·a) for new development areas and 2 MWh/(m·a) for existing building areas (FHH & BUKEA, 2019).

The comparison of linear heat densities in Table 1 shows that the average values in Germany, Finland, and Switzerland are considerably higher than those in Austria and Denmark. Interestingly, Denmark has the highest share of district heating, suggesting that even areas with relatively low linear heat densities can technically support a widespread district heating network. For Hamburg, the theoretical techno-economic potential of district heating is estimated at approximately 80 % of the building heat demand (BUKEA, 2025a).

Primary energy factor

The non-renewable primary energy factor (PEF) is defined as the ratio of non-renewable primary energy to final energy. The approach was developed in studies by the Wuppertal Institute for Climate, Environment and Energy in the 1990s and has become established in the energy assessment of buildings. Its application is regulated in Section 22 of the GEG. According to the GEG, only the non-renewable portion of primary energy is assessed. Some of the primary energy factors specified in the GEG are based on political decisions and therefore deviate from a physical definition (GEG, 2020).

Emission factor

The greenhouse gas (GHG) emission factor (EF) is a parameter used to assess the climate impact of processes or products. It is defined by the ratio of GHG emissions caused to the final energy provided and is specified in the GEG in the unit g CO_2 equivalent per kWh. For the calculation of the EF, a time horizon of 100 years is usually considered. District heating operators report a specific GHG emission factor for the respective network as part of the energy assessment in accordance with AGFW worksheet FW 309-1. The methodological derivation and the parameters and GHG emission factors required for the calculation for district heating systems are presented in detail in this worksheet. (AGFW, 2023) In the Hamburg Heat Register, heating networks are characterised using the GHG emission factor according to FW 309-1 (corresponding to the calculation in Annex 9 of the GEG) as well as the GHG emission factor determined by the reference value method (also known as the Finnish method). The calculation according to FW 309-1 is based on the electricity credit method, which results in lower GHG emission factors for heat generated in CHP plants under the current electricity mix. FW 309-6 (2023) describes the Carnot method, based on Car-

not efficiency, which provides a physically grounded approach for allocating heat and electricity production. Nevertheless, most district heating certifications apply only the electricity credit method according to FW 309-1. The Umweltbundesamt (2016) provides an overview of the relevant allocation methods for CHP.

Resource exergy factor

The resource exergy factor (REF) is a key metric of resource exergy analysis (REA) and enables the thermodynamic evaluation and comparison of energy systems. REF is defined as the ratio of resource exergy consumption to the final energy delivered and can be calculated for various energy systems and fuels following the methodology outlined in the REA (Jentsch, 2025).

An exergy-based assessment considers not only the quantity of energy but also its quality, allowing exergy losses to be identified and optimization potentials to be highlighted comprehensively. Conventional primary energy or GHG emission factors do not permit a meaningful comparison between renewable energy sources, as they are often assigned zero. However, a comparison of the resource exergy consumption of a hydrogen combustion boiler with that of a fossil-fuel combined heat and power (CHP) plant demonstrates that renewable energies are not inherently equivalent, and resource consumption must be considered in a future climate-neutral energy system to avoid indirect GHG emissions due to inefficiencies (Jentsch, 2024).

The following simplified formulas from the REA were applied to calculate the REFs in this study (Jentsch, 2025):

Air-to-water heat pumps:

$$f_{R,WP} = \frac{f_{R,el}}{APF} \qquad \text{Equation 1}$$

Where

$f_{R,el}$ =REF of the drive energy

APF=Annual performance factor

The calculation according to equation 1 is only applicable under the assumption that the outside air temperature corresponds to the reference temperature T_0 and the heat pump is electrically operated.

Heating plants/boilers:

$$f_{R,HB,i} = \frac{f_{R,i}}{\eta_{th}} \qquad \text{Equation 2}$$

Where

$f_{R,i}$ =REF of the fuel

η_{th} =annual thermal efficiency; related to the Higher Heating Value

CHP plants:

$$f_{R,CHP,i} = f_{R,i} \cdot \frac{\alpha_{th}}{\eta_{th}}$$ Equation 3

The allocation factor α_{th} (5) is based on the Carnot factor f_C (4):

$$f_C = 1 - \frac{T_0}{T_{mn}}$$ Equation 4

$$\alpha_{th} = \frac{\eta_{th} \cdot f_C}{\eta_{el} + \eta_{th} \cdot f_C}$$ Equation 5

η_{el} =annual electrical efficiency

T_0 =reference temperature

T_{mn} =logarithmic average temperature of the district heating network (annual average of supply and return temperatures)

District heating system:

$$f_{R,DH} = \frac{\sum(x_i \cdot f_{R,i}^{plant}) + \omega \cdot f_{R,el}}{1 - e_{loss}}$$ Equation 6

x_i =share of the generation plant i

$f_{R,i}^{plant}$ =plant-specific REF

ω =share of pump power consumption in relation to the produced heat (district heating: 0.015; waste heat: 0.02 according to (IEA, 2022))

e_{loss} =relative heat losses as a share of heat production (assumed to be 14% according to (IEA, 2022))

Table 2 summarises the key parameters considered in this study.

Table2 : Key parameters considered in the analysis

Key parameter	Unit	Definition	Source	Evaluation
Primary energy factor PEF	-	$\frac{primary\ energy}{final\ energy}$ *	FW 309-1/ Geoportal Hamburg	Comparison of energy sources based on primary energy consumption (non-renewable)
GHG emission factor **EF**	$\frac{g\ CO_2 equiv.}{kWh}$	$\frac{greenhouse\ gas\ emissions}{final\ energy}$	FW 309-1/ Geoportal Hamburg	Estimation of greenhouse gas emissions, comparison of energy sources
Resource exergy factor REF	-	$\frac{ressource\ exergy}{final\ energy}$	Calculation according to (Jentsch, 2025)	Assessment of thermodynamic efficiency & optimisation potential

*PEFs specified in the Building Energy Act often deviate from this definition

Electrification of heat demand

Several studies analyse potential transformation pathways for the energy transition, considering different levels of electrification (dena, 2018; Trutnevyte, 2019; Thelen et al., 2024). The Fraunhofer Institute study prioritises direct electrification in the building, transport and industry sectors as the most cost-effective option (Thelen et al., 2024). However, full electrification of all sectors conflicts with the principle of diversification and increases the vulnerability of the energy system to failures (Li, 2005). According to iSelect (2025), Germany is already among the ten countries with the highest risk of large-scale blackouts, with previous studies documenting the catastrophic effects of power outages on the population (Petermann et al., 2011).

Additionally, an electrified scenario with numerous decentralized heat pumps is likely to impose significant electrical loads on the power grid, necessitating its expansion or reinforcement. The current study by Fakhrooeian et al. (2024) concludes that most existing electricity grids are not designed to provide the additional energy required for charging electric vehicles and operating heat pumps.

System temperatures

Despite the recommendations made during the development of the district heating transformation strategy (Maaß et al., 2015), there have been few initiatives to date aimed at lowering the system temperature in Hamburg's city network. Lowering flow and return temperatures in existing district heating networks is, however, constrained by multiple factors, including the technical limitations of the network (e.g., pipe dimensions and hydraulic restrictions), the existing building stock with high heating requirements, and economic and institutional conditions such as investment costs and pre-existing contractual arrangements.

However, there are several neighbourhood and sub-networks that already operate at lower supply and return temperatures. From an exergetic point of view, lowering the supply and return temperatures could offer significant advantages: heat losses would be reduced, and more waste heat sources and renewable energies could be integrated into the network (Schmidt, 2018).

Methodology

This study examines three urban areas in Hamburg that are currently supplied by the municipal gas network. Preliminary heat planning has already been completed for all areas. In the Hamburg Heat Register, most of these areas are designated as decentralised supply areas, excluding existing building-related heat network structures (Geoportal Hamburg).

In order to evaluate the heat planning from an environmental perspective, primary energy, GHG emission and resource exergy factors of the district heating networks were calculated and compared to air-water heat pumps. For the Hamburg Othmarschen case study, direct utilisation of waste heat in a local heating network was assumed. The results were subsequently compared, and the relevance of the evaluated indicators was assessed, with a discussion of aspects not captured by the evaluation.

PEFs and EFs for the heating networks were obtained from the Hamburg Heat Register (Geoportal Hamburg). For the heat pump and CHP variants, the respective factors were calculated in accordance with the GEG (GEG, 2020). REFs are calculated in accordance with the the REA methodology (Jentsch, 2025). Annual utilisation rates and other assumptions were adapted from the IEA (2022). The compositions of the district heating mixes were based on the available certificates according to AGFW FW 309, Parts 1 and 7 (HEnW, 2022 & HEnW 2025a) and on documents provided by network operators (E.ON SE, (2023) & EAM Natur Energie GmbH, (2021)). Supply and return temperatures were taken from the operators' Technical Connection Conditions (TABs) where available (HEnW, 2025b & HEnW, 2025c). For networks without publicly accessible TABs, temperatures were requested directly from the operators. The arithmetic mean values of the minimum and maximum supply and return temperatures from the TABs were assumed as the average annual network temperatures.

Case study 1: Hamburg Alsterdorf

The garden city of Alsterdorf "Gartenstadt Alsterdorf" is composed primarily of single-family homes, most of which were built in the 1930s. Heating is mainly provided by gas or oil boilers. The linear heat density in the neighbourhood ranges from 1 to 1.5 MWh/(m·a). Despite its close proximity to the city's district heating network, the area was classified as "unsuitable for district heating" in the Hamburg Heat Register preliminary target scenario due to its relatively low linear heat density (see Figure 1). The adjacent network is Hamburg's city network, operated by Hamburger Energiewerke (HEnW).

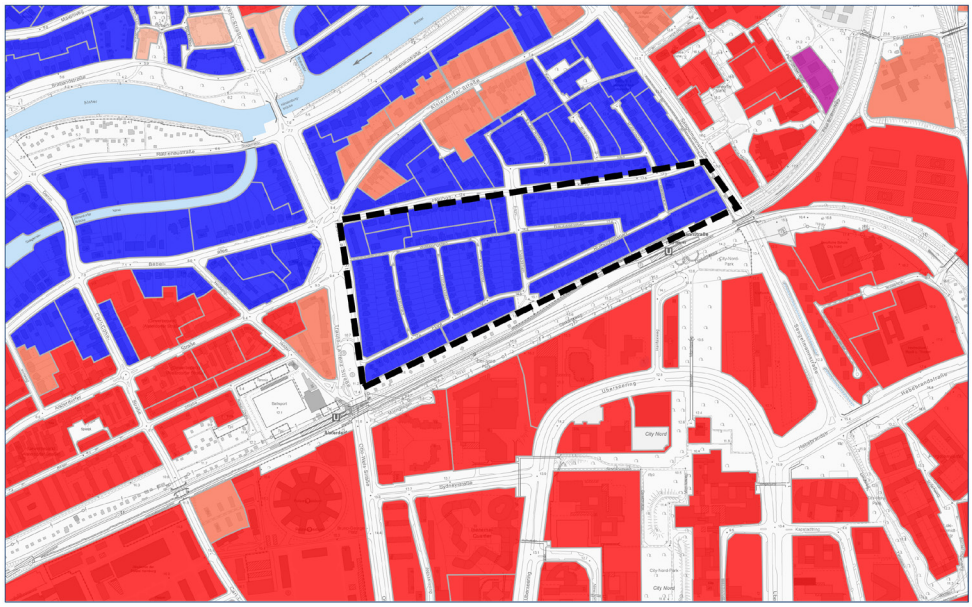

Figure1: Preliminary target scenario for the heat supply of the "Gartenstadt Alsterdorf" neighbourhood (map excerpt from the Hamburg Heat Register; scale 1:5,000; accessed 17 March 2026). Blue: decentralized heat supply; red: existing district heating networks; light red/beige: district heating expansion likely; pink: decentralized and district heating both possible; black dotted area: study area.

Case study 2: Hamburg Neuallermöhe and Nettelnburg

The Neuallermöhe and Nettelnburg neighbourhoods (formally part of Bergedorf) have different building structures. Neuallermöhe is dominated by multi-family houses and modern, well-insulated new buildings, whereas Nettelnburg, particularly outside the S-Bahn corridor, consists mainly of detached and semi-detached houses. The settlement in Nettelnburg was built in the 1960s, implying a comparatively low insulation standard of the building envelope. Due to the differing settlement patterns, the linear heat densities also vary. In some multi-family buildings, linear heat densities may exceed 5 MWh/(m·a), whereas values in Nettelnburg range between 1 and 1.5 MWh/(m·a). Several heating networks operate in the surrounding area, with the largest operated by HenW, EAM Natur Energie GmbH and HanseWerk Natur. Despite the proximity to multiple heating networks and some existing building networks, a decentralised heat supply is planned for most of the buildings not yet connected to the network. Some areas are identified as optimally suited for district heating; however, their implementation would require initiative by the building owners themselves (areas highlighted in beige in Figure 2).

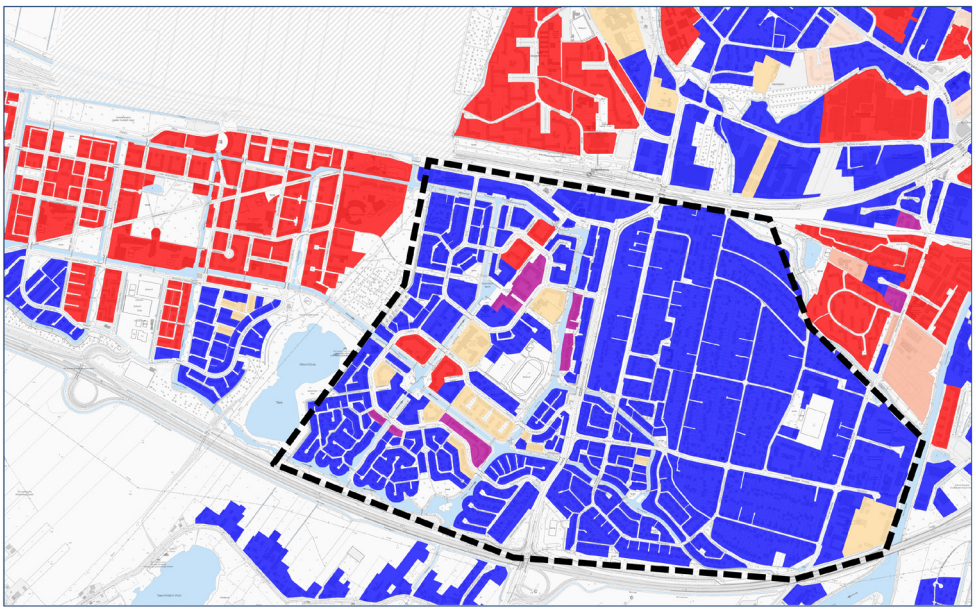

Figure2: Preliminary target scenario for the heat supply in the Neuallermöhe and Nettelnburg districts (map excerpt from the Hamburg Heat Register, scale 1:10,000; accessed: 17 March 2026). Blue: decentralized heat supply; red: existing district heating networks; light red/beige: district heating expansion likely; pink: decentralized and district heating both possible; black dotted area: study area.

Case study 3: Hamburg Othmarschen

The district of Othmarschen, located in the borough of Hamburg-Altona, features a heterogeneous building structure. Old villas and detached houses dominate along the Elbe river, while apartment buildings predominate near the S-Bahn. In addition to the Hamburg municipal heating network, smaller local heating networks are present in the immediate vicinity, such as the Bahrenfeld and Lyserstraße networks. The preliminary target scenario developed by BUKEA predominantly foresees decentralized heat supply solutions for most residential buildings. Exceptions mainly include non-residential buildings, such as schools and daycare centers (areas highlighted in beige in Figure 3).

Zimmermann et al. (2025), in their spatial assessment of waste heat potential in Hamburg, identify a theoretically high waste heat potential for Othmarschen. According to their evaluation methodology, the waste heat is classified as level 3, corresponding to an annual volume of over 10,000 MWh at temperatures above 100 °C. The study, however, does not specify individual sources for each district.

High temperature waste heat sources relevant for heat planning primarily arise from industrial production (e.g. steel, chemical industry, glass, paper), waste disposal and energy conversion (BMWSB, 2024). The Hamburg Heat Register lists the German Electron Synchrotron DESY and Airbus Operations GmbH as nearby waste heat sources.

To account for waste heat utilisation efficiency in this study, direct use of the waste heat potential via a local heating network is assumed for Othmarschen. In practice, direct feed-in is often not feasible, as waste heat usually requires a temperature boost via a heat pump. Nevertheless, direct use is theoretically possible for high-temperature waste heat above 100 °C and low flow temperatures in the building heating system. Due to the absence of detailed data, direct waste heat utilisation is assumed in this analysis.

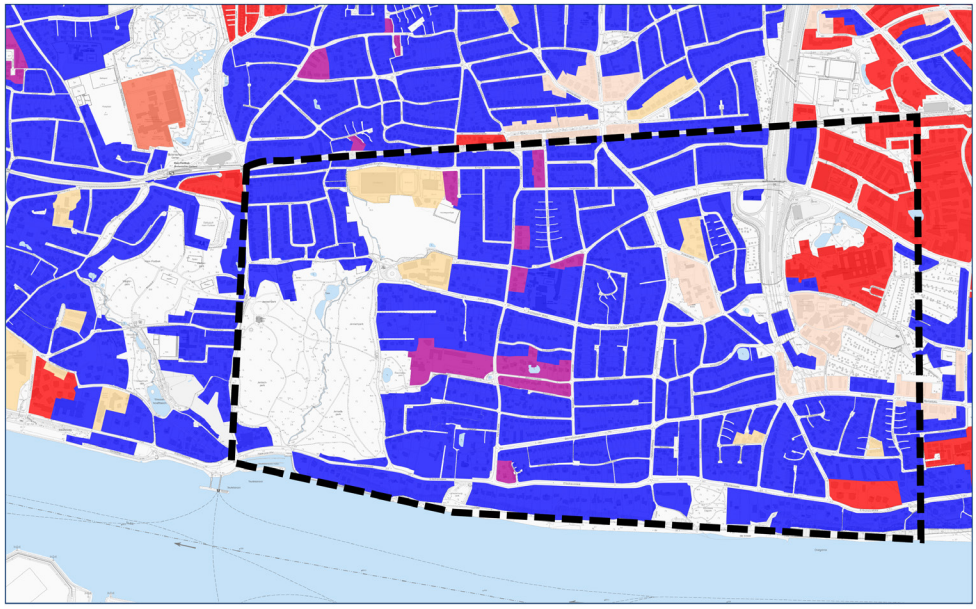

Figure3: Preliminary target scenario for the heat supply in the Othmarschen district (map excerpt from the Hamburg Heat Register, scale 1:10,000; accessed: 11 March 2026). Blue: decentralized heat supply; red: existing district heating networks; light red/beige: district heating expansion likely; pink: decentralized and district heating both possible; black dotted area: study area.

Results and Discussion

The calculated factors, along with the underlying assumptions, are detailed in Table 3. The potential local heat supply options were evaluated against three scenarios: pure waste heat utilization, decentralized air-to-water heat pump operation with APFs of 3 and 4, and a coal-fired CHP configuration. Due to unknown assumptions in the Hamburg Heat Register, GHG emissions for the waste heat, heat pump and CHP variants were not calculated using the Finnish method.

The results demonstrate significant differences in assessment logic across the various methods. According to the GEG and FW 309-1, CHP plants are strongly favoured in terms of PF and EF. This preference results from electricity credit method, which values exported electricity with a high GHG emission factor of 860 g CO_2 equivalent/kWh and deducts it from the total emissions. As a result, EF values for CHP are significantly lower compared to the Finnisch method, which benchmarks cogeneration against separate generation of electricity and heat. For perspective, the latest GHG emission factor of the German electricity mix in 2023 is 445 g CO_2 equivalent/kWh, which is lower than the GEG reference value (UBA, 2024). This discrepancy illustrates how the choice of assessment methodology strongly influences which heat supply alternatives are classified as low-emission. For future GHG emission assessments, the Carnot method could be applied in certificates and in the Heat Register, as it enables a thermodynamically consistent allocation of electricity and heat in CHP plants.

The REF results show a differentiated picture. CHP plants are particularly advantageous from an exergetic perspective. According to the REF methodology, conventional coal or natural gas CHP plants can outperform individual heat pumps operated with the current electricity mix (see Table 3.). Among the investigated networks, only one existing system—characterized by a high share of heat supplied by a wood-fired power plant operated by HanseWerk Natur GmbH—achieves a better REF than a decentralised air-source heat pump with an APF of 3. The primary reason for this is the high proportion of natural gas boilers in the district heating mixes analyzed, which diminishes the exergetic efficiency of these systems. Therefore, increasing the share of CHP in local district heating networks could substantially enhance their thermodynamic efficiency. Upon exclusion of the electricity credit method, utilization of waste heat via local heating networks emerges as the most efficient and environmentally sustainable option, considering both exergy and greenhouse gas emissions.

Table 3: Results for the factors used to evaluate primary energy consumption, greenhouse gas emissions and resource exergy consumption

Heat supply options:		**HEnW Alsterdorf**	**HEnW Allermöhe/ Bergedorf-West**	**EAM Glasbläserhöfe/ Am Güterbahnhof**	**HWN Lohbrügge**	**Waste heat utilisation (Othmarschen)**	**Heat pump APF=3**	**Heat pump APF=4**	**Coal-fired CHP**
Energy source	*REF (Jentsch, 2025)*	*Shares*	*Shares*	*Shares*	*Shares*	*Shares*	*Shares*	*Shares*	*Shares*
Hard coal CHP	$1.16 \cdot \frac{\alpha_{th}}{\eta_{th}}$	28.2 %	-	-	-	-	-	-	100 %
Natural gas CHP	$1.26 \cdot \frac{\alpha_{th}}{\eta_{th}}$	23.2 %	48 %	-	-	-	-	-	-
Natural gas boiler	1.26	19.9 %	24 %	32 %	19 %	-	-	-	-
Heating oil boiler	1.22	2 %	-	-	-	-	-	-	-
Biogenic waste CHP	$1 \cdot \frac{\alpha_{th}}{\eta_{th}}$	12 %	-	55 %	-	-	-	-	-
Biogenic waste	1	-	-	13 %	5 %	-	-	-	-
Wood-fired power plant	$1.16 \cdot \frac{\alpha_{th}}{\eta_{th}}$	-	-	-	76 %	-	-	-	-
Incineration of waste wood	1.02	4.9 %	-	-	-	-	-	-	-
Waste heat from waste CHP	$1 \cdot \frac{\alpha_{th}}{\eta_{th}}$	4.1 %	-	-	-	-	-	-	-
Industrial waste heat	$=f_C$	2 %	-	-	-	100 %	-	-	-
Waste heat from wastewater	$APF \cdot f_{C,ww}$	3.7 %	-	-	-	-	-	-	-
Electricity grid	2.63	-	9 %	-	-	-	33.3 %	25 %	-
Environmental heat	0	-	19 %	-	-	-	66.7 %	75 %	-
Annual average supply/return temperature	-	111.5/40 °C	87.5/30 °C	80/50 °C	85/50 °C	70/40 °C	-	-	111.5/40 °C
Primary energy factor PEF according to FW 309-1/GEG		**0.3**	**0.46**	**0.24**	**0.23**	**0**	**0.6***	**0.45***	**0.31****
Emission factor EF FW 309-1/GEG in g CO_2 eq. /kWh		**64**	**28**	**0**	**0**	**40**	**187***	**140***	**7****
Emission factor EF Finnish method in g CO_2 eq./kWh		**258**	**238**	**139**	**43**	**-**	**-**	**-**	**-**
Resource exergy factor REF		**0.89**	**0.96**	**1.01**	**0.85**	**0.32**	**0.88**	**0.66**	**0.56**

*The PEF and EF of the heat pump were calculated using an electricity PEF of 1.8 and an electricity EF of 560 g equivalent/kWh; (FW 309-1:2023).

** The PEF and EF of the coal-fired CHP were calculated using a PEF of 1.1 and an EF of 300 g equivalent/kWh for hard coal, and a PEF of 2.8 and an EF of 860 g equivalent/kWh for the exported electricity mix (FW 309-1:2023).

The analysis acknowledges several critical factors that were not incorporated into the current assessment methods, including economic efficiency and material/resource consumption comparisons between district heating and decentralized heat pumps. Incorporating a holistic approach that combines exergy analysis with life cycle assessment (LCA) in future municipal heat planning could provide a more comprehensive evaluation of system efficiency and material use, especially relevant as renewable energy sources proliferate. This is crucial because the current primary energy and emission factors do not distinguish between different types of renewables, potentially obscuring their true sustainability profiles.

The case study analysis suggests that municipal heat planning in Hamburg currently leans toward promoting decentralized heat supply solutions in areas connected to the natural gas network. However, this approach may lead to several significant challenges:

- **Retention of fossil fuel heating systems:** The upcoming repeal of the 65% renewable energy obligation may cause many homeowners to continue using gas or oil systems.
- **Persistent low insulation standards:** Older buildings in decentralized areas with poor insulation are likely to rely on fossil fuels for longer, often supplemented by hybrid systems with heat pumps.
- **Rising electricity demand:** As heating electrification and growth in electric vehicle use increase, electricity prices might climb, and significant grid expansion and fortification may be necessary.
- **Grid dependency and blackout risk:** Increased reliance of all sectors (mobility, electricity, and heating) on the electricity grid combined with high share of renewables raise the risk of power outages.
- **Untapped waste heat potential:** Existing waste heat resources may remain underutilized.

Conclusion

The analysis indicates that municipal heat planning in Hamburg is largely influenced by economic considerations, but relying on linear heat density as a key criterion has notable limitations. In some neighboring countries, alternative linear heat density thresholds are considered economically viable, highlighting the context-specific nature of planning criteria. Developing a resilient and environmentally sound heat infrastructure therefore requires a more comprehensive, holistic approach that accounts for political, economic, and technical factors. Among the investigated factors, the primary energy factor (PEF) appears to be politically dependent, while the GHG emission factor (EF) varies significantly depending on the calculation methodology. For the assessment of GHG emissions, the electricity credit method is outdated, and a scientifically robust approach based on standardized methodologies must be applied to ensure a fair comparison between CHP plants and decentralized solutions. The resource exergy factor (REF) is proposed as a politically neutral and valuable metric for initial assessments of local heating options, providing a more objective basis for decision-making and complementing GHG emission assessments. The analysis reveals that several critical aspects of sustainable heat planning are not fully captured by current evaluation tools. Looking forward, the integration of exergy analysis with life cycle assessments (LCA) is seen as a promising approach to gain a more holistic understanding of system efficiency and material consumption. Such combined methods could significantly contribute to the development of more sustainable and resilient heat infrastructures.

Based on a qualitative assessment of the case studies, the results suggest that current strategies, which promote decentralized solutions, could lead to long-term infrastructure lock-in. For example, heat pumps installed today are likely to operate throughout their lifespan, potentially limiting flexibility and adaptation to future technological or policy changes. Moreover, recent policy shifts, such as the potential repeal of the 65% renewable obligation in buildings, might lead residents to retain fossil-fuel heating systems longer, resulting in environmentally less favorable outcomes. Conversely, district heating networks, benefiting from existing infrastructure and transformation strategies, are comparatively more aligned with climate goals

and indicate a techno-economic potential in Hamburg capable of supplying up to 80% of the city's building heat demand.

The study results indicate that waste heat utilization generally represents the most sustainable heat supply option. Lowering system temperatures would further facilitate the integration of waste heat and renewable energy sources into district heating networks. Therefore, it is recommended to identify areas in Hamburg with high waste heat potential and to explore the development of low-temperature subnetworks or local heating networks to optimize utilization.

Literature

AGFW – The Energy Efficiency Association for Heating, Cooling and CHP e. V. (2023). FW 309-1:2023 – Energy assessment of district heating and cooling: Primary energy and emission factors according to the electricity credit method. AGFW.

AGFW – The Energy Efficiency Association for Heating, Cooling and CHP e. V. (2023). FW 309-6: Energy evaluation of district heating and district cooling – Emission factors according to the work allocation method and the Carnot method. AGFW.

BDEW Bundesverband der Energie- und Wasserwirtschaft. (2025). Wie heizt Deutschland? Ergebnisse der BDEW-Studie 2023 [How Germany Heats: Results of the BDEW Study 2023].

BMWSB Bundesministerium für Wohnen, Stadtentwicklung und Bauwesen. (2024). Leitfaden Wärmeplanung: Empfehlungen zur methodischen Vorgehensweise für Kommunen und andere Planungsverantwortliche. [Heat Planning Guide: Recommendations for Methodological Approaches for Municipalities and Other Planning Authorities].

Bundesregierung; Fraktionen der CDU/CSU & SPD. (2026, February 24). Eckpunkte zum neuen Gebäudemodernisierungsgesetz [Key Points of the New Building Modernization Act].

BUKEA Behörde für Umwelt, Klima, Energie und Agrarwirtschaft (2025a). Leitlinien klimaneutrale Wärmeversorgung von Gebäuden: Kommunale Wärmeplanung der Freien und Hansestadt Hamburg [Guidelines for Climate-Neutral Heat Supply in Buildings: Municipal Heat Planning of the Free and Hanseatic City of Hamburg]. Freie und Hansestadt Hamburg.

dena Deutsche Energie-Agentur. (2018). dena-Leitstudie Integrierte Energiewende: Impulse für die Gestaltung des Energiesystems bis 2050. [dena Integrated Energy Transition Study: Impulses for Shaping the Energy System until 2050]. Deutsche Energie-Agentur GmbH.

Dochev, I., Peters, I., Seller, H., & Schuchardt, G. K. (2018). Analysing district heating potential with linear heat density: A case study from Hamburg. Energy Procedia, 149, 410–419. https://doi.org/10.1016/j.egypro.2018.08.205

EAM Natur Energie GmbH. (2021). Hamburg Am Guterbahnhof Glasbläserhöfe Informationsblatt 2021 [Hamburg Am Guterbahnhof Glasbläserhöfe Information Sheet 2021]. Retrieved March 2026.

E.ON SE. (2023). Hamburg-Lohbrügge-Nord – Lieferjahr 2023: Anteil eingesetzter Energieträger und Wärme- oder Kältegewinnungstechnologien im Gesamtenergiemix [Hamburg-Lohbrügge-Nord – Supply Year 2023: Share of Energy Carriers and Heat or Cooling Generation Technologies in the Overall Energy Mix]. Retrieved March 2026.

Fakhrooeian, P., Pitz, V., & Scheppat, B. (2024). Systematic evaluation of possible maximum loads caused by electric vehicle charging and heat pumps and their effects on common structures of German low voltage grids. World Electric Vehicle Journal, 15(2), 49. https://doi.org/10.3390/wevj15020049

FHH Freie und Hansestadt Hamburg, BUKEA Behörde für Umwelt, Klima, Energie und Agrarwirtschaft. (2019). Wärmekataster Handbuch. [Heat register handbook]

FHH Freie und Hansestadt Hamburg. (2023). Klimaschutzplan 2023: Energie, Gebäude und Wärmeversorgung [Climate Protection Plan 2023: Energy, Buildings, and Heat Supply]. Hamburg: Senatskanzlei.

FHH Freie und Hansestadt Hamburg, BUKEA Behörde für Umwelt, Klima, Energie und Agrarwirtschaft. (2024). Gebäudewärme.

FHH Freie und Hansestadt Hamburg, BUKEA Behörde für Umwelt, Klima, Energie und Agrarwirtschaft. (2026). Bericht zum Wärmeplan der Freien und Hansestadt Hamburg [Report on the heat plan of the Free and Hanseatic City of Hamburg].

GEG. (2020) Gesetz zur Einsparung von Energie und zur Nutzung erneuerbarer Energien zur Wärme- und Kälteerzeugung in Gebäuden [Building Energy Act: Law on Energy Savings and the Use of Renewable Energies for Heating and Cooling in Buildings].

HenW Hamburger Energiewerke GmbH. (2022). Bescheinigung nach AGFW FW 309 Teil 5 und 7 für das Stadtnetz Hamburg [Certificate according to AGFW FW 309 Parts 5 and 7 for the Hamburg City Network].

HenW Hamburger Energiewerke GmbH. (2025a). Bescheinigung nach AGFW FW 309 Teil 1 und 7 für das Wärmenetz „Verbundsystem Allermöhe / Bergedorf-West“ [Certificate according to AGFW FW 309 Parts 1 and 7 for the “Allermöhe / Bergedorf-West” District Heating Network].

HenW Hamburger Energiewerke GmbH. (2025b). Technische Anschlussbedingungen (TAB-Allermöhe / Burgwedel-Schnelsen) [Technical Connection Conditions (TAB-Allermöhe / Burgwedel-Schnelsen)].

HenW Hamburger Energiewerke GmbH. (2025c). Technische Anschlussbedingungen (TAB-Stadtnetz) [Technical Connection Conditions (TAB-City Network)].

IEA International Energy Agency. (2022). GHG emissions and resource exergy savings from district heating in Europe and China: Final project report. IEA Technology Collaboration Programme on District Heating and Cooling.

iSelect. (2025, Oktober). The Global Energy Outage Report. iSelect.

Jentsch, A. (2024). REA: Resource Exergy Analysis – A Key to Climate Sustainability. International Sustainable Energy Conference - Proceedings, 1. https://doi.org/10.52825/isec.v1i.1055

Jentsch, A. (2025). REA: Resource Exergy Analysis – Calculation Guide for Energy Systems including District Heating and District Cooling (Version 1.1). AGFW | The Energy Efficiency Association for Heating, Cooling and CHP e. V.

Landesbetrieb Geoinformation und Vermessung Hamburg. Geoportal Hamburg [online map service]. Freie and Hansestadt Hamburg. https://geoportal-hamburg.de/, retrieved March 18, 2026.

Li, X. (2005). Diversification and localization of energy systems for sustainable development and energy security. Energy Policy, 33(17), 2237–2243. https://doi.org/10.1016/j.enpol.2004.05.002

Maaß, C., Sandrock, M., & Schaeffer, R. (2015). FERNWÄRME 3.0: Strategien für eine zukunftsorientierte Fernwärmepolitik [DISTRICT HEATING 3.0: Strategies for a Future-Oriented District Heating Policy]. HIR Hamburg Institut Research GmbH.

Nussbaumer, T., & Thalmann, S. (2014). Status report on district heating systems in IEA countries (IEA Bioenergy Task 32, Swiss Federal Office of Energy & Verenum). Verenum; Swiss Federal Office of Energy.

Petermann, T., Bradke, H., Lüllmann, A., Poetzsch, M., & Riehm, U. (2011). Was bei einem Blackout geschieht: Folgen eines langandauernden und großräumigen Stromausfalls [What Happens in a Blackout: Consequences of a Long-Lasting and Widespread Power Outage].

Pfnür, A., Winiewska, B., Mailach, B., & Oschatz, B. (2016). Dezentrale vs. zentrale Wärmeversorgung im deutschen Wärmemarkt: Vergleichende Studie aus energetischer und ökonomischer Sicht. [Decentralised vs. centralised heat supply in the German heating market: A comparative study from an energy and economic perspective]. Technical University of Darmstadt, Research Centre for Commercial Real Estate Management.

Rambøll. (2020). WEDISTRICT_WP2_D2.3: District Heating and Cooling stock at EU level.

Sandrock, M., Bürger, V., & Jaeschke, N. (2025). Entwicklungsszenarien für neue Klimaziele – Aktualisierung Klimaschutzzielszenario (Szenario B) [Development Scenarios for New Climate Targets – Update of the Climate Protection Target Scenario (Scenario B)]. Behörde für Umwelt, Klima, Energie und Agrarwirtschaft der Freien und Hansestadt Hamburg.

Schmidt, D. (2018). Low temperature district heating for future energy systems. Energy Procedia, 149, 595–604. https://doi.org/10.1016/j.egypro.2018.08.224

Thelen, C., Ganter Næss, L., Nolte, H., Kaiser, M., Jürgens, P., Müller, P., Senkpiel, C., & Kost, C. (2024). Paths to a climate-neutral energy system in Germany: Federal states in the transformation process. Fraunhofer Institute for Solar Energy Systems ISE.

Trutnevyte, E., Bauer, N., Kriegler, E., Pye, S., & Brecha, R. (2019). Reviewing the role of electrification in energy system decarbonisation scenarios for Germany. Energy Strategy Reviews, 26, 100397. https://doi.org/10.1016/j.esr.2019.100397

UBA Umweltbundesamt. (2024). Entwicklung der spezifischen Treibhausgas Emissionen des deutschen Strommix in den Jahren 1990 – 2023 [Development of Specific Greenhouse Gas Emissions of the German Electricity Mix from 1990 to 2023] (Climate Change, 23/2024).

Umweltbundesamt. (2016). Die Nutzung von Exergieströmen in kommunalen Strom-Wärme-Systemen zur Erreichung der CO_2-Neutralität von Kommunen bis zum Jahr 2050: Endbericht [The use of exergy flows in municipal electricity-heat systems to achieve carbon neutrality of municipalities by 2050: Final report] (Climate Change 35/2016).

WPG. (2023). Gesetz für die Wärmeplanung und zur Dekarbonisierung der Wärmenetze [Heat Planning and Decarbonization of Heating Networks Act]. Bundesgesetzblatt.

Zimmermann, T., Gerlach, M.-J., Landsberg, F., Pieper, H., Möhring, P., & Wiechers, E. (2025, September 2). Räumliche Erfassung von Abwärmepotenzialen in Hamburg: Abschlussbericht [Spatial Survey of Waste Heat Potentials in Hamburg: Final Report]. Hamburg Institut & PlanEnergi.

Description of solid-rich suspensions in the model of internal structure

Marcel Ramler-Kowollik
ramler@hs-koblenz.de Koblenz University of Applied Sciences, Koblenz

Abstract

Solid-rich suspensions play a crucial role in many areas of civil engineering, including fresh concrete, controlled low-strength materials, fluidized backfill materials, and bentonite support suspensions used in geotechnical applications. Due to the interaction between granular particles and the surrounding fluid phase, these materials exhibit complex rheological behavior that cannot be fully described by classical generalized Newtonian fluid models. In particular, structural changes within the granular network during deformation often lead to deviations between experimentally observed flow behavior and numerical predictions. This contribution presents a conceptual framework for describing such materials using an internal structure model. The approach introduces two phenomenological parameters: the angle of internal structure, representing the preferred orientation of contact networks and momentum transfer within the material, and a cohesive potential, describing the intrinsic ability of the granular-fluid system to maintain structural integrity. These parameters are interpreted as state variables that evolve with deformation and energy dissipation in the system. The model concept is motivated by observations from granular mechanics, rheological experiments, and structural analyses of particle networks. Experimental findings from oscillatory and rotational rheometry on solid-rich suspensions demonstrate how structural rearrangements influence energy dissipation and resistance to shear. The proposed framework aims to incorporate these structural effects into the description of momentum diffusion in the Navier–Stokes equation, thereby improving the representation of highly concentrated suspensions in analytical and numerical models. The presented concept provides a phenomenological bridge between classical continuum rheology and the evolving granular microstructure of solid-rich suspensions. Future work will focus on deriving explicit formulations for the modified momentum diffusion term and implementing the model in numerical simulations.

Introduction

Solid-rich or highly concentrated suspensions are widely used in civil engineering. Typical examples include fresh concrete, controlled low-strength materials (CLSM), and fluidized backfill materials, often referred to as liquid soils (ZFSV). Bentonite suspensions used as support fluids in geotechnical engineering also belong to this class of materials. All these materials share a common characteristic: they are multiphase systems consisting of a dispersed solid phase embedded in a continuous liquid phase. The interaction between particles and fluid gives rise to complex rheological phenomena. These include rate-independent (scleronomous) behaviors such as shear thinning, shear thickening and structural viscosity, as well as time-dependent (rheonomous) effects such as thixotropy and rheopexy. The accurate determination and parametrization of these properties, as well as their implications for material behavior, remain active areas of research. This paper provides an overview of possible interpretations of such behavior within a material model that explicitly accounts for the internal structure of solid-rich suspensions.

DOI: 10.34712/142.81-6

Controlled Low-Strength Materials (CLSM / ZFSV)

Controlled low-strength materials (CLSM), referred to in German as *zeitweise fließfähige, selbstverdichtende Verfüllbaustoffe (ZSFV)*, are highly concentrated suspensions primarily used for backfilling trenches, especially in urban construction. Immediately after mixing, these materials exhibit a fluid to plastic consistency similar to self-compacting concrete. After placement and sufficient resting time, they undergo a transition toward a consolidated state. In contrast to conventional concrete, however, the resulting structure remains comparable to that of granular soils rather than forming a rigid solid. This characteristic enables subsequent excavation without heavy equipment. In the fresh state, CLSM must satisfy two competing requirements: sufficient flowability for placement and resistance to segregation. In the hardened state, the material should exhibit mechanical behavior similar to the surrounding soil while maintaining excavability.

Historically, the characterization of these properties relied heavily on empirical index tests derived from concrete technology standards (e.g., (*DIN EN 12350-5*, 2019)). For instance, flowability was often specified solely by a target slump flow diameter (typically 50-70 cm). While such tests provide qualitative insight, they do not allow for a clear separation of influencing parameters such as density and rheological properties. In addition, the only other parameterized property was defined as the re-excavation capability via the uniaxial compressive strength.

Recent guidelines (*M ZFSV*, 2025) and (DWA-A 127-2, 2024) introduce more refined and measurable properties. In the fresh state, requirements such as suspension stability are defined, accounting for the prevention of segregation. A key parameter in this context is the yield stress, which, together with particle size and density governs stability of the suspension (Equation (1)):

$$\tau_0 = \frac{4}{3} \cdot (\gamma_{Korn} - \gamma_{Fluid}) \cdot r_{Korn} \quad (1)$$

Flowability is now categorized under both static (self-weight-driven flow) and dynamic conditions. Although still based on index tests, strong correlations between these measures and the yield stress have been observed. In addition to the new guideline (M ZFSV, 2025), the DWA-A 127-2 Worksheet Static Calculation of Drainage Systems - Part 2, 2024 sets out specific requirements for CSLM. Another important aspect is the uplift force acting on pipes embedded in CLSM. In addition to classical buoyance, a contribution arising from the yield stress acts in the flow direction (Equation (2)). Own experimental studies have shown that the buoyancy force can be up to twice as a result of the proportion of the yield point compared to the sole approach according to Archimedes.

and takes into account the special features of the building material in the static calculation. In particular, the increased buoyancy effect on the pipe when backfilled with ZFSV should be mentioned here. In addition to the conventional part of Archimedes' buoyancy, a force component acts on the tube in the direction of flow due to the yield point (equation (2)). Own investigations have shown that the buoyancy force can be up to twice as a result of the proportion of the yield point compared to the sole approach according to Archimedes.

$$f_A = \frac{\pi \cdot d_a^2}{4} \cdot \gamma_{Susp} - G_{Rohr} + 3 \cdot \pi \cdot d_a \cdot (\tau_f - \tau_{0,min}) \quad (2)$$

A major challenge remains in the determination of rheological parameters, particularly the yield stress, for highly concentrated suspensions. While methods in accordance with (*DIN EN ISO 3219-2*, 2021) are necessary to determine the rheological parameters (viscosity and yield stress); however, the prescribed test geometries only allow for particle sizes up to 0.2 mm, which is why relative rheometric methods are predominantly used in construction material rheology. Similar to the index tests described above, these

relative rheometric methods allow only qualitative statements about material behavior; the exact derivation of physical parameters is therefore not directly possible. However, the modified ViscoScale test listed in (*M ZFSV*, 2025) presents an absolute rheometric method for determining the yield stress of highly concentrated suspensions. Under idealized boundary conditions, the yield stress is defined as the maximum resistance that the material can oppose the withdrawal of an anchor body. No separate distinction is made between shear-rate-dependent and static components of the resistance, even though the underlying deformation rates are kept to a minimum in the experimental setup. However, the yield stress determined in this way shows a good correlation with observable phenomena such as flow behavior and suspension stability.

In accordance with the nature of the CLSM, various analytical models and parameters are available, categorized according to the different states of the liquid soil. In the flowable state, material behavior is described strictly using parameters from classical rheology; in the solid state, soil mechanics or comparable solid-state models are applied. An attempt at a comprehensive material description is made using the model of internal structure. In the next section, the model is first introduced using basic structural concepts based on granular materials, then further specified, and its parameters and initial application are described.

Structure-descriptive approaches

It is evident that the material behavior of highly concentrated suspensions in the liquid state depends significantly on the intergranular interaction of the individual components (Figure 1). The following section presents several approaches from past studies aimed at identifying and quantifying specific contact orientations and contact frequencies in relation to their resulting effects. For the sake of simplicity, we begin with approaches from soil mechanics, which provide good insight into the underlying considerations.

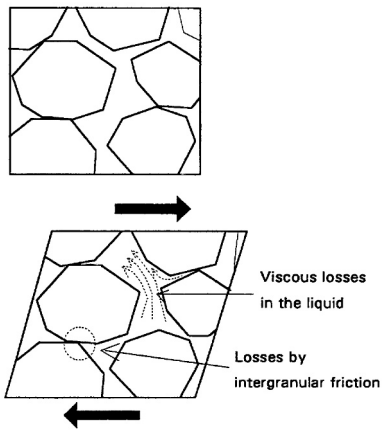

Figure 1: Influence of the granular structure at shear deformation (Ferraris' & Larrard, 1998)

Within the scientific field of soil mechanics, extensive studies have been conducted on the granular structure of regular and irregular aggregates (Guo, 2000; Oda, 1972a, 1972b, 1972c, 1974, 1993; Oda & Konishi, 1974; Wiebicke et al., 2021). The methodology of the studies involved quantifying various dry piles under a range of configurations and boundary conditions using microscopy. The quantification, for example, focused on the frequency of different contact orientations under the various boundary conditions (Figure 2 and Figure 3).

It was found that the material behavior, specifically the relationship between deformation and the stress state, depends on the internal material structure. Furthermore, it was identified that the material structure, characterized by the specific contact formation, is subject to a load-dependent change. Under load, some configurations exhibited the ability to orient contacts specifically in the direction of the dominant principal stress. The resulting loads that could be applied to the test specimen were greater than those of comparable specimens lacking this ability to change structure.

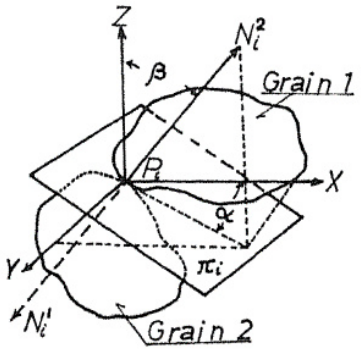

Figure 2: Contact orientation (Oda, 1972b)

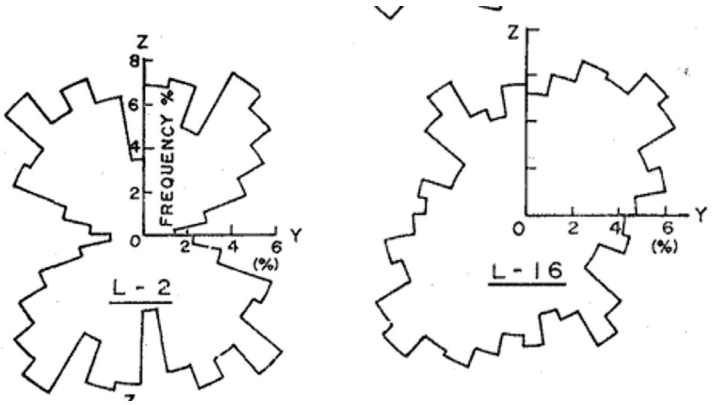

Figure 3: Frequency distribution of contact direction in the vertical plane (Oda & Konishi, 1974)

Early considerations regarding the physical interpretation of liquids at the atomic level were made. Various models from gas theory and crystal theory (models for solids) were adapted for this purpose. However, due to the absence of long-range order in the molecular structure of fluids, these models yielded results that were not physically meaningful. It turns out that in liquids, only a short-range order exists in the vicinity of the nearest or next-nearest molecule (Bernal, 1959). Bernal described a distribution function to characterize general fluids. The distribution function $g(r)$ represented the probability of finding another molecule at a distance r. The difference from solids is that the molecular structure is subject to constant change due to the weak bonds between the individual molecules.

Derivation of the model of internal structure

Building on the phenomena described above — which arise from the internal structure, whatever its nature, whether due to specific grain contacts within the aggregate or to the exchange of momentum between molecules during relative motion — it is now to develop a model that captures these characteristics and describes them using simple parameters. At the current stage of development, two descriptive parameters are initially used for the model. The first parameter accounts for the geometric factor of contacts or momentum orientation and is referred to as the angle of internal structure ω. A second parameter defines an internal cohesive potential f_t (Figure 4). The basic idea of the model of internal structure is a phenomenological consolidation of the internal factors governing impulse diffusion via the mediating parameter of

the angle of internal structure. This parameter represents a state variable of the system and, in simplified terms, describes the systems ability to concentrate loads. In addition, a second variable — the cohesive potential — represents the intrinsic cohesion of the material or system and its ability to maintain stability without external support. Visually, the cohesive potential of the material corresponds to an internal tension spring and could correlate with the elastic potential of the material.

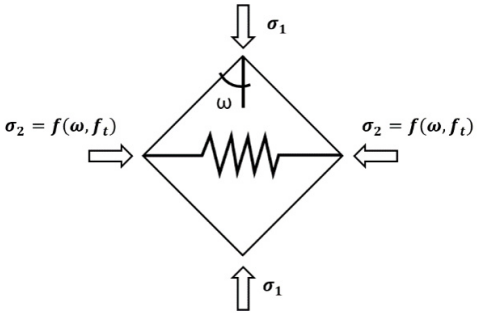

Figure 4: Idealized representation of the model in the plane stress space

To simplify, for example, a maximally possible planar stress state in σ_1 and σ_2 can only be maintained if the supporting stress σ_2 can accommodate the stress propagation from depending on the internal structure and the cohesive potential (Equation (3)).

$$\sigma_1 = (\sigma_2 + f_t) \cdot \cot(\omega) \tag{3}$$

Considering the previous investigations into the quantification of the internal structure, it can be inferred that there may be capacity for structural change, which must naturally be described, at least initially, as material dependent. For example, in an initial increase in the concentration of contact orientations in the vertical direction, i.e., the principal loading direction (Figure 5). This is represented in the model of internal structure by a reduction in the angle of the internal structure ω . On the one hand, this results in a reduction in load propagation and thus a reduction in the necessary support stresses within the structure; on the other hand, it also allows the representation of plastic deformation within the context of classical plasticity theory (Hill, 1998). A change in the structure, at the mesoscopic scale of the granular solid, occurs through relative motion of the grains. In the process, energy is released, among other things, through gran-to-grain friction, which is no longer available to the system as elastic potential. A change in the angle of the internal structure is thus equivalent to energy loss.

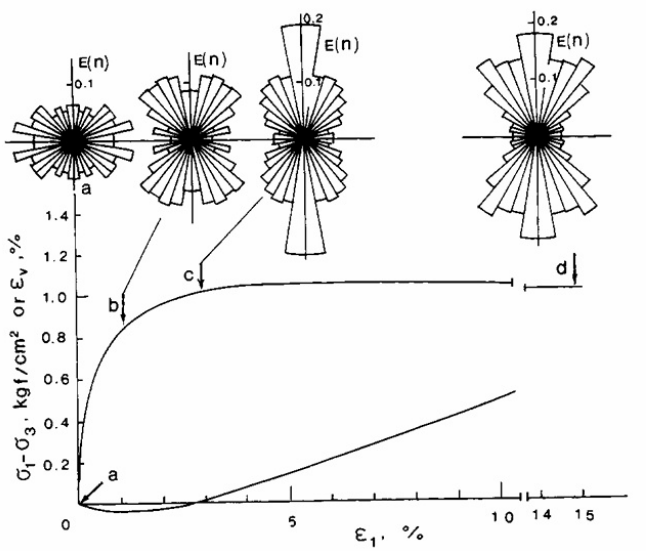

Figure 5: Structural change under triaxial loading (Oda, 1993)

This interpretation of the internal structure and its capacity for change, in combination with the material's cohesive potential, is the starting point for describing the plastic transition behavior of highly deformable sealing compound materials. It was demonstrated that utilizing the entire deformation range of the diaphragm material beyond the elastic region, up to the uniaxial compressive strength, is justified. This observation is consistent with Kayser's observation of single-phase diaphragm wall mixtures (Kayser, 1995). Internal material redistribution (concentration of the internal structure) upon reaching the material's tensile strength allows the plastic transition zone to be explained beyond the elastic deformation range without the internal tensile stresses exceeding the material's tensile strength or cohesive potential. This rules out the possibility of sustained crack formation in the microstructure (Figure 6: Structural change in the plastic deformation range). As a result, a novel design concept utilizing a reduced material stiffness could be implemented in the current draft of the DWA-M 512-3 standard.

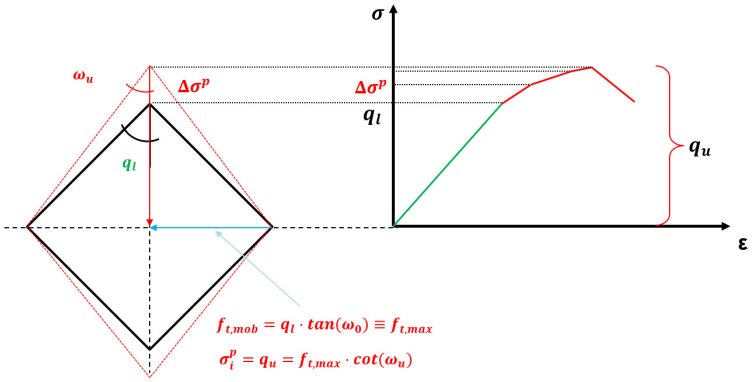

Figure 6: Structural change in the plastic deformation range

Rheological Fundamentals

Rheology is the key discipline for describing the deformation of bodies, whether liquid or solid. For the mathematical description of liquid materials, a categorization according to the underlying parameters is presented in Figure 7. For context, it is necessary to show few basic concepts.

The shear rate or fluid deformation is a quantity derived from the velocity field $\boldsymbol{u}$, which is correlated with the shear stresses in the fluid. To separate pure deformation or change in shape from rotational motions, the symmetric part of the velocity gradient $\boldsymbol{\nabla u}$ is used in the continuum. (Equation (4)):

$$\boldsymbol{D} = \frac{1}{2}(\nabla \boldsymbol{u} + (\nabla \boldsymbol{u})^T) \tag{4}$$

Furthermore, for most generalized Newtonian fluids, the proportionality between shear stress $\boldsymbol{\tau}$ and the deviatoric component of the deformation (referred to here as the shear rate) is defined according Equation (5):

$$\tau = 2 \cdot \mu \cdot \left(D - \frac{1}{3} \cdot tr(D) \right) \tag{5}$$

When assuming a functional relationship between viscosity and shear rate (for non-Newtonian fluids), a scalar quantity is determined using the Frobenius norm instead of the two-dimensional shear rate tensor (Equation (6))

$$\dot{\gamma} = \sqrt{2} \cdot |D| \tag{6}$$

The proportionality is formed by the initially constant factor μ or η , the dynamic viscosity. Based on the relationship between shear rate and shear stress, different types of material behavior are distinguished at the macroscopic scale (Figure 7). In addition to the viscous stress components described above, which only come into play during a shear rate gradient within the structure, there is also the parameter of the rheological yield stress τ_f. In simple terms, the yield stress or yield point describes the shear stress required to transition the material from a solid state to a state of viscous flow. This enables the CLSM to form a stable suspension.

Description of highly concentrated suspensions

As previously described, highly concentrated suspensions consist of a mixture of dispersed solids and a surrounding liquid phase. For example, according to (*DIN 1045-2*, 2023), normal concrete has a volumetric solid content of approx. 70 Vol.-%, approx. 63 Vol.-% (SCC), and based on experience 53 Vol.-% (CLSM). At the microscopic scale, however the cement paste or the carrier suspension surround the aggregate can already be considered a solid-rich suspension. However, at the mesoscopic scale, within the size range of the aggregate, it behaves as a fluid. In Figure 8, the schematic relationship between the volumetric solid content, relative to the percolation limit ϕ_{max} , and the resulting development of the rheological parameters is shown. Model experiments on the deaeration behavior of highly concentrated suspensions (Sosinka, 2021) illustrate a significant effect that can arise due to the granular structure of highly concentrated suspensions. For instance, the release of air bubbles and the size of the corresponding air bubbles in pure bentonite suspensions and suspensions with relatively low solid content correlate well with the rheological yield point. As the solid saturation of the suspension increased, sustained changes in the microstructure were observed due to the movement of the air bubbles. The result was a local change in the solid concentration and thus in the local rheological properties of the material (Figure 9). This is an effect that is not captured in either the numerical or analytical analysis of the material's behavior.

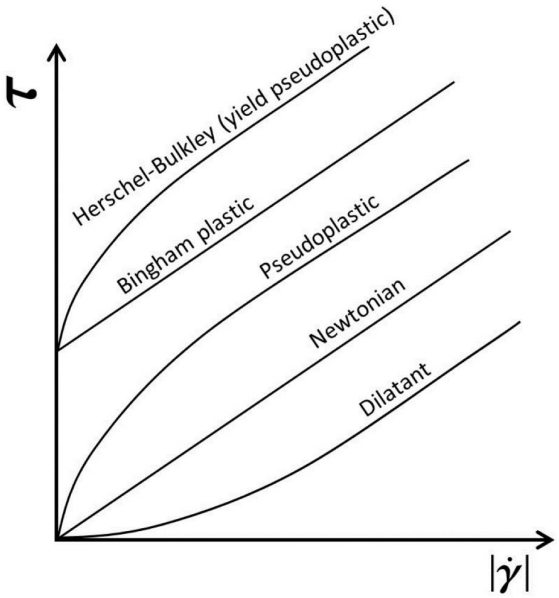

Figure 7: Qualitative behavior of various rheological models. (Mehta et al., 2018)

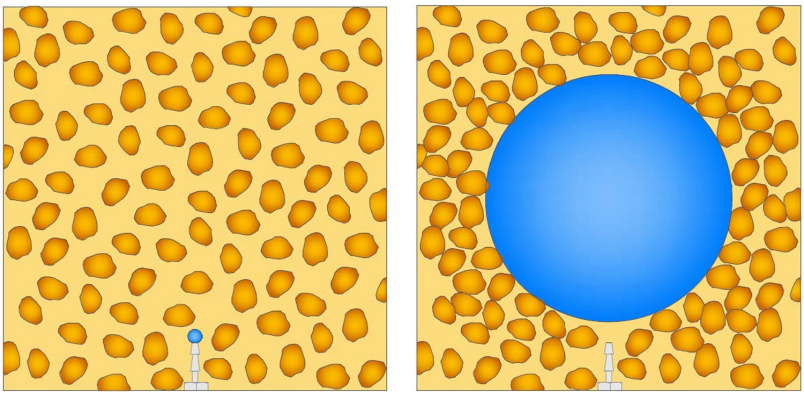

Figure 8: Change in the granular structure of the suspension. (Sosinka, 2021)

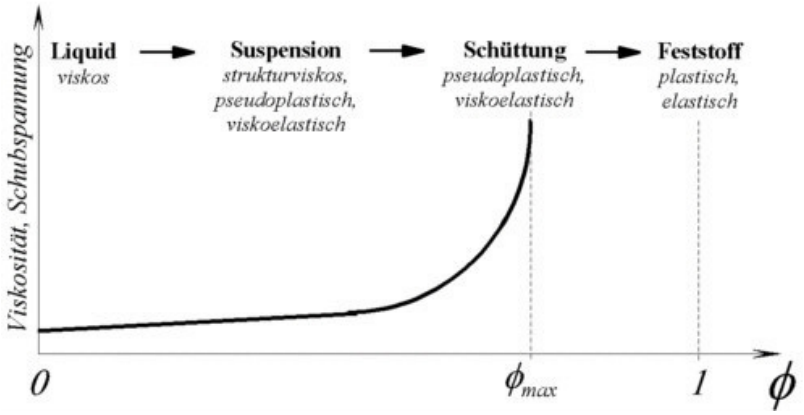

Figure 9: Influence of the volumetric solids content. (Mattke, 2006)

Another challenge arises in the numerical description of solid-rich suspensions in the context of CFD (computational fluid dynamics). The representation of non-Newtonian fluids within continuum mechanics is typically carried out using generalized Newtonian models as described above. The problem can be easily illustrated using the Bingham model, which is the most commonly used model for flowable construction materials; here, the viscosity used in the momentum equation is defined as a function of the shear rate (Equation (6)). When implementing this Bingham model equation numerically, the fluid's viscosities can become virtually infinite as the shear rate approaches the limit of zero. A conventional interpretation therefore employs a biviscous model according to (Tanner & Milhorpe, 1983) by dividing the flow behavior into two regions of different viscosities. Up to a limit value of the shear rate $\dot{\gamma}_{crit}$, the material is assigned a fictitious very high viscosity to simulate a stiff or solid like behavior. As the shear rate transitions $\dot{\gamma} \geq \dot{\gamma}_{crit}$, the viscosity is determined according to equation (7). The complete relationship is shown in equation (8)

$$\eta(\dot{\gamma}) = \frac{\tau_0}{\dot{\gamma}} + \eta_{pl} \cdot \dot{\gamma} \tag{7}$$

$$\eta(\dot{\gamma}) = \min\left(\eta_0, \frac{\tau_0}{\dot{\gamma}} + \eta_{pl} \cdot \dot{\gamma}\right) \tag{8}$$

Although it appears that simulation results based on determined rheological parameters are in good agreement with the vertical flow model according to equation (2), there are significant differences when comparing the simulation (Figure 10) with the real slumb tests in the laboratory. The complex spatial flow system and the resulting structural changes in the granular components of the suspension are considered to be the reason for this.

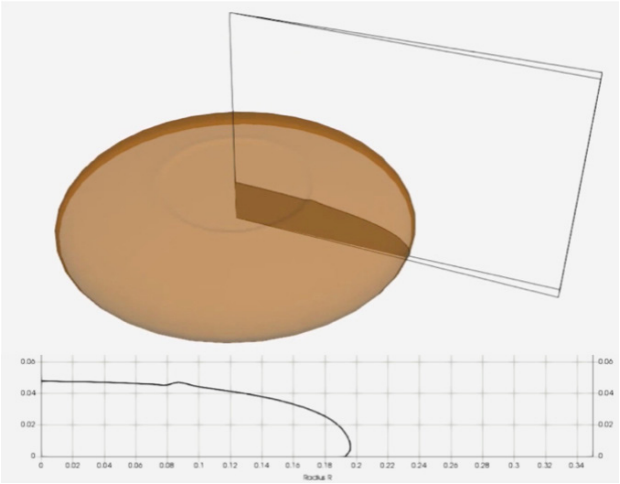

Figure 10: CFD simulation of the slumb test

To approach this, a detailed look at the mathematical formulation of liquid flow is needed. The flow behavior of solids or liquids is generally described by the Navier-Stokes equation in the continuum (simplified for incompressible fluids):

$$\rho \cdot \left(\frac{\partial \boldsymbol{u}}{\partial t} + (\boldsymbol{u} \cdot \nabla)\boldsymbol{u}\right) = -\nabla p + \mu \Delta \boldsymbol{u} + \boldsymbol{f} \tag{9}$$

On the left-hand side, the local change and the advection of momentum are shown. On the right-hand side, ∇p denotes the pressure gradient and $\boldsymbol{f}$ involve volume forces such as the gravitational force. Particular attention should be paid to the diffusion term $\mu \Delta \boldsymbol{u}$, as this describes the momentum diffusion. For simple Newtonian fluids, this corresponds to the direct momentum exchange between neighboring

molecular layers under relative motion (Chapman & Cowling, 1970; Greenshields & Weller, 2022). Using an analogy to the elastic collision of spheres, the measure of internal structure should also be incorporated into the description of momentum diffusion here.

Oscillatory rheometry has proven to be a promising method for identifying structural change processes in solid-rich suspensions. The basic principle involves exciting the material via a harmonic displacement or force amplitude at a given frequency. The material's response also oscillates and consists of a corresponding amplitude, frequency and phase shift (Figure 11). Two limit values can be defined for the material's response function. If the response is in phase with the deflection, this corresponds to linear elastic material behavior according to Hooke. If a phase shift of $\delta = 90°$ relative to the deflection occurs, the response is consequently in phase with the time derivative of the deflection — the shear rate — and the material exhibits ideal viscous behavior. For phase shifts of $0° < \delta < 90°$, the material exhibits both elastic recovery and viscous energy losses. In addition, Lissajous diagrams are frequently generated from the measured values. Figure 12 shows characteristic Lissajous diagrams from an oscillation test using an amplitude sweep. A solid-rich bentonite-sand suspension was investigated with a volumetric solids content of approx. 51 Vol.-% and a grain size distribution of 0.1 – 1 mm. At low amplitude of deflection, the material exhibits an elliptical force-displacement relationship. This suggests that viscous friction losses occur within the material; the area enclosed by the ellipse corresponds to the energy loss. As the amplitude is further increased, plastic structural changes occur in the material, as illustrated by the nonlinear progression of the Lissajous diagram in Figure 12 (right). As the deflection increases, the granular structure within the material becomes increasingly compacted, as in the deaeration experiments (Sosinka, 2021), local concentrations of solids form, leading to a higher degree of branching in the force network within the grain structure. At a deflection of approximately 0,5°, the measuring body thus encounters stiffer material with higher momentum and force diffusion, which is represented by the steeper rise in the force-displacement-curve. The structural transformation was also demonstrated using rotational rheometry. In this method, the material was sheared continuously through the measuring body (vane cell). In the plots from Figure 13, it is clearly evident that for the suspension with lower solid content (top), no significant change in the material's resistance can be detected during the entire shearing process. In contrast, in the material with a higher solids content (bottom), it is visible that after an initially stronger resistance to shearing — due, for example, to the mobilization and orientation of specific contact networks — the resistance drops to a constant residual value. This can be explained by the fact that, along the shear path, the structure changes in such a way that the granular solids move away from the shear gap to certain extent and can therefore no longer be mobilized to contribute to the resistance.

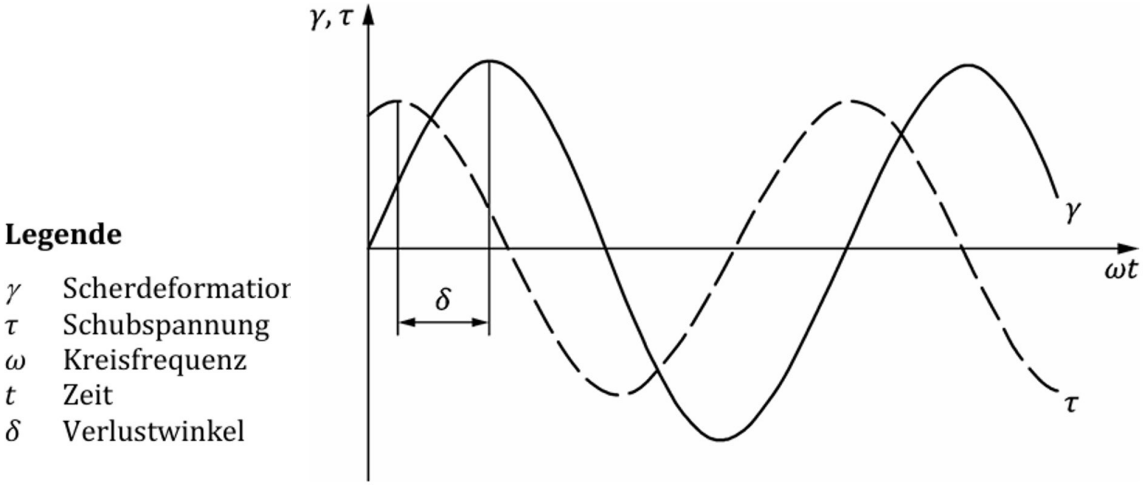

Figure 11: Oscillatory rheometry. (DIN EN ISO 12345)

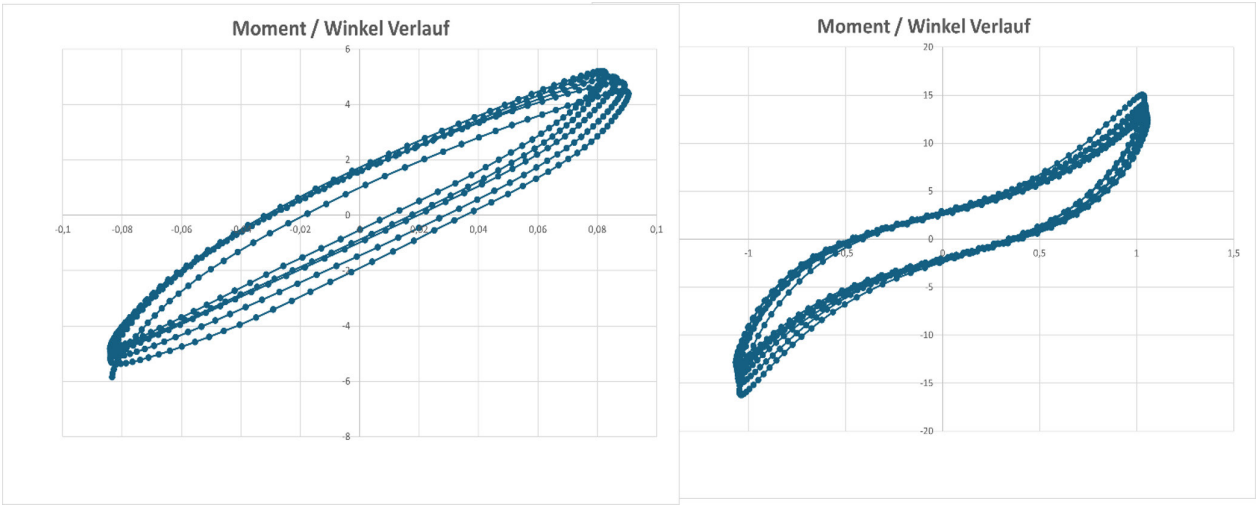

Figure 12: Lissajous figure after amplitude sweep, left at an amplitude of 0,2°, right at an amplitude of 1,0°. Constant frequency of 0,1 Hz

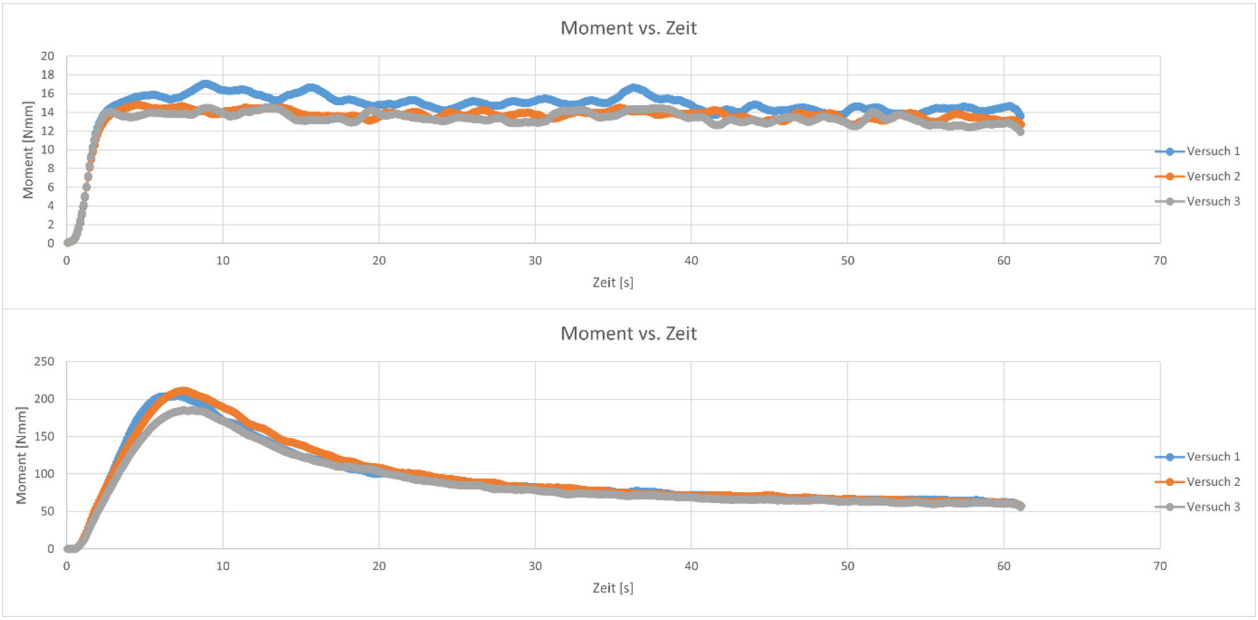

Figure 13: Results of rotational rheometric analysis of materials with diffrent solid concentrations. Top: 36 Vol.-%, bottom 49 Vol.-%

Conclusion and Outlook

Current considerations indicate that the complex behavior of solid-rich suspensions can be phenomenologically explained using the model of internal structure. Based on the findings, the next step will be to derive a measure of structural transformation and the underlying parameters e.g., the spatial stress state of the fluid. The goal is to reduce the discrepancy that arises when modeling non-Newtonian material laws. For the concrete formulation of momentum diffusion, various granulometric parameters, such as the particle size distribution, will be incorporated in combination with statistical descriptions — for example, regarding contact probability — as a measure of the structure that builds up and is represented by the angle of internal structure ω.

Furthermore, the model of internal structure is already incorporated into the description of solids in uniaxial compression tests (Ramler-Kowollik & Quarg-Vonscheidt, 2024). In addition, a team at the Koblenz University of Applied Sciences is working to describe the material behavior of cold asphalt and BSM (bitumen stabilized material) on the fundamental principles of the model.

Literature

Bernal, J. D. (1959). A Geometrical Approach to the Structure Of Liquids. Nature, 183(4655), 141–147. https://doi.org/10.1038/183141a0

Chapman, S., & Cowling, T. G. (1970). The mathematical theory of non-uniform gases: An account of the kinetic theory of viscosity, thermal conduction and diffusion in gases (3rd ed). Cambridge University Press.

DIN 1045-2:2023-08, Tragwerke aus Beton, Stahlbeton und Spannbeton_- Teil_2: Beton. (2023). DIN Media GmbH. https://doi.org/10.31030/3445766

DIN EN 12350-5:2019-09, Prüfung von Frischbeton_- Teil_5: Ausbreitmaß; Deutsche Fassung EN_12350-5:2019. (2019). DIN Media GmbH. https://doi.org/10.31030/3045714

DIN EN ISO 3219-2:2021-08, Rheologie_- Teil_2: Allgemeine Grundlagen der Rotations- und Oszillationsrheometrie (ISO_3219-2:2021); Deutsche Fassung EN_ISO_3219-2:2021. (2021). DIN Media GmbH. https://doi.org/10.31030/3225958

Greenshields, C. J., & Weller, H. G. (2022). Notes on computational fluid dynamics: General principles. CFD Direct Limited.

Guo, P. (2000). Modelling granular materials with respect to stress-dilatancy and fabric: A fundamental approach (S. xxiii, 375 leaves : ill.; 30 cm.). University of Calgary. https://doi.org/10.11575/PRISM/23431

Hill, R. (1998). The mathematical theory of plasticity. Clarendon Press ; Oxford University Press.

Kayser, J. (1995). Spannungs-Verformungs-Verhalten von Einphasen-Dichtwandmassen. TU Braunschweig.

M ZFSV. (2025). https://www.fgsv-verlag.de/m-zfsv

Mattke. (2006). Rheologie disperser Systeme. https://rheologie.hier-im-netz.de/kurs6.html

Oda, M. (1972a). Deformation Mechanism of Sand in Triaxial Compression Tests. Soils and Foundations, 12(4), 45–63. https://doi.org/10.3208/sandf1972.12.4_45

Oda, M. (1972b). Initial Fabrics and their Relations to Mechanical Properties of Granular Material. Soils and Foundations, 12(1), 17–36. https://doi.org/10.3208/sandf1960.12.17

Oda, M. (1972c). The Mechanism of Fabric Changes During Compressional Deformation of Sand. Soils and Foundations, 12(2), 1–18. https://doi.org/10.3208/sandf1972.12.1

Oda, M. (1974). A Mechanical and Statistical Model of Granular Material. Soils and Foundations, 14(1), 13–27. https://doi.org/10.3208/sandf1972.14.13

Oda, M. (1993). Inherent and induced anisotropy in plasticity theory of granular soils. Mechanics of Materials, Special Issue on Mechanics of Granular Materials, 16(1), 35–45. https://doi.org/10.1016/0167-6636(93)90025-M

Oda, M., & Konishi, J. (1974). Microscopic Deformation Mechanism of Granular Material in Simple Shear. Soils and Foundations, 14(4), 25–38. https://doi.org/10.3208/sandf1972.14.4_25

Ramler-Kowollik, M., & Quarg-Vonscheidt, J. (2024). Vorschlag zur Beschreibung des einaxialen Druckverhaltens von hochverformbaren Dichtwandmassen im Modell der inneren Struktur. geotechnik, 47(4), 243–253. https://doi.org/10.1002/gete.202400012

Sosinka, K. (2021). Katharina Sosinka—Entlüftungsverhalten zeitweise fließfähiger und selbstverdichtender Baustoffe. https://www.shaker.de/de/site/content/shop/index.asp?lang=de&ID=8&ISBN=978-3-8440-7818-3

Tanner, R. I., & Milhorpe, J. F. (1983). Numerical simulation of the flow of fluids with yield stress. In Numerical methods in laminar and turbulent flow (S. 680–690).

Wiebicke, M., Herle, I., Andò, E., & Viggiani, G. (2021). Measuring the fabric evolution of sand – application and challenges. geotechnik, 44(2), 114–122. https://doi.org/10.1002/gete.202000019

Exergy-Based LCA of Buildings: Bridging Gaps Through Enriched Material Databases

Samira Shokouhi

samira.shokouhi@hcu-hamburg.de HafenCity University, Hamburg

Abstract

Exergy-based life cycle assessment (Ex-LCA) extends conventional LCA by incorporating the second law of thermodynamics, capturing both the quantity and quality of resource use. However, its application in building analysis is constrained by inconsistent and incomplete data on material exergies. This paper discusses the methodological origins of these discrepancies and proposes a framework for enriching material databases through multi-source reconciliation, reference environment harmonization, and uncertainty quantification. By integrating the approach within existing LCA workflows and aligning it with standards, the study aims at enhancing data reliability and comparability. The resulting framework enables more rigorous, exergy-informed sustainability assessments across building life cycles.

Introduction

Life cycle assessment (LCA) is a standardized methodology for quantifying the environmental impacts of products or systems across their entire life cycle, from raw material extraction through production, use, end-of-life treatment, and disposal. Standardized under ISO 14040/44 (International Organization for Standardization, 2006a, 2006b), LCA typically evaluates impacts in categories such as global warming potential, resource depletion, and acidification, often relying on energy content as a proxy for resource use (M. Nwodo & Anumba, 2021). Exergy-based LCA extends this by incorporating the second law of thermodynamics, measuring the maximum useful work obtainable from a system as it reaches equilibrium with its environment. Exergy distinguishes between energy forms based on quality; high-grade electricity carries more exergy than low-grade heat, thus revealing inefficiencies invisible in first-law analyses.

In building contexts, exergy-based LCA addresses three key impact categories: material consumption, energy consumption, and emissions arising from both. Exergy consumption of materials quantifies the thermodynamic potential embedded in structural elements like concrete and steel during extraction and processing. Resource exergy consumption of energy evaluates fuels and electricity used in manufacturing and operations, accounting for conversion losses. Exergy of emissions expresses the work potential still contained in pollutants, treating them as degraded resources whose abatement reflects their remaining usefulness (Michalakakis et al., 2021).

The exergy of materials, calculated as cumulative exergy demand, arises from standard chemical reactions to form the material from reference substances and all upstream exergy invested into their production. For construction staples, it is calculated via elemental composition using models like Szargut's reference environment (Szargut, 2005). Among the three categories, exergy of energy consumption is the best documented, with robust inventories in tools like Ecoinvent for fuels and grids, enabling precise operational assessments (Koroneos et al., 2012). In contrast, material exergies and those tied to emissions from material and energy processes remain underexplored, suffering from sparse data and methodological inconsistencies. Further diligence is required to aggregate reliable values, as current gaps hinder holistic building sustainability evaluations (Ari, 2011).

Challenge

The practical application of exergy-based LCA in buildings is limited by a lack of standardized data on the exergy of construction materials, compounded by discrepancies across available sources. Several reviews underscore this issue: while energy inventories are mature, material exergy databases are fragmented,

DOI: 10.34712/142.81-7

with values for elements like steel varying from 22 to 34 MJ/kg depending on alloy specifics, reference states, and inclusion of process exergies (Ari, 2011), (M. Nwodo & Anumba, 2021), (Koroneos et al., 2012). Concrete shows analogous spreads (0.54-1.7 MJ/kg), driven by cement-to-aggregate ratios and clinker production assumptions not uniformly documented (M. Nwodo & Anumba, 2021), (Koroneos et al., 2012).

These inconsistencies trace to methodological divergences. Standard chemical exergy tables, such as those from Szargut's, provide elemental baselines but require aggregation for composites, introducing errors when sources diverge on reference environments (Szargut, 2005). Studies applying exergy-based LCA to buildings report variance in embodied exergy totals due to such inputs, eroding result comparability. Global reviews further highlight underrepresentation of regional materials, exacerbating biases in international assessments (Ari, 2011). Handbook analyses confirm that neglecting physical exergy components or recycling credits amplifies these gaps (Kotas, 1985), (Lizarraga & Picallo-Perez, 2019).

Without unified repositories, exergy-based LCA cannot reliably inform design choices or certifications.

Discussion

Addressing the data challenges in exergy-based LCA demands a multifaceted strategy focused on standardization, aggregation, and validation processes. Key aspects warrant development: First, methods should support multiple, well-documented reference environments, since exergy is inherently state-dependent and rigid reliance on one global model risks misrepresenting regional and sector-specific conditions. Practitioners can still use one model as a common baseline, but any adaptations for local relevance should be explicitly justified and transparently documented.

Secondly, multi-source data compilation is essential. Inventories should be developed by cross-referencing elemental exergies from validated tables (e.g., Szargut's) (Szargut, 2005) with compound-level studies, weighting by recency and peer-review status. For discrepant values, either (a) statistical reconciliation can be employed or (b) values can be recalculated by breaking down compounds into elemental compositions and re-deriving exergies to systematically recheck existing sources.

Enrichment protocols should leverage proxies for data voids: decompose materials into elements and sum standard molar exergies, validating results against benchmarks such as component or assembly case studies. Collaborative platforms, similar to ecoinvent's structure, could host community-updated exergy libraries that explicitly incorporate recycling loops and other circularity features.

Comprehensive system coverage is critical. For material exergies, calculations should use detailed inventory data on constituent substances and production processes, ensuring complete coverage of upstream and life cycle stages. For the exergy of emissions, substance-level emission data should be accounted for prior to characterization, enabling precise exergy calculations for individual emissions before aggregation, and capturing downstream effects that manifest as negative environmental impacts, such as climate change. In this way, material exergy reflects not only the embedded work potential of emission elements but also the environmental impacts they impose.

Fifth, uncertainty quantification must become routine. Categorize sources by pedigree (e.g., lab-measured vs. modeled) and propagate errors using Monte Carlo approaches in LCA software, ensuring exergy inputs reflect real-world variability (M. Nwodo & Anumba, 2021). For emissions exergy, extend abatement models to include dispersion potentials, bridging the gap with energy-focused inventories.

Sixth, integration workflows are critical: embed enriched data in open LCA tools, running sensitivity tests to assess impacts on building totals (e.g., 15% embodied exergy shift from steel harmonization). Theoretical development involves hybrid metrics, exergy per functional unit (m^2 floor area), to compare renovations vs. new builds, critiquing potential energy-LCA's underestimation of material dominance.

Finally, institutional aspects require attention: advocate for exergy inclusion in standards like EN 15978 (European Committee for Standardization, 2011), with guidelines mandating checklist adherence (standardize, compile, quantify, reconcile, validate). Pilot applications in German contexts (e.g., KfW 40+ renovations) can demonstrate feasibility, fostering adoption. This holistic development, processual, statistical, and collaborative, transforms exergy-LCA from niche to mainstream, resolving literature contradictions through rigorous, evidence-based evolution.

Conclusion

Exergy-based LCA contributes to sustainability accounting by providing a thermodynamically solid framework that considers both the quality and quantity of resources, enabling comprehensive, physically grounded assessments of embedded materials, use-phase processes, and emissions. By addressing data gaps through the proposed processes, standardization, multi-source reconciliation, uncertainty handling, and validation, this approach enhances authenticity and reproducibility, supporting the development of single-indicator metrics for design optimization and policy formulation.

These guidelines pave the way for broader adoption, supporting certifications like DGNB by delivering consistent exergy inventories that outperform energy proxies in revealing true sustainability trade-offs. Ultimately, they promote a paradigm shift toward exergy-informed practices, fostering resource-efficient construction and progress in global sustainability goals.

References

Ari, V. (2011). Energetic and exergetic assessments of a cement rotary kiln system. Scientific Research and Essays, 6(6), 1428–1438. https://doi.org/10.5897/sre11.030

European Committee for Standardization. (2011). EN 15978:2011 Sustainability of construction works—Assessment of environmental performance of buildings—Calculation method. CEN.

International Organization for Standardization. (2006). ISO 14040:2006 Environmental management—Life cycle assessment—Principles and framework. ISO.

International Organization for Standardization. (2006). ISO 14044:2006 Environmental management—Life cycle assessment—Requirements and guidelines. ISO.

Koroneos, C. J., Nanaki, E. A., & Xydis, G. A. (2012). Sustainability Indicators for the Use of Resources—The Exergy Approach. Sustainability, 4(8), 1867–1878. https://doi.org/10.3390/su4081867

Kotas, T. J. (1985). The exergy method of thermal plant analysis. In Elsevier eBooks. https://doi.org/10.1016/c2013-0-00894-8

Lizarraga, J. M. P. S., & Picallo-Perez, A. (2019). Exergy analysis and thermoeconomics of buildings. In Elsevier eBooks. https://doi.org/10.1016/c2018-0-01196-2

Michalakakis, C., Fouillou, J., Lupton, R. C., Hernandez, A. G., & Cullen, J. M. (2021). Calculating the chemical exergy of materials. Journal of Industrial Ecology, 25(2), 274–287. https://doi.org/10.1111/jiec.13120

Nwodo, M., & Anumba, C. J. (2021). Exergy-Based Life Cycle Assessment of Buildings: case studies. Sustainability, 13(21), 11682. https://doi.org/10.3390/su132111682

Szargut, J. (2005). Exergy Method: Technical and ecological applications.

On the theoretical axial resistance of district heating joints

Ingo Weidlich
ingo.weidlich@hcu-hamburg.de HafenCity University, Hamburg

Abstract

District heating networks consist of different pipe segments, straight pipes, pipe bends and T-branches, which are connected on site. A large number of connections must therefore be made in order to create a branched district heating network. In this paper the state of art in pipeline engineering is reviewed and analyzed for the determination of the theoretical axial resistance of district heating joints, since an anchor effect of the joints was expected. Based on the findings a calculation method for the expected resistance is proposed and in a parameter study the deviations to a straight pipe are shown for typical joint applications.

Keywords: District heating construction, District heating joints, axial resistance

Introduction

District heating networks consist of different pipe segments, straight pipes, pipe bends and T-branches, which are connected on site. A large number of connections must therefore be made on site to create a branched district heating network. This is particularly the case with typical rigid pipe segments in accordance with EN 253 [EN253:2024] and EN 488 [EN488:2025], as pipes with a maximum length of 6 or 12 meters are mainly used for straight sections. The structure of a district heating pipe connection is shown in Figure 1.

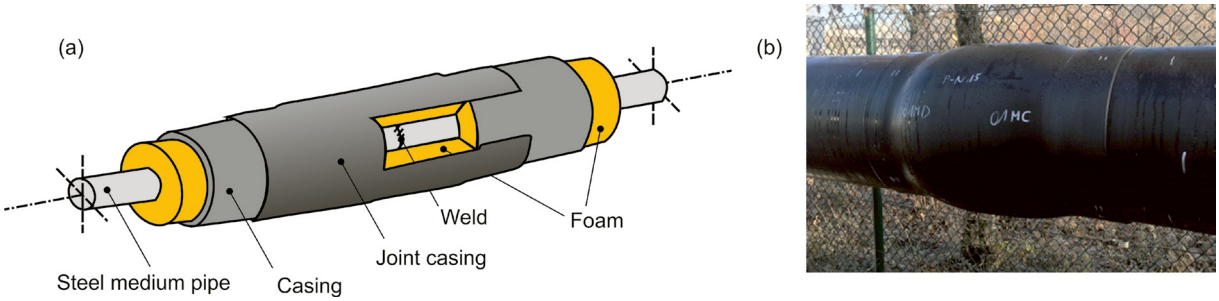

Figure 1. District heating joint system, (a) technical scheme, (b) Foto

The pipes and connections are subjected to a combination of primary loads due to temperature and internal pressure and secondary reaction loads due to the interaction between the pipe and the ground.

The load level according to EN 13941 [EN 13941:2022] and EN 253 with peak temperatures of up to 120°C of the medium and an internal pressure of up to 25 bar can be safely operated if all pipe static verifications have been carried out according to EN 13941. Axial earth resistance is particularly important in calculations for pipe statics, as almost all verifications depend on its quantity. The temperature-related expansion of the pipes is partially constrained by the axial bedding reaction, which results in smaller displacements and bending moments in the curved areas, while the axial stresses in the pipe are significantly lower than in fixed systems due to the permitted movements. This makes it possible to achieve an economical design despite high loads. The key relationships between pipe statics and soil mechanics phenomena are explained in [ACHMUS & WEIDLICH 2016].

Normatively, a constant line load is applied for the calculation of the axial reaction stress, which corre-

DOI: 10.34712/142.81-8

sponds to friction, particularly in granular backfill materials. Figure 1 shows that joints can have larger diameters than straight pipes. The change in diameter leads to increased resistance during axial displacement, which is not reflected by a constant line load that relates solely to the straight pipe. A theoretical calculation approach for the axial bedding reaction resistance for district heating joint systems is developed below.

Methodology

In this paper the state of art in pipeline engineering is reviewed and analysed for the determination of the theoretical axial resistance of district heating joints. Based on the findings a calculation method for the expected resistance is proposed. In a parameter study the expected results and deviations to a straight pipe are shown for typical joint applications.

State of knowledge

Changes in direction, elongation compensation elements, branches, diameter changes and the integration of other components in district heating networks require connections. The construction of the connection results in a change in cross-section compared to a straight pipe. The geometric changes usually occur in the course of the manufacturing process on site due to the internal pressure generated during foaming and the high temperatures of the exothermic foaming reaction, which soften the casing. The change in diameter increases soil resistance during temperature-induced movements throughout subsequent operation. According to EN 253 from 1994, the average outer diameter of the casing must not increase by more than 2% [EN 253:1994]. According to AGFW code of practice FW 401 T14, an increase in diameter of 2% is therefore also considered permissible for the connection area and the joint casing. Today, this requirement no longer exists in the current version of EN 253:2024. Since the EN 253:2015-12 version, only minimum and maximum values for the diameter of the casing are specified. The specifications refer to the composite pipe system and include manufacturing tolerances, including the increase due to foaming.

According to GRAGE and HERBST, the formation of these connections can lead to either an increase or a decrease in cross-sectional area [GRAGE & HERBST 2013]. In some single cases no difference between the cross sections is observed. Figure 2 illustrates the joint shape factor ξ according to Equation 1. GRAGE and HERBST report joint shape factors for DN 80/160 of ξ = 0.96 (decreased joint diameter) to ξ = 1.17 (increased joint diameter) and for DN 150/250 of ξ = 0.97 to ξ = 1.12.

$$\xi = \frac{D_J}{D_P} \qquad \text{Equation 1}$$

Where ξ =Shape factor, D_J=Joint Diameter, D_P=Pipe Diameter.

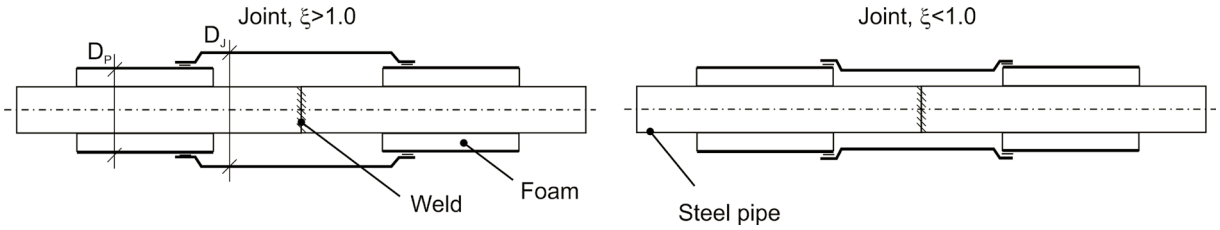

Figure 2. cross sections at the joint

Decreased joint diameters are not allowed according to FW401 Part 14, because this is an indicator of insufficiently foamed joints or an incorrect mixing ratio of the foam components [FW 401 P14:2007]. Thus, the increased diameter at the joint is the more relevant here. An increase factor ξ_i according to EN253:1994 can be defined according to Equation 2.

$$\xi_i = \frac{|D_j - D_P|}{D_P} < 2\% \qquad \text{Equation 2}$$

At HafenCity University, as part of quality assurance tests on DN 80/160 DH-pipes, the foaming process was measured and the joint temperatures and diameter changes were determined [ANDRETZKY et al. 2024]. It was found that during foaming, temperatures rise by up to 20 Kelvin compared to the initial state and can reach temperatures of up to 40°. At the same time, the joint casing expands significantly, but the permanent deformations are smaller after subsequent cooling than during foaming. After the connections had been made, the joint shape factors were determined for five different types in the project. They varied for the nominal diameter DN 80/160 in the range from ξ=1.10 to 1.21. Figure 3 shows a comparison of the permissible form factors derived from AGFW FW401 Part 14, Table 1, with the measured values. It can be seen that higher tolerances result for small diameters than for large diameters. Permissible values for joint diameters below DN 80 base pipe are not specified.

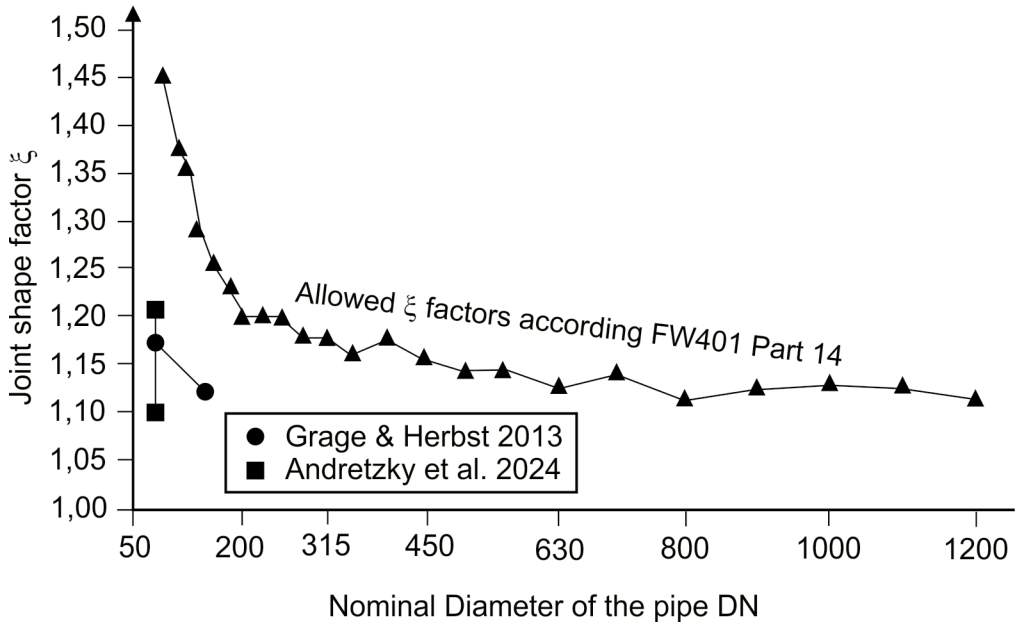

Figure 3. Joint shape factor ξ in comparison

Axial bedding reaction occurs in plugged sewer-pipe connections when there is relative movement between the pipe and the ground. This is phenomenologically comparable to the axial resistance of a district heating joint connection. NETZER and HELBIG describe according to figure 4 in [NETZER & HELBIG 2018] the resistance R_J of the joint according to Equation 3 using the earth pressure coefficients according to RANKINE.

$$R_J = \frac{\pi}{4}\left(D_j^2 - D_C^2\right) \cdot \gamma_s \cdot H \cdot \left(K_p - K_a\right) \qquad \text{Equation 3}$$

Where:

R_J=axial soil resistance of the sewer joint due to the diameter difference

D_J=Joint Diameter

D_p=Outer Pipe Diameter

γ_s= weight of the soil

H = Overburden height of the pipe axis

K_P= passive earth pressure coefficient according to RANKINE

$$K_p = \frac{1 + sin\varphi'}{1 - sin\varphi'}$$

φ' = internal friction angle

K_A = active earth pressure coefficient according to RANKINE

$$K_a = \frac{1 - sin\varphi'}{1 + sin\varphi'}$$

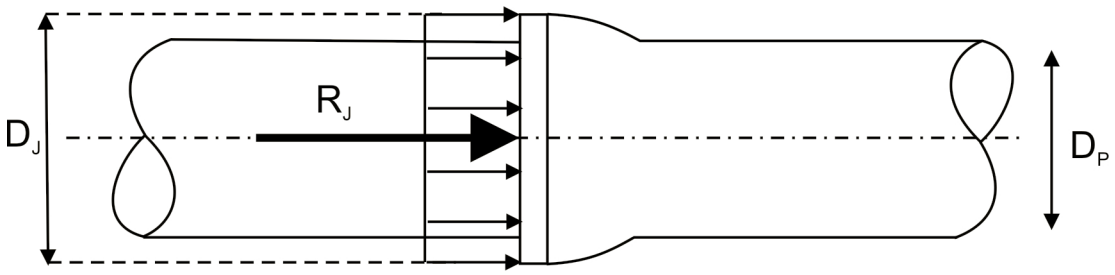

Figure 4. Soil resistance at a sewer joint according to NETZER and HELBIG

Consequently, additional axial bedding resistance must also be expected in district heating pipes if they move axially in the ground as a result of the increased diameter at the joint. In addition, the axial bedding reaction resistances on straight pipes are a function of the diameter. This can be seen in equation 4 according to [ACHMUS & WEIDLICH 2016] for the calculation of axial soil resistance with the K_0-method. A bigger diameter then applies for the joint section.

$$R_f = \gamma_s \cdot H \cdot \left(\frac{1 + K_0}{2}\right) \cdot \pi \cdot D \cdot L_J \cdot \mu \qquad \text{Equation 4}$$

Where:

R_f=axial soil resistance

γ_s = weight of the soil

H = Overburden height to the pipe axis

K_0= earth pressure coefficient at rest = 1-sin φ'

φ' = internal friction angle

D= Diameter

L_J= length of the joint

μ = coefficient of friction between the casing and surrounding soil

The total resistance at the joint R_{tot} is illustrated in Figure 5.

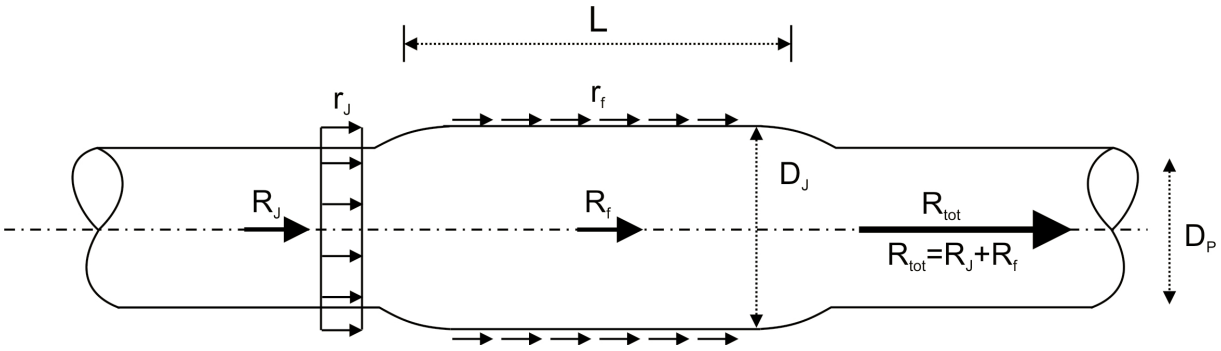

Figure 5. Total axial soil resistance at the joint

The length of the joint is determined by the free steel pipe length required for welding and an overlap on the base pipe. Typical delivery lengths from manufacturers range from 700 mm to 1000 mm; lengths of 605 mm to 805 mm were measured at HCU. For straight DH pipes with a length of 6 m to 12 m, the connections thus account for approx. 10% of the 6 m pipe and 5% of the 12 m pipe in the construction.

Results

The above explanations show that the resistance during axial displacement of the joint is determined by the diameter difference and the additional friction at the joint due to its larger diameter. The combination of Equation 3 and 4 results in Equation 5.

$$R_{tot} = \gamma_s \cdot H \cdot \pi \left[\left(D_J^2 - D_P^2 \right) \cdot \frac{\left(K_p - K_a \right)}{4} + \left(\frac{1 + K_0}{2} \right) \cdot D_J \cdot L_J \cdot \mu \right] \qquad \text{Equation 5}$$

In order to gain a better impression of the magnitude of the additional forces resulting from the increased diameter of the joint, a parameter study was carried out using the parameter set shown in Table 1, and the additional forces were normalised by introducing the indicator I_{plus} of increased forces according to Equation 6. The results are shown in Figure 6.

Parameter	Symbol	Value
Length of the base pipe	L_B	6 m
Length of the joint	L_J	$0.1 * L_B$
Overburden height to the pipe axis	H	1.5 m
Internal friction angle	φ'	32.5°
Friction coefficient PE-Sand	μ	0.4
Weight of the soil	γ_s	20.0 kN/m³
Joint shape factor	ξ	Allowed shape factor derived from AGFW FW401 Part 14

Table 1: Parameter set for calculation example

$$I_{plus} = \frac{R_{tot} + 0.9 \cdot R_{f,B}}{R_{f,B}} \qquad \text{Equation 6}$$

Where:

R_{tot}=total axial soil resistance of the joint system

$R_{f,B}$=axial soil resistance of the base pipe according to Equ. 4 with D = D_P

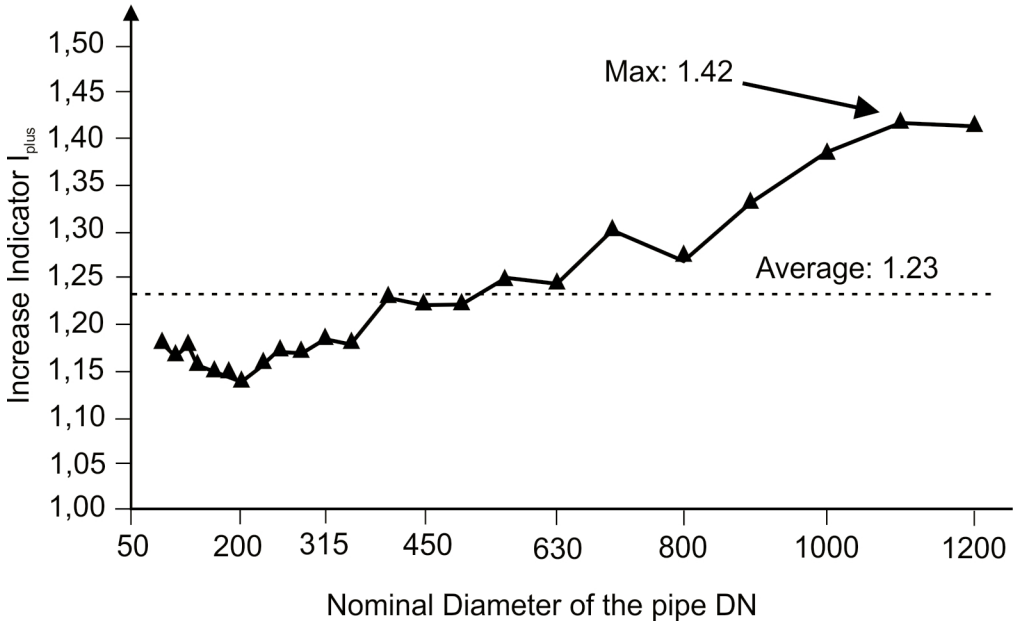

Figure 6, Results of the parameter study

Discussion and Conclusion

In this study, common calculation methods from pipe engineering are used to provide a theoretical basis for calculating joint resistance in the event of axial pipe displacement. This allows the increase in displacement resistance to be estimated for known joint geometry. In particular, the diameter of the joint casing must be known in order to perform a calculation. A parameter study with a soil cover of 1.5 m above the pipe axis and the permissible diameter changes at the joint casing according to FW401 T14 showed that the resistance increases significantly. Based on a 6 m pipe, normalised indicators for increased forces of up to 1.42 maximum and 1.23 average were obtained. The results apply to large axial displacements in which passive earth resistances are fully developed (K_p approach according to RANKINE). With small displacements, the anchor effect of the joint is lower. Furthermore, the permitted diameter changes according to the AGFW code of praxis appear to be much higher than observed values. Because of its limits these theoretical considerations must be validated by measurements. Sandbox tests according to type testing in accordance with EN 489 [EN 489:2022] seem to be unsuitable for this purpose, as constraints and related stresses arise in the small sandbox that are atypical for the actual installation situation in situ. An evaluation should therefore be carried out on field measurements that are more realistic. Furthermore, the proposed calculation approach is only applicable to monotonic initial displacement. The alternating loads that typically occur in district heating pipes are not taken into account here. The calculation approach must therefore be expanded in order to fully capture the phenomenon.

Acknowledgements

This article was elaborated in the framework of the research project ABM4Energy (FKZ 03EN3125A). The author thanks the Federal Ministry of Economy and Energy for the funding.

Literature

EN 253:2024. District heating pipes - Bonded single pipe systems for directly buried hot water networks - Factory made pipe assembly of steel service pipe, polyurethane thermal insulation and a casing of polyethylene; German version EN 253:2019+A1:2023

EN 488:2025. District heating pipes - Bonded single pipe systems for directly buried hot water networks - Part 1: Factory made steel shut-off valve assembly for steel service pipes, polyurethane thermal insulation and a casing of polyethylene; German version EN 488-1:2025

EN 489:2022. District heating pipes - Bonded single and twin pipe systems for buried hot water networks - Part 1: Joint casing assemblies and thermal insulation for hot water networks in accordance with EN 13941-1; German version EN 489-1:2019

EN 13941:2022. District heating pipes - Design and installation of thermal insulated bonded single and twin pipe systems for directly buried hot water networks - Part 1: Design; German version EN 13941-1:2019+A1:2021

Achmus M., Weidlich I., (2016) „Interaktion zwischen Fernwärmeleitungen und dem umgebenden Boden", Bautechnik 93, Heft 9, Ernst & Sohn Verlag für Architektur und technische Wissenschaften GmbH & Co. KG, Berlin, Seiten 663-671, 2016

EN 253:1994. Preinsulated bonded pipe systems for underground hot water networks - Pipe assembly of steel service pipes, polyurethane thermal insulation and outer casing of polyethylene; EN 253:1994

EN 253:2015. District heating pipes - Preinsulated bonded pipe systems for directly buried hot water networks - Pipe assembly of steel service pipe, polyurethane thermal insulation and outer casing of polyethylene; German version EN 253:2009+A2:2015

Grage T., Herbst V., (2013) „Praxisgerechte Qualitätsprüfungen von KMR-Muffensystemen – Erddruckprüfungs von Muffen", EuroHeat&Power, 42. Jg., Heft 9, pp. 46-53, ISSN 0949-166X-D9790 F

FW 401 P14:2007. AGFW-Arbeitsblatt FW 401 - Teil 14, Verlegung und Statik von Kunststoffmantelrohren (KMR) für Fernwärmenetze, - Bau und Montage; Muffenmontage, Installation and calculation of preinsulated bonded pipes for district heating networks – Installation; joint construction - Dezember 2007

Andretzky M., Prein T., Weidlich I., Madan V., Langroudi P., Illguth M., (2024) „Qualitätsprüfung von KMR-Systembauteilen Prüfung von Kunststoffmantelrohrverbindungen" Abschlussbericht zum Vorhaben, Technik und Normung Heft 01/2024, ISBN 3-89999-102-8, Verlag: AGFW-

Netzer W., Helbig U., (2018) Erdverlegte Rohrleitungen unter alpinen Bedingungen, In: Horlacher H.-B. und Helbig U., Rohrleitungen 2, 2. Auflage, Springer Verlag, ISBN 978-3-662-50354-6, Seiten 869-871

Experimental Setup for Thermal and Cyclic Axial Loading of District Heating Pipes

Aaron Wieland
aaron.wieland@hcu-hamburg.de HafenCity University, Hamburg

Abstract

In Europe, pre-insulated district heating (DH) pipes are typically evaluated for quality control in accordance with EN 253; however, the standard does not include testing under simultaneous thermal and axial cyclic loads. The present work advances beyond the standard by introducing a test setup that superimposes thermal loads and cyclic axial shear stresses on pre-insulated DH pipes, thereby reflecting more realistic stress conditions in DH pipes. The configuration extends the EN 253 methodology by integrating welded connections for heat-carrier circulation, a pendulum-bearing for controlled cyclic axial loading, and a pipe casing fixation system. A structured multi-stage test procedure—comprising thermal conditioning, cyclic axial loading, and quasi-static axial shear testing—was developed, incorporating precise temperature control and 3D-digital image correlation for displacement tracking. The contribution of this work lies in the conceptual design, rationale, and realisation of a flexible thermo-mechanical test configuration that remains compatible with existing standards while enabling testing beyond their current scope. The proposed setup provides a methodological foundation for future investigations into ageing mechanisms, adhesion performance, and load interaction effects in pre-insulated DH pipes under realistic operational conditions. As the experimental campaign is still ongoing, this paper presents the test methodology and setup, while final test results will be reported elsewhere.

Introduction

Most DH pipes consist of a high-density polyethylene (HDPE) casing, an insulating layer of rigid polyurethane (PUR) foam, and a steel service pipe for transporting the heat carrier (Pelda, 2024). One purpose of this design is that the bond between the three components guarantees the pipes' mechanical performance. Another criterion of this design is an acceptable thermal performance. During operation, DH pipes undergo temperature changes due to variations in customer demands, seasonal heat losses, and operational loads according to weather conditions. These changes lead to mechanical and thermal loads on the pipes. Temperature fluctuations lead to variable thermal expansion of the steel service pipe, which induces an axial shear stress due to restraint by the surrounding soil. Throughout its service life, the composite must withstand the resulting shear stresses to fulfil its load-bearing function, especially in the gliding zones where axial forces vary due to soil friction. The service life of pre-insulated DH pipe systems with PUR insulation is typically at least 30 years when normative specifications (EN 253 and EN 13941) are complied with. However, a strong bond between the service pipe and insulation is required to ensure the functionality of DH pipes. Total loss of the bond, which some operators define as the end of service life, can result in serious damage to connections and bends. While EN 253 provides a robust framework for evaluating the factory-made quality of pre-insulated DH pipes, the standard is limited to quasi-static testing at 23°C and 140°C. Procedures for assessing simultaneous thermal and cyclic axial loading are not included. As a result, the interaction effects that occur under operating conditions, such as dynamic temperature changes, cyclic axial stress, and material fatigue, remain largely unaddressed. To address these gaps, the present study introduces an experimental setup specifically designed to reproduce the combined thermo-mechanical loads acting on pre-insulated DH pipes.

Methodology

The methodological approach of this work was designed to develop a test setup capable of superimposing controlled thermal and cyclic axial loads on pre-insulated DH pipes. The methodology consists of three

DOI: 10.34712/142.81-9

core components: (i) a review of existing testing approaches, (ii) the derivation of functional and boundary requirements for a new setup, and (iii) the conceptual and technical development of the proposed thermo-mechanical test configuration. Particular attention was given to studies involving thermal ageing, axial shear testing, cyclic loading, or combined thermo-mechanical influences. Relevant standards (e.g., EN 253 and EN 13941-1), experimental reports, and research projects were analysed to extract design parameters. In addition, data presented graphically in the literature were digitised and converted into numerical form to support the evaluation and comparison of test conditions. The present contribution focuses on the conception, rationale, and realisation of the test setup. The methodology presented here establishes the foundation for subsequent work, in which validated thermo-mechanical results and ageing-related performance assessments will be reported.

Existing Test Setups

The industry standard for testing factory-made pre-insulated DH pipe systems is the EN 253. However, in recent years, various tests which deviate from the standard have been conducted to investigate the material behaviour of pre-insulated DH pipes beyond the standard.

For instance, between 2007 and 2011, within the research project by Thieme et al. (2011), experiments to analyse the effect of cyclic axial stress on the residual strength and service life of new and thermally aged (150 °C / 5,000 h) pre-insulated DN 50 DH pipes were conducted. Therefore, they split their experiments into two. First, they performed Wöhler tests under different load horizons until failure to create S-N curves (Wöhler curves). Second, they repeated the experiments, but defined a limited number of load cycles not resulting in failure, following axial shear strength tests according to EN 253 to determine the residual axial shear strength of the pipes. Their goal was to statistically show the probability of survival and to ultimately estimate the service life based on linear damage accumulation. The test setup included a test rig with a servo-hydraulic test cylinder, a force transducer, and a single-channel controller. The tests were performed in a force-controlled manner with a sinusoidal force curve at varying oscillation frequencies between 0.005 Hz and 0.8 Hz and constant amplitudes, and no travel recording. The experiments were performed at room temperature, with a stress ratio (R)[1] of 0.1. Depending on the experiment, the number of applied cycles varied. For the Wöhler test, until failure, 25 to 100,000 cycles could be observed. For the Wöhler tests without failure, an axial shear stress of 0.04 MPa was applied, and a target cycle count of 10,000 was set, which, according to the authors, corresponds to at least 30 years of operation under daily load cycles. Furthermore, the influence of specimen length on the shear stress distribution in the pipe was analysed using the finite element method (FEM). They concluded that, as test specimen length decreases, a more uniform shear stress distribution is achieved, and they recommended a specimen length of 100 mm. Nevertheless, they tested specimens ranging from 50 mm to 200 mm in length, which aligns with findings of Weidlich et al. (2018) regarding specimen length. Based on the findings, Thieme et al. (2011) concluded that, as the oscillation frequency decreases, the oscillation resistance also decreases. They hypothesised that this could be caused by increasing cyclic creep effects at low oscillation frequencies. Since load cycles in DH pipes occur at very low frequencies, they subsequently planned to extrapolate the frequency range of load cycles to operating conditions to estimate the residual strength and failure. However, due to project-specific restrictions, it was not possible to proceed.

Thereafter, within the research project by Schleyer et al. (2016), a similar servo-hydraulic test setup inside a temperature-controlled chamber was used to conduct static and cyclic axial shear stress tests to analyse the effects of mechanical and thermal loads on new and thermally conditioned (140 °C /2,000 h, and 170 °C / 2,000 h) 150 mm-long pre-insulated DH DN 50/140 pipes with PUR. Following the methodology from Thieme et al. (2011), Schleyer et al. (2016) also performed Wöhler tests under different load horizons until failure to create S-N curves. Subsequently, they repeated the Wöhler tests with a limited number of load cycles, not resulting in failure. Following axial shear strength tests according to EN 253, to determine the residual axial shear strength of the pipes. The differences in their approach were: a different preconditioning of the pipe specimens, a temperature of the pipe specimen of 30 °C during testing, applying two

1 The stress ratio (R) is described by the ratio of the minimmum to the maximum occuring axial shear stress during cyclic loading (Götz and Eulitz (2022)).

different stress ratios of R = -1 and R = 0.1, as well as a test frequency of 0.5 Hz for all tests. The target cycle count for the non-destructive cyclic tests was set to 10,000, while the axial shear stress amplitudes were individually set for each experiment and ranged from 0.04 MPa to 0.06 MPa. They observed that the axial shear strength increased after cyclic loading. They concluded that, based on current knowledge, it remains controversial to what extent the cyclic axial loads applied here could increase the axial shear strength of thermally and oxidatively pre-aged pre-insulated DH pipes. Furthermore, they stated that cyclic axial loading, in compliance with limit loading conditions according to current standards and guidelines for pipe static network dimensioning, is less significant than thermal-oxidative ageing.

Moreover, in 2020, within the research project by Hay et al. (2020), experiments using a modified version of the test setup introduced by Schleyer et al. (2016) were conducted to investigate the fatigue behaviour of thermally conditioned pre-insulated DN 60/125 DH pipes with PUR foam insulation under superimposed cyclic axial stress and thermal loading. Therefore, they performed Wöhler tests on thermally preconditioned pipes at 120 °C, 140 °C, and 160 °C until failure occurred. For testing, 150 mm long cut-out pipe specimens were heated using an electric heating element to 90 °C and 120 °C in a nitrogen-flushed chamber to prevent thermo-oxidative ageing processes during the experiments. The temperature inside the chamber was set to 30 °C. In addition to applying a cyclic axial shear stress, they also compressed the PUR foam by 1 % to simulate earth load. The test frequency was set to 1 Hz for all tests, while the applied axial shear stress was individually set for each experiment, ranging from 0.04 MPa to 0.12 MPa. Due to time constraints, they limited the target cycle count of the Wöhler tests to 1,000,000. Based on their findings, they concluded that PUR foam reacts elastically and can therefore be described using a simple spring model to determine the modulus of elasticity. However, as the conditioning temperature increased, the elasticity decreased until, at 160 °C, no elastic behaviour could be observed, or only slight behaviour. They also concluded that the decrease in axial shear strength caused by thermal ageing due to preconditioning of the pipes leads to a higher load level for the same stress amplitude.

Similarly, in their study, Doyle & Weidlich (2021) evaluated the effect of cyclic axial shear stress superimposed with thermal load on the residual shear strength, shear modulus, toughness and failure behaviour of PUR foam in pre-insulated DH pipes, compared with unaged reference samples. The study focused particularly on the initiation and propagation of cracks in the foam. Therefore, they developed a rig with a heatable chamber that could simultaneously test five 200 mm-long DN 20/90 pipes. Electronic control of the mechanical cycling rig was coupled with a thermocouple placed in the middle of the specimen. This ensured that the maximum force was applied simultaneously with the maximum temperature. Three different cyclic loading trials were carried out. The first trial subjected the pipes to temperature-induced stress only with a temperature interval of 25 °C to 100 °C using a heating and cooling ramp of 30 min corresponding to a gradient of 150 K/h. The second trial represented a worst-case scenario in which thermal and axial loads are superimposed with a temperature interval from 25 °C to 100 °C and an axial shear stress interval from 0 MPa to 0.12 MPa over 250 cycles. The third trial represented a scenario under mild conditions in which thermal and axial loads are also superimposed with a temperature interval from 25 °C to 100 °C and an axial shear stress interval from 0 MPa to 0.04 MPa for 125 cycles. Following the trials, an axial shear strength test according to EN 253 was carried out. The researchers concluded that simultaneously applying axial shear stress and thermal loads reduces the foam's strength and increases its stiffness, and that this change is not caused by degradation of the foam's molecular structure.

Vega et al. (2021) aged and analysed DH pipes with PUR foam insulation at elevated temperatures by applying cyclic axial loads over two years, with a special focus on chemical degradation. They heated four DN 50/160 DH pipes, each 3.4 m long, to 130 and 140 °C using electricity, while a fifth one was kept at room temperature (23 ± 2 ◦C). Two of the heated pipes were additionally subjected to a cyclic axial shear stress at a rate of 2 mm/min until 20 kN was reached, which was associated by the researchers with an axial shear stress of 0.031 MPa. The piston was then locked in the loaded position for 28 minutes, after which it returned to the starting position, and no load was applied for a further 28 minutes. This cycle was repeated over 16,000 times in less than two years. The exact number of applied axial load cycles and the corresponding ageing time were reported in (Banushi et al., 2021). The axial shear strength was analysed using the so-called "Pipeopsy" method, a plug method described in (Jakubowicz et al., 2025). The researchers found that the adhesion strength of pipes exposed to both thermal and axial loads decreased faster than

that of pipes exposed only to thermal ageing.

Takeaways from Existing Test Setups

A review of five existing experimental approaches for assessing thermo-mechanical behaviour in pre-insulated DH pipes reveals substantial variation in specimen orientation, thermal and cyclic axial loading strategies, and control modes. Overall, existing literature mainly targets the fatigue behaviour of pre-insulated DH pipes using two dominant strategies: (1) development of Wöhler curves, and (2) residual axial shear strength testing according to EN 253. Most studies conducted their experiments in vertical universal testing machines, using short specimens whose dimensions were aligned with EN 253 requirements. Only Vega et al. (2021) deviated from this by employing a horizontal test setup and considerably longer specimens of 3.4 m, aiming to better approximate real installation conditions. A consistent observation across the literature is that existing test setups orient their maximum applied axial shear stress levels toward established standards and common engineering practice, as shown in Figure 1: Overview of the max. applied axial shear stress vs. max applied temperature. An exception to this observation is Thieme et al. (2011) and Schleyer et al. (2016), who applied destructive axial shear stresses beyond common standards.

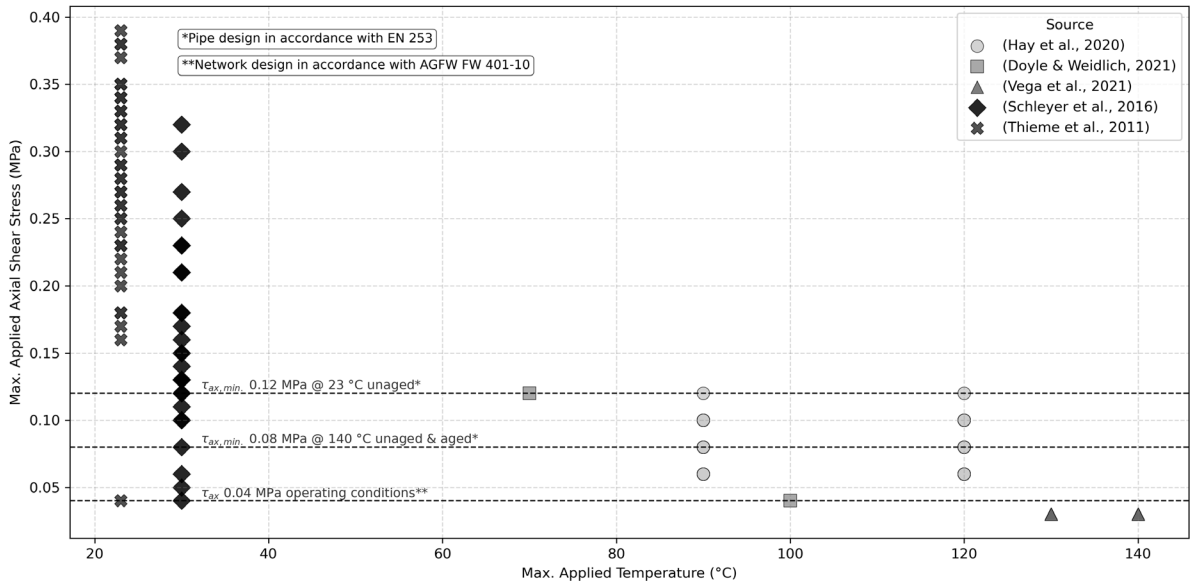

Figure 1: Overview of the max. applied axial shear stress vs. max applied temperature

In the literature, thermal loading is typically imposed by heating the steel service pipe and maintaining a constant temperature during mechanical cycling. An exception is Doyle & Weidlich (2021), who applied synchronised alternating thermal and mechanical loading. Furthermore, the max. applied temperatures, as seen in Figure 1: Overview of the max. applied axial shear stress vs. max applied temperature, fall within the range of typical operating temperatures of DH networks today (Heißler, 2020), except for Vega et al. (2021), who analyse peak temperatures for 3rd-generation DH networks. Another essential point from the literature is the number of applied cycles. Thieme et al. (2011) and Schleyer et al. (2016) limited the number of applied cycles to 10,000, corresponding to the expected number of load cycles over a 30-year service life (assuming a cycle per day), while also testing until failure without a fixed number of cycles. Likewise, Vega et al. (2021) derived their cycle count from the expected number of load cycles over a 30-year service life, whereas Doyle & Weidlich (2021) strictly followed EN 13941 for transmission pipelines. Hay et al. (2020) used 1,000,000 cycles as a termination criterion, reflecting a high-frequency fatigue approach. Figure 2: Overview of the number of cycles vs. max. applied temperature shows an overview of the applied number of cycles and the maximum applied temperature. It can be seen that the number of applied cycles falls within the range of an expected service life of 30 years, assuming one cycle per day.

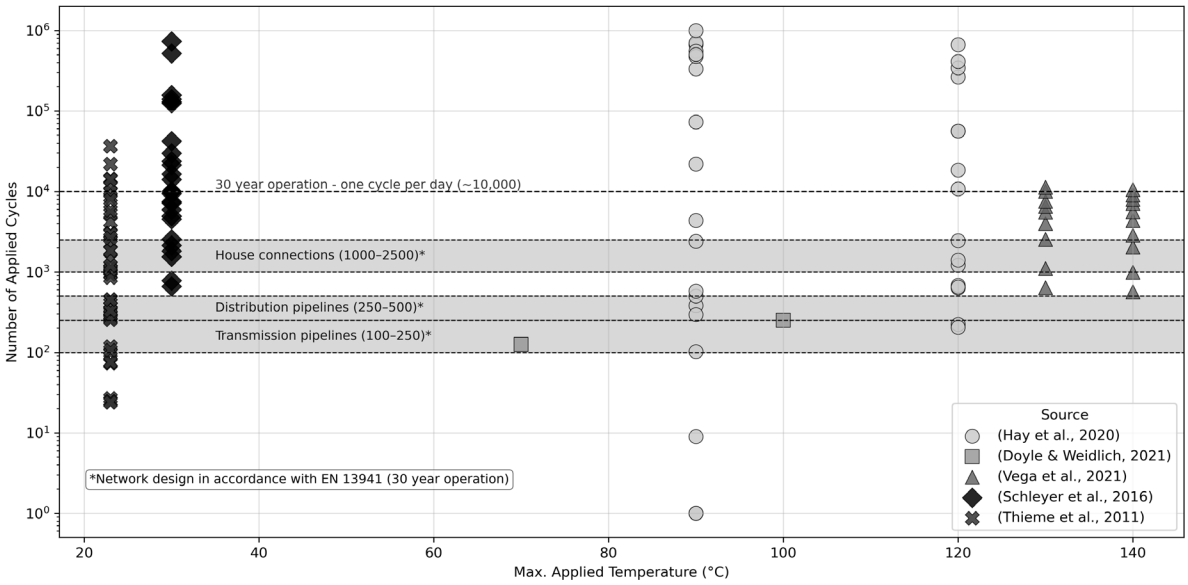

Figure 2: Overview of the number of cycles vs. max. applied temperature

Regarding load ratios, Schleyer et al. (2016) and Hay et al. (2020) adopted a stress ratio of R = –1, corresponding to fully reversed cyclic loading. On the other hand, Thieme et al. (2011) used a stress ratio of R = 0.1, Doyle & Weidlich (2021) and Vega et al. (2021) used a stress ratio of R = 0, corresponding to cold laying of DH pipes. Not only is the ratio between maximum and minimum applied shear stress of importance, but also the frequency at which the axial load is applied to the test object. Except for Doyle & Weidlich (2021) and Vega et al. (2021), most studies rely on high loading frequencies or short test durations followed by an extrapolation of the results into low-cycle-fatigue ranges commonly observed in DH systems. Which, on the other hand, do not capture long-term creep, relaxation, or other time-dependent deformation processes. A comparative overview of test frequencies and stress ratios is given in Table 1: Applied test frequencies and stress ratios.

Table 1: Applied test frequencies and stress ratios

Source	Test Frequency [Hz]	Stress Ratio (R)
(Doyle & Weidlich, 2021)	< 0.001*	0*
(Hay et al., 2020)	1	-1
(Schleyer et al., 2016)	0.5	-1, 0.1
(Thieme et al., 2011)	0.8, 0.2, 0.1, 0.05, 0.01, 0.005	0.1
(Vega et al., 2021)	0.00028*	0*
*not explicitly reported in the source		

Environmental control also differs significantly. Hay et al. (2020) conducted tests in a nitrogen-flushed chamber to suppress oxidation, while simultaneously simulating earth load by compressing the PUR foam by 1 % (stress-strain ratio) and preconditioning the pipes thermally at high temperatures. By contrast, most other studies were tested under an ambient laboratory atmosphere. Furthermore, nearly all non-destructive investigations performed axial shear strength tests after cyclic loading following EN 253 procedures, except Vega et al. (2021), who additionally applied the alternative “PipeOpsy” method. When an elevated thermal load was applied, it was universally applied to the steel service pipe to represent operational conditions. Schleyer et al. (2016) and Hay et al. (2020) are the only researchers who applied a constant temperature of 30 °C to simulate Earth’s temperature at the casing in operating conditions. It is worth mentioning that, besides Doyle & Weidlich (2021), no one has reported the applied temperature change rate to heat and cool the steel service pipe. Even though standards such as EN 253 require a temperature change rate of a maximum of 10 K/h. However, actual DH networks may experience much slower or higher variations depending on the operation strategy.

In brief, these takeaways raise fundamental questions about which approach to choose when dealing with fatigue and thermo-mechanical material behaviour of pre-insulated DH pipes. On one hand, high-cycle fatigue Wöhler tests following extrapolation into low-cycle-fatigue ranges applicable for DH systems or long-term low-cycle-fatigue testing simulating operation conditions following residual axial shear strength tests. Furthermore, the question of the representativeness of laboratory conditions arises: Which axial shear stresses, temperature levels, loading frequencies, and stress ratios appropriately reflect real network operation? These methodological uncertainties highlight the challenges in developing reproducible laboratory tests that balance realism, standard conformity, and practical feasibility. They also underscore why a consistent and transparent definition of boundary conditions is essential when designing new experimental setups for evaluating the thermo-mechanical behaviour of pre-insulated district heating pipes.

Implications for the Present Study and Conceptual Design of the Test Setup

The findings from the literature review directly informed the conceptual design of the thermo-mechanical testing approach developed in this study. A central requirement was that the test setup should be capable of superimposing thermal and cyclic axial mechanical loads, thereby replicating the combined loading conditions experienced by pre-insulated DH pipes in operation. To reflect the full spectrum of real network conditions, the setup should allow testing across the entire range of temperature loads commonly encountered in DH systems, ideally including the capability to couple peak temperature with peak axial load, since this combination best represents critical in-situ operating scenarios. The temperature range should theoretically cover all five generations of district heating and cooling systems with the corresponding temperature change rates. Given the diversity of thermo-mechanical loading patterns in DH networks, the setup should further enable both high-cycle fatigue and low-cycle fatigue testing. This includes accommodating different stress ratios relevant for DH operation. For example, a stress ratio of R = 0.1 reflects the typical installation under cold-laying conditions where a minimum thermal load is always present once the network is in operation. Alternatively, once steady-state operation is reached, seasonal or operational temperature fluctuations could be represented by a stress ratio of R = 0, provided the maximum axial shear stress is adjusted accordingly. To ensure methodological continuity with existing industry practice and to maintain comparability with established data, the design of the test setup should be oriented closely towards EN 253. The setup should therefore not only follow the principles of EN 253 but also remain capable of performing tests according to the standard when required. In addition, the number of mechanical load cycles should be aligned with the network design criteria defined in EN 13941-1, balancing realistic assumptions on load frequency with the practical limitations imposed by laboratory equipment and available testing time. Ideally, an advanced test configuration would also incorporate the ability to suppress thermo-oxidative processes during elevated-temperature testing (e.g., by nitrogen flushing) and to simulate earth loads based on statistically relevant soil cover depths. While these additional features represent desirable extensions for future system development, the present study prioritised feasibility within the constraints of the available universal testing machine and laboratory infrastructure. Overall, the conceptual design aimed to create a test setup that is realistic enough to capture the essential thermo-mechanical interactions occurring in real DH pipes, standard-aligned enough to ensure comparability with established testing practice, and flexible enough to explore new loading scenarios beyond the scope of existing standards.

Test Setup

The experimental setup was derived from the requirements of EN 253 and extended to enable combined thermal loading and cyclic axial loading in the form of axial shear stresses. Three modifications were implemented to adapt the standard configuration to the intended application:

- welded connections for the circulation of the heat carrier fluid,
- a pendulum bearing assembly enabling controlled application of tensile and compressive axial forces to the steel service pipe, and
- a clamping device for fixing the test specimen in the axial direction.

The test setup according to EN 253 is shown in Figure 3 a). The modified test setup is illustrated in Figure 3 b). Figure 3 c) gives an image of the test setup. For all tests, tensile and compressive axial forces can

be applied to the steel medium pipe via a hydraulic universal testing machine. The axial force F_{ax} , which needs to be specified for the universal testing machine to achieve the defined axial shear stress level, can be calculated as follows

$$F_{ax} = \tau_{ax} * L * D_s * \pi \quad (1)$$

Where

τ_{ax} = the axial shear strength, in MPa;

F_{ax} = the axial force including the weight of the steel medium pipe, in N;

L = the length of the PE jacket, in mm;

D_s = the outer diameter of the steel medium pipe, in mm.

To transmit tensile and compressive forces, the pendulum bearing, which is welded to the test specimen, is connected to the universal testing machine via a metal pin. The force is measured using a 20 kN force transducer with an accuracy class 0.5. The clamping device, which cages the specimen, consists of two mounting rings connected by steel rods, which are fitted to the upper and lower ends of the test specimen and prevent longitudinal movement of the pipe casing, thereby generating an axial shear stress along the service pipe and the insulating foam. Furthermore, the universal testing machine can be operated either in distance-time-controlled mode or in force-time-controlled mode, resulting in two fundamentally different loading scenarios. Figure 4: Hypothesised a) Fax constant over time and resulting traverse path vs. b) traverse path constant over time and resulting Fax illustrates these two possible control strategies and their expected outcomes. In scenario A, a constant axial force is applied over time. It is hypothesised that, due to material creep and temperature-induced softening, this setting will result in an increasing traverse displacement to maintain the target axial load. In contrast, scenario B applies a constant traverse displacement over time, which typically leads to a decreasing axial force as the material relaxes.

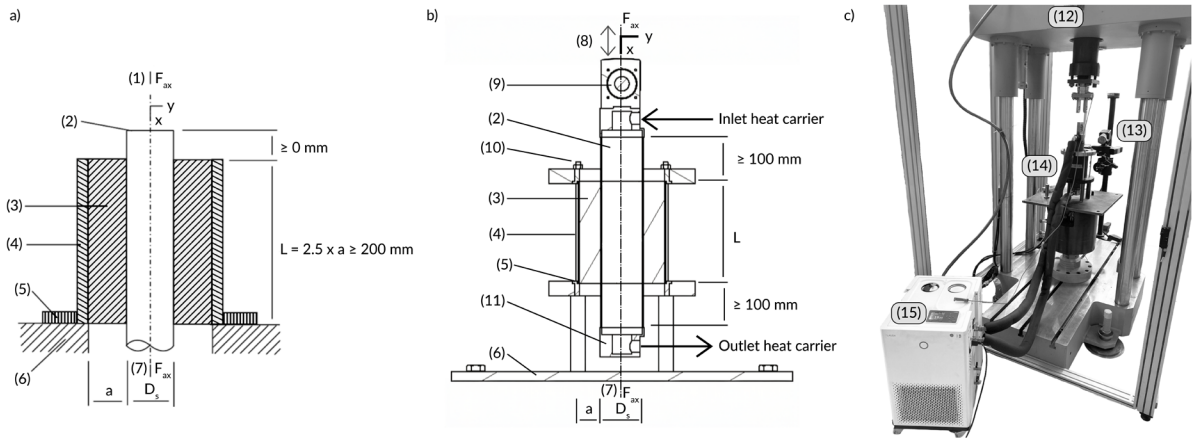

a) Test setup according to EN 253, b) Test setup, c) Image of the test setup, Legend - (1): applied axial force, (2): steel service pipe, (3): thermal insulation foam, (4): pipe casing, (5): mounting ring, (6): base plate of the testing machine, (7): alternative applied axial force, (8): applied cyclic axial force, (9): pendulum bearing, (10): anchoring of the test object, (11): welded attachment for the heat carrier, (12): universal testing machine, (13): 3D digital image correlation, (14): test object, (15): process thermostat – Figure not to scale

Figure 3: Test setup in comparison to the setup according to EN 253

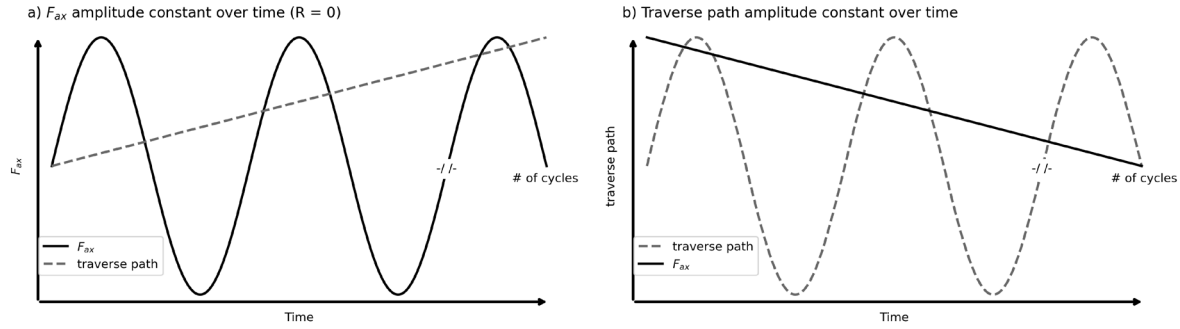

Figure 4: Hypothesised a) Fax constant over time and resulting traverse path vs. b) traverse path constant over time and resulting Fax

The displacement is recorded using three-dimensional digital image correlation (3D-DIC). For this purpose, the GOM ARAMIS 6M stereo camera system with a resolution of 2,752 × 2,200 pixels was used. Images are captured at 5 Hz during static and cyclic tests. Reference point markers are used to record and track the 3D coordinates during the tests. Continuous digital data acquisition includes force, relative displacement, and temperature. Where relative displacement describes the displacement of the steel medium pipe in relation to the casing. During testing, temperature control is provided by a Lauda INTEGRAL IN 150 XT process thermostat using thermal oil. With a working range of –45 °C to 220 °C and a temperature stability of ±0.05 K, the device ensures a stable test temperature during all temperature test phases. The test objects should be manufactured from factory-made district heating pipes and cut out at right angles to the pipe axis. According to EN 253, the test specimen shall be a length of pipe assembly where the length of the casing is equal to 2,5 times the thickness of the thermal insulation, but not less than 200 mm. For that reason, to allow welding, both ends of the pipe must be stripped back a minimum of 100 mm to expose the steel service pipe. Furthermore, the coaxiality tolerance according to EN 253 must be maintained for all test specimens. Following a successful inspection of the test specimens, welding work can be carried out to fit the inlets and outlets for the heat carrier and the pendulum bearing.

The test programme for low-cycle fatigue testing comprises four consecutive stages to ensure well-defined thermal and axial loading conditions.

1. Axial shear test: Before low-cycle-fatigue testing, a reference value according to EN 253 is established.
2. Heating phase: Each specimen is heated to the target test temperature and held isothermally for one hour to ensure a uniform temperature distribution throughout the pipe.
3. Cyclic axial loading: While maintaining the target temperature, a defined number of axial loads is applied to the steel medium pipe.
4. Axial shear test: After completion of cyclic loading without failure, a quasi-static axial shear test is performed under the target temperature with a crosshead speed of 5 mm/min until failure of the composite occurs. A lower shear strength would then indicate fatigue compared to the monotonic-loaded specimen.

On the other hand, the test programme for high-cycle-fatigue testing consists of three consecutive stages to ensure defined thermal and axial loading conditions.

1. Axial shear test: Before low-cycle-fatigue testing, a reference value according to EN 253 is established.
2. Heating phase: Each specimen is heated to the target test temperature and held isothermally for one hour to ensure a uniform temperature distribution throughout the pipe.
3. Cyclic axial loading: While maintaining the target temperature, a high number of axial loads is applied to the steel medium pipe until failure of the bond is observed.

Discussion and Conclusion

The test setup presented opens the way for a wider investigation into the thermo-mechanical behaviour of pre-insulated DH pipes. The work aimed to design a test methodology that enables superimposed thermal and cyclic axial loading of short-length pre-insulated DH pipe specimens beyond the scope of existing standards. The review of existing test setups revealed large variations in thermal loads, cycle counts, stress ratios, and frequencies. Many approaches involve high-frequency fatigue tests with subsequent extrapolation into the low-cycle regime, which may not adequately reflect long-term operational behaviour. This highlights the methodological challenge of defining laboratory test conditions that appropriately represent in-situ behaviour over decades. The present setup, therefore, offers a flexible platform that can support both high-cycle and low-cycle testing under controlled and adjustable thermal conditions. Temperature control proved to be a critical aspect of the test concept. Although the setup allows testing up to 220°C, it does not currently include a nitrogen-flushed chamber. As a result, thermo-oxidative ageing at elevated temperatures cannot be fully suppressed and may influence long-term material behaviour. Future extensions of the setup could integrate nitrogen purging or controlled atmospheric conditions to distinguish between thermal and thermo-oxidative effects. Likewise, simulating earth loads by applying defined pre-compression of the insulation remains a potential extension for cases where soil-pipe interaction is of interest. Despite these limitations, the test setup closely aligns with EN 253 requirements wherever feasible and remains compatible with EN 13941-1-based load cycle considerations. It also enables testing at representative stress ratios for cold-laid pipes and steady-state temperature variations. In its present form, the configuration allows systematic exploration of the roles of temperature level, axial shear stress amplitude, and cycle frequency in the degradation behaviour of pre-insulated DH pipes. In summary, the newly developed test setup expands the methodological toolkit for evaluating pre-insulated DH pipes under more realistic thermo-mechanical loads. It enables controlled application of axial cyclic loads, elevated temperatures, and EN 253-compliant test procedures within a single configuration. This makes it suitable for investigating ageing mechanisms, adhesion performance, and load interaction effects under conditions that more closely resemble real network operation than existing standards allow. As the full experimental programme is still ongoing, future work will apply the setup to further quantify the combined effects of thermal ageing and cyclic axial loading and to develop improved indicators for long-term performance and service life prediction of pre-insulated DH pipe systems.

Acknowlegements

The author gratefully acknowledges the support of the Baulabor team at HafenCity University Hamburg, led by Marcus Illguth. Special thanks are extended to Alexandros Apostolou for the close collaboration in designing the test setup, and to Mickael Cheung for helping construct the setup. I also thank Jorge González Lizcano for his continuous assistance throughout the process, and Ingo Weidlich for his critical insights and valuable discussions that significantly supported the execution of this work.

References

Banushi, G., Vega, A., Weidlich, I., Yarahmadi, N., Kim, J., Jakubowicz, I., & Sällström, J. H. (2021). Durability of District Heating Pipelines Exposed to Thermal Aging and Cyclic Operational Loads. Journal of Pipeline Systems Engineering and Practice, 12(1), Article 04020067. https://doi.org/10.1061/(ASCE)PS.1949-1204.0000521

DIN German Institute for Standardization (2022). District heating pipes - Design and installation of thermal insulated bonded single and twin pipe systems for directly buried hot water networks - Part 1: Design; German version EN 13941-1:2019+A1:2021 (DIN EN 13941-1). DIN Media GmbH.

DIN German Institute for Standardization (2024). District heating pipes - Bonded single pipe systems for directly buried hot water networks - Factory made pipe assembly of steel service pipe, polyurethane thermal insulation and a casing of polyethylene; German version EN 253:2019+A1:2023 (DIN EN 253). DIN Media GmbH.

Doyle, L., & Weidlich, I. (2021). Effects of thermal and mechanical cyclic loads on polyurethane pre-insulated pipes. Fatigue & Fracture of Engineering Materials & Structures, 44(1), 156–168. https://doi.org/10.1111/ffe.13347

Götz, S., & Eulitz, K.-G. (2022). Betriebsfestigkeit: Bauteile sicher auslegen! (2., korrigierte Auflage). Springer Vieweg.

Hay, S., Huther, H., Grimm, S., Heiler, D., Dony, J., & Nielsen, H.-J. (2020). „EnEff:Wärme - Technische Gebrauchsdaueranalyse von Wärmenetzen unter Berücksichtigung volatiler erneuerbarer Energien" : Teil I: Untersuchungsergebnisse zur Materialdegradation : Akronym: „TGdA" : Schlussbericht : Laufzeit des Vorhabens: 01.10.2015-31.05.2019. Forschung und Entwicklung / AGFW, Heft 55. https://doi.org/10.2314/KXP:170169347X

Heißler, K. M. (2020). 5th generation district heating networks. Dissertation (1. Edition) [XIX, 200 Seiten].

Jakubowicz, I., Vega, A., Sällström, J. H., & Yarahmadi, N. (2025). Pipeopsy: A Novel Method for Status Assessment of District Heating Pipes in Operation. Journal of Pipeline Systems Engineering and Practice, 16(1), Article 04024061. https://doi.org/10.1061/JPSEA2.PSENG-1689

Pelda, J. D. (2024). Aspekte der Transformation von Fernwärmesystemen: Verteilung, Quellen und Senken. https://doi.org/10.15488/17597

Schleyer, A., Geßner, A., Uhlig, U., Baumgart, G., Zimmermann, D., Thieme, T., Thieme, G., Schuricht, W., Just, M., Döking, T., Hildebrandt, S., Kaulfuß, G., Lehmann, B., Döhnert, F., Fiedler, H., Ridzewski, J., Döring, K.-D., Finnberg, J., Rätzsch, E., . . . Meyer, M. (2016). Abschlussbericht zum Forschungsvorhaben „Qualitätssicherung für zukünftige Kunststoffmantelrohrsysteme in der Fernwärmeversorgung - Alterungsprüfmethoden, Wechselbeanspruchung, zerstörungsfreie Muffenprüfungen, Diffusionshemmung, Zeitstandsverhalten, Versagensmechanismen, Projektkoordination". https://doi.org/10.2314/GBV:872406350

Thieme, T., Thieme, G., Schuricht, W., Just, M., Kaufmann, U., Ridzewski, J., Döring, K.-D., Finnberg, J., Rätzsch, E., Friebel, G., Wagenknecht, U., Leuteritz, A., Besier, R., Rosenberg, N., Böhm, A., Uhlig, U., Baumgart, G., Zimmermann, D., Manderfeld, M., . . . Pape, H.-G. (2011). Zeitstandsfestigkeit von Kunststoffmantelrohren - Permeations- und Degradationsverhalten, Wechselbeanspruchung, Alterungsgradient, Muffenbewertung, Versagensverhalten: Abschlussbericht zum Forschungsvorhaben, 17. https://opac.tib.eu/DB=1/LNG=DU/SID=ff1a38fd-2/CMD?ACT=SRCHA&IKT=1016&SRT=YOP&TRM=Zeitstandsfestigkeit+von+Kunststoffmantelrohren+

Vega, A., Yarahmadi, N., & Jakubowicz, I. (2021). Cyclic axial loads and thermal ageing of district heating

pipes. Energy Reports, 7, 105–109. https://doi.org/10.1016/j.egyr.2021.09.033

Weidlich, I., Illguth, M., & Banushi, G. (2018). Reserves in axial shear strength of district heating pipes. Energy Procedia, 147, 78–85. https://doi.org/10.1016/j.egypro.2018.07.037

ISBN: 978-3-947972-92-0

DOI: 10.34712/142.81